



National Library
of Canada

Bibliothèque nationale
du Canada

Acquisitions and
Bibliographic Services Branch

Direction des acquisitions et
des services bibliographiques

395 Wellington Street
Ottawa, Ontario
K1A 0N4

395, rue Wellington
Ottawa (Ontario)
K1A 0N4

Your file / Votre référence

Our file / Notre référence

NOTICE

AVIS

The quality of this microform is heavily dependent upon the quality of the original thesis submitted for microfilming. Every effort has been made to ensure the highest quality of reproduction possible.

La qualité de cette microforme dépend grandement de la qualité de la thèse soumise au microfilmage. Nous avons tout fait pour assurer une qualité supérieure de reproduction.

If pages are missing, contact the university which granted the degree.

S'il manque des pages, veuillez communiquer avec l'université qui a conféré le grade.

Some pages may have indistinct print especially if the original pages were typed with a poor typewriter ribbon or if the university sent us an inferior photocopy.

La qualité d'impression de certaines pages peut laisser à désirer, surtout si les pages originales ont été dactylographiées à l'aide d'un ruban usé ou si l'université nous a fait parvenir une photocopie de qualité inférieure.

Reproduction in full or in part of this microform is governed by the Canadian Copyright Act, R.S.C. 1970, c. C-30, and subsequent amendments.

La reproduction, même partielle, de cette microforme est soumise à la Loi canadienne sur le droit d'auteur, SRC 1970, c. C-30, et ses amendements subséquents.

Canada

**The Reduction of Nitric Oxide by Carbon Monoxide
over Excessively-Exchanged Copper ZSM-5 Zeolite**

Ian Thomas Gilchrist

Department of Chemical Engineering
McGill University
Montreal, Canada

August, 1994

A Thesis Submitted to The Faculty of Graduate Studies and Research
in partial fulfilment of the requirements of the degree of
Master of Engineering

© Ian Gilchrist, 1994



National Library
of Canada

Bibliothèque nationale
du Canada

Acquisitions and
Bibliographic Services Branch

Direction des acquisitions et
des services bibliographiques

395 Wellington Street
Ottawa, Ontario
K1A 0N4

395, rue Wellington
Ottawa (Ontario)
K1A 0N4

Your file / Votre référence

Our file / Notre référence

THE AUTHOR HAS GRANTED AN IRREVOCABLE NON-EXCLUSIVE LICENCE ALLOWING THE NATIONAL LIBRARY OF CANADA TO REPRODUCE, LOAN, DISTRIBUTE OR SELL COPIES OF HIS/HER THESIS BY ANY MEANS AND IN ANY FORM OR FORMAT, MAKING THIS THESIS AVAILABLE TO INTERESTED PERSONS.

L'AUTEUR A ACCORDE UNE LICENCE IRREVOCABLE ET NON EXCLUSIVE PERMETTANT A LA BIBLIOTHEQUE NATIONALE DU CANADA DE REPRODUIRE, PRETER, DISTRIBUER OU VENDRE DES COPIES DE SA THESE DE QUELQUE MANIERE ET SOUS QUELQUE FORME QUE CE SOIT POUR METTRE DES EXEMPLAIRES DE CETTE THESE A LA DISPOSITION DES PERSONNE INTERESSEES.

THE AUTHOR RETAINS OWNERSHIP OF THE COPYRIGHT IN HIS/HER THESIS. NEITHER THE THESIS NOR SUBSTANTIAL EXTRACTS FROM IT MAY BE PRINTED OR OTHERWISE REPRODUCED WITHOUT HIS/HER PERMISSION.

L'AUTEUR CONSERVE LA PROPRIETE DU DROIT D'AUTEUR QUI PROTEGE SA THESE. NI LA THESE NI DES EXTRAITS SUBSTANTIELS DE CELLE-CI NE DOIVENT ETRE IMPRIMES OU AUTREMENT REPRODUITS SANS SON AUTORISATION.

ISBN 0-315-99964-0

Canada

THE REDUCTION OF NO by CO over
excessively-exchanged CU-ZSM-5

Abstract

Nitric oxide (NO) is a major pollutant which is produced by the combustion of fossil fuels. Current three-way catalyst (TWC) technology, used for the reduction of NO in automobile exhaust, is effective only under stoichiometric or net reducing conditions which cause incomplete use of the fuel and CO and hydrocarbon pollution. Excessively-exchanged Cu-ZSM-5 zeolite was investigated as a catalyst for the reduction of NO in net oxidizing exhaust mixtures, which would allow for greater fuel efficiency and lower NO, CO and hydrocarbon emissions.

Cu-ZSM-5 powder was pelletized by extrusion and the activity for the reduction of NO by CO on the presence of O₂ was measured at temperatures of 200°C to 550°C and a space velocity of 450 hour⁻¹. The activity of the Cu-ZSM-5 was compared to that of a TWC at 550°C. Under stoichiometric or net reducing conditions the conversion to N₂ over both catalysts was about 100%. Under net oxidizing conditions (when the equivalence ratio, λ , is greater than 1) the conversion decreased with increasing oxygen concentration for both catalysts, but the Cu-ZSM-5 was much more active; at $\lambda=1.3$ the conversion was 53% compared to 26%. The Cu-ZSM-5 was found to deactivate after 30 hours of use. The deactivation was accompanied by a change in the Cu-ZSM-5 structure, and a change in the chemical composition. The deactivation was not found to be a function of the composition, or of the oxidative nature of the conditioning gas used (20% O₂, inert, or 20% CO). Regeneration of the Cu-ZSM-5 proved unsuccessful.

Résumé

Le monoxyde d'azote (NO) est un polluant majeur produit par la combustion de combustibles fossiles. La technologie actuelle des catalyseurs à trois voies (three way catalyst, TWC), utilisés pour la réduction du NO dans le système d'échappement des automobiles, est efficace seulement dans des conditions stoechiométriques ou réductives; une conversion incomplète du carburant résulte, ce qui entraîne des émissions polluantes de CO et d'hydrocarbures. Le catalyseur Cu-ZSM-5 excessivement échangé (excessively exchanged) est proposé pour la réduction du NO dans des gaz d'échappements oxydants, ce qui permettrait une utilisation plus efficace du carburant tout en diminuant les émissions de NO, de CO et d'hydrocarbures.

De la poudre de Cu-ZSM-5 a été agglomérée en boulettes par extrusion et l'activité de réduction du NO par le CO en présence d'O₂ a été mesurée à des températures variant de 200 à 550 °C avec un temps de résidence moyen de huit secondes. L'activité du Cu-ZSM-5 a été comparée à celle du TWC à 550 C. Pour les conditions stoechiométriques ou réductives, la conversion en azote pour les deux catalyseurs est d'environ 100%. Pour les conditions oxydante (quand le ratio d'équivalence est plus d'un, $\lambda > 1$) la conversion diminue avec une augmentation de la concentration en oxygène pour les deux catalyseurs. Cependant, le Cu-ZSM-5 demeure beaucoup plus actif: par exemple, pour $\lambda = 1.3$, la conversion est de 53% pour le Cu-ZSM-5 comparée à 26% pour le TWC. Il a été observé que le Cu-ZSM-5 se désactive après 30 heures d'utilisation. Cette désactivation est accompagnée d'un changement dans la structure du Cu-ZSM-5 ainsi que d'une modification de sa composition chimique. La désactivation ne varie pas en fonction de lambda ou de la nature oxydante du gaz de pré-traitement utilisé (20% O₂, gaz inerte ou 20% CO). Le catalyseur n'a pas pu être régénéré avec succès.

Acknowledgements:

This work was made possible through grants from the Natural Sciences and Engineering Research Council (NSERC). Catalyst samples were provided free of charge from Allied Signal Incorporated (in conjunction with UOP Incorporated), Mobil Chemical Company, and Degussa Canada Limited.

I would like to thank my research supervisor, Dr. Dimitrios Berk for his guidance, advice, and continuous encouragement throughout the length of the project.

My appreciation goes out to all members, past and present, of the 'Berklabs' Reaction Engineering Group, including Messrs Nedim Altaras and Matt Collyer, and especially Ms. Christine Bryce, for the friendship and camaraderie which made the research such an enjoyable experience. Thanks are also due to Mr. David Mulligan for his advice and assistance with the experimental apparatus and Mr. Patrice Nadeau for his assistance with the translation of the abstract.

Messrs Mark Weber, Gary Ng, Eric Cheluget, and Jaspreet Singh deserve a special thanks for their continued friendship and the many thoughtful discussions.

Mr. Jean Dumont efficiently procured much of the necessary hardware, and his contribution to the good humour of the department cannot go without note.

I would also like to thank Messrs Andy Krish, Alain Gagnon, and Walter Greenland for their assistance in the construction and repair of the experimental apparatus, Mr. Ed Siliauskas for his assistance in the use of the analytical equipment, and Messrs Frank Sebo and Nabil Habib for their procurement of sundry items.

I am grateful for the direct financial support provided by NSERC and the Department of Chemical Engineering.

A final note thanks goes to my family and friends, especially Ms. Anita Stepan, for their unfailing encouragement, and support throughout the duration of the work.

Table of Contents

Abstract	i
Résumé	ii
Acknowledgements:	iii
List of Figures	vii
List of Tables	x
Nomenclature	xi
1 Introduction	1
1.1 Nitric Oxide, Surface Ozone, Photochemical Smog, and Acid Rain	2
1.2 Regulation of NO _x Pollution	4
1.3 NO Production and Abatement	4
1.4 Thermodynamic Considerations	9
1.5 Nitric Oxide Reduction and Direct Decomposition Testing Over the Last Two Decades	9
1.6 Cu-ZSM-5 Zeolite Properties and Structure	11
1.7 Overview of the Thesis	14
2 Objectives of the Research	15
2.1 Statement of Objectives	16
3 Literature Review	17
3.1 Conversion of NO to N ₂ over Cu-ZSM-5	17
3.2 Redox Properties of Cu-ZSM-5	23
4 Materials and Methods	25
4.1 Catalyst Material and Gas Supplies	25
4.2 Pelletization of the Allied Signal Cu-ZSM-5 Powder	25
4.2.1 Direct Pelletization of the Cu-ZSM-5	27
4.2.2 Pelletization by Extrusion of Cu-ZSM-5 Paste	28
4.3 Ion Exchange of ZSM-5 Pellets	28
4.4 Catalyst Characterization	28
4.4.1 X-Ray Crystallography	28
4.4.2 Chemical Analysis	29
4.4.3 Surface Area, Porosity, and Pore Volume Distribution Analysis	30
4.5 Wet Chemical Analysis	31
4.6 Experimental Setup	31

4.7	Description of a Typical Experimental Run	35
4.8	Data Evaluation	36
4.9	Reactor Flow Characterization	38
5	Gas Analysis	40
5.1	Introduction	40
5.2	The NO ₂ Trap	41
5.3	The Analysis by Gas Chromatography	42
5.3.1	Description of the Sampling System and Analysis Hardware	42
5.3.2	GC Preparation and Gas Sampling Procedure	46
5.3.3	Description of the GC Analysis, by Component, in Order of Measurement	47
5.4	Interpretation of the GC Area Results: Calculation of the Composition of the Gas Streams and Conversions	48
5.4.1	The Analysis of NO and Calculation of x_{NO}	50
5.4.2	The O ₂ Analysis	53
5.4.3	The N ₂ Analysis and Calculation of x_{N_2}	54
6	Results and Discussion	56
6.1	Preliminary Experiments	56
6.1.1	Characterization of the Reactor	56
6.1.2	Determination of Homogeneous Reaction Products	58
6.1.3	Preliminary Experiments for Catalytic Activity	59
6.1.3.1	Catalytic Activity of the Cu-ZSM-5-M	61
6.1.3.2	Catalytic Activity of the Cu-ZSM-5-AS	61
6.1.3.3	Activity for NO Reduction of the Montmorillonite	62
6.1.3.4	Dependence of Activity on Reaction Time	62
6.1.4	Test for External Diffusion Control	67
6.2	Reduction of NO by CO in the Presence of O ₂	68
6.2.1	Reduction Activity of Fresh Cu-ZSM-5	70
6.2.2	Reduction Activity of the Three-Way Catalyst	77
6.2.3	Reduction Activity of Reused Cu-ZSM-5	77
6.2.4	Effect of Regeneration Treatments on the Cu-ZSM-5	83
6.2.5	Effect of Pretreatment of Cu-ZSM-5 on Reduction Activity	83
6.2.6	Effect of the Feed Redox Ratio on Cu-ZSM-5 Deactivation	83
6.3	Activity of Cu-ZSM-5 for CO Oxidation	85
6.4	Characterization of Virgin and Used Cu-ZSM-5	88
6.4.1	Chemical Analysis of the Cu-ZSM-5	88
6.4.2	Crystallographic Analysis of the Cu-ZSM-5 by X-ray Diffraction	90
6.5	Redox State and Observed Colour of the Cu-ZSM-5	97

7	Conclusions and Recommendations	100
7.1	Conclusions	100
7.2	Recommendations for Future Work	101
Appendix A	Mass Flow Controller Calibration	102
Appendix B	Gas Chromatography Calibration	103
Appendix C	Test For Mass Transfer Control	104
Appendix D	Survey of Analytical Methods	106
Appendix E	GC Column and Program Selection	111
Appendix F	Measurement of NO in the Product Stream in the Absence of O ₂ , and Calculation of x _{NO}	114
Appendix G	Measurement of N ₂ and Calculation of x _{N₂}	116
List of References	122

List of Figures

Figure 1.1	Chemical transformations of atmospheric NO _x	3
Figure 1.2	Exhaust components concentration as a function of λ	6
Figure 1.3	Conversion efficiency of a typical PGM three-way catalyst	8
Figure 1.4	Schematic structure of Cu-ZSM-5	12
Figure 1.5	Simplified schematic of Na-ZSM-5 and Cu(II)-ZSM-5	13
Figure 3.1	Correlation between exchange level of copper ions (as Cu ²⁺) and conversion of NO to N ₂ and O ₂	18
Figure 3.2	Arrhenius plots for NO decomposition over Cu-ZSM-5 (4% NO in helium)	21
Figure 4.1	Schematic diagram of the experimental setup	32
Figure 4.2	Diagram of the gas handling system, showing the mass flow controllers, rotameters, and sample ports	33
Figure 4.3	The tube reactor with the catalyst bed	34
Figure 5.1	The gas chromatograph with the bypass valve activated	43
Figure 5.2	A typical chromatogram showing the CO ₂ , N ₂ , O ₂ , Ar, and CO peaks.	44
Figure 5.3	Typical chromatogram of a mixture of N ₂ , Ar, and NO	45
Figure 5.4	Measured and Actual NO and O ₂ in one experiment, product normalized by Ar ($y_i^p \cdot y_{Ar}^f / y_{Ar}^p$) (10% CO, 2% NO, 4% O ₂)	52
Figure 6.1	Residence Time Distribution: Concentration of Argon in Reactor Effluent after a Step Input Change, and Model Results . . .	57
Figure 6.2	Homogeneous steady state oxidation of CO by O ₂ at different temperatures (Feed: 10% CO, 4% O ₂ , balance Ar and He)	60
Figure 6.3	Activity of Cu-ZSM-5-AS for the decomposition of NO. (Feed: 2% NO, balance Ar)	63
Figure 6.4	Activity of Cu-ZSM-5-AS for reduction of NO (Feed: 10% CO, 2% NO, balance Ar)	64
Figure 6.5	Decomposition activity as a function of time (Feed: 2% NO, 98% Ar)	65
Figure 6.6	Reduction activity as a function of time (Feed: 10% CO, 2% NO, balance Ar)	66
Figure 6.7	Reduction activity at $\lambda < 1$ ($\lambda = 0.2$; 10% CO, 2% NO, 0% O ₂) ($\lambda = 0.75$; 10% CO, 2% NO, 2.75% O ₂)	71
Figure 6.8	Reduction activity at $\lambda = 1$ (Feed: 10% CO, 2% NO, 4% O ₂ , balance inert)	72
Figure 6.9	Reduction activity at $\lambda = 1.3$ (Feed: 10% CO, 2% NO, 5.5% O ₂ , balance inert)	73
Figure 6.10	Reduction activity trends over Cu-ZSM-5. Space velocity = 450 hr ⁻¹ Space time (W/F) = 4.8 g·s/cm ³	74

Figure 6.11	Lambda-plot for Cu-ZSM-5: Conversion to N ₂ at fixed temperatures for a space velocity of 450 hour ⁻¹ (space time of 4.8 g-s/cm ³)	76
Figure 6.12	Pore volume distribution of the PGM TWC from Degussa	78
Figure 6.13	Lambda-plot at 550°C for the alumina PGM three-way catalyst from Degussa	79
Figure 6.14	Reduction activity of a spent catalyst and trend for new catalyst at lambda = 1	80
Figure 6.15	Reduction activity for a used catalyst sample at lambda = 1.18 . . .	81
Figure 6.16	Lambda-plot, including results obtained with used catalyst samples	82
Figure 6.17	Reduction activity at lambda = 1, with pretreatment gas indicated (Feed = 2% NO, 4% O ₂ , 10% CO, balance inert)	84
Figure 6.18	Conversion of CO by O ₂ (Feed: 10% CO, 4% O ₂ , balance Ar and He)	86
Figure 6.19	CO conversion for comparison with the λ = 1 case	87
Figure 6.20	X-ray diffraction pattern of virgin Cu-ZSM-5, with H-ZSM-5 reference data	91
Figure 6.21	X-ray diffraction pattern of virgin Cu-ZSM-5, with Na-ZSM-5 reference data	92
Figure 6.22	X-ray diffraction patterns: Untreated, reduced, oxidized, and spent Cu-ZSM-5	93
Figure 6.23	X-ray diffraction patterns: Untreated, reduced, oxidized, and spent Cu-ZSM-5	94
Figure 6.24	Partial x-ray diffraction pattern: Untreated and Spent Cu-ZSM-5	95
Figure 6.25	Partial x-ray diffraction pattern: Untreated and spent Cu-ZSM-5	96
Figure A.1	GC Calibration Curve for NO	103
Figure A.2	N ₂ measured in consecutive feed samples. (10% CO, 2% NO, 4% O ₂ , 38% Ar, 0% N ₂)	117
Figure A.3	The N ₂ measured in the CO supply	117
Figure A.4	Data from Figure A.2; the N ₂ measured in feed gas mix with 0% N ₂	118
Figure A.5	N ₂ measured in feed gas samples of constant volume, and, for reference, maximum amount producible by reaction of the feed mixture.	120

List of Tables

Table 1.1	California and U.S. Federal Automobile Emissions Standards, in Grams per Mile	5
Table 1.2	Equilibrium Constant, K_p , versus Temperature for Pertinent Reactions	10
Table 3.1	Decomposition of NO (in Helium) over Cu-ZSM-5; Reported Results	20
Table 4.1	The Gasses Used for the Feed Supply	26
Table 6.1	Experimental Conditions for Measuring the Activity for the Reduction of NO by CO in the Presence of O ₂	69
Table 6.2	Elemental Analysis of Cu-ZSM-5 Samples	89
Table 6.3	Colour of the Cu-ZSM-5 Under Various Conditions	98

Nomenclature

Cu-ZSM-5-146-27 = copper ZSM-5 zeolite, with an exchange ratio of 146 (may not be specified) and a Si/Al ratio of 27 (may not be specified)

C_i	=	Concentration of species i (mol/cm ³)
F_i^s	=	molar flow rate of species i in stream s (mol/s)
k	=	rate constant
k_m	=	mass transfer coefficient
K	=	equilibrium constant
$\bar{K}_{N_2}^f$	=	average amount of N ₂ co-injected with feed samples
m_i^s	=	moles of species i measured in a gas sample from stream s (mol)
M	=	mass of the catalyst (g)
n_i^s	=	moles of species i in a gas sample from stream s (mol)
n_a	=	moles of active metal in the catalyst bed (mol)
r_i	=	rate of reaction of species i (mol/s)
$r \frac{N_2}{i}$	=	ratio of N ₂ to species i in the feed supply of species i
TOF	=	rate of reaction of NO to 1/2N ₂ per mole of Cu in the catalyst (s ⁻¹)
Q_f	=	volumetric flow rate of the feed (cm ³ /s) at 25°C and 1 atmosphere unless otherwise stated
x_i	=	conversion of species i , $i \neq N_2$
x_{N_2}	=	conversion of NO to 1/2N ₂
Y_i	=	yield of species i
y_i	=	mole fraction of species i
λ	=	equivalence ratio of a gas mixture.
θ	=	residence time (s)
$\bar{\theta}$	=	mean residence time (s)
ρ	=	density (g/cm ³)

Superscripts:

s	=	gas stream s
f	=	feed stream
p	=	reactor effluent (product) stream, downstream of the cold trap
x	=	reactor effluent (exit) stream, upstream of the cold trap

Subscripts:

i	=	gas species i
-----	---	-----------------

Chapter 1

Introduction

The emission of nitrogen oxides (NO_x) from automobiles has been of great concern for over a quarter century. Photochemical smog, surface ozone, and acid rain caused by nitrogen oxides continues to plague many areas world wide. In industrialized nations regulation and technological advance has lead to significant reductions in the emissions from other sources, but the automobile remains the largest source, accounting for well over half of all emissions (Bosch and Jansen, 1987). Furthermore, the move towards fuel efficiency and requirements for lower carbon monoxide and hydrocarbon exhaust emissions makes the abatement of NO_x more difficult. The research presented in this thesis is aimed at improving the abatement under these difficult circumstances.

Current NO_x abatement technology for automobiles is based on the use of three-way catalysts (TWC) which are alumina-supported rare-earth-promoted platinum-group metal (PGM) catalyst materials coated on ceramic honeycomb type monoliths. The TWC catalyze the reduction of NO and the oxidation of CO and hydrocarbons (HC) in the exhaust stream. Apart from being very expensive, these catalysts are easily poisoned by Pb, S, P and other agents commonly found in gasoline (including unleaded) and motor oil, and have short lifetimes, about 80,000 km (Church *et al.*, 1989). To be effective for NO_x removal, they must be used under stoichiometric or net reducing conditions which are incompatible with maximum engine efficiency and which result in hydrocarbon and carbon monoxide pollution.

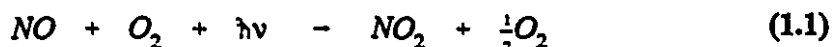
This research is a preliminary investigation of the activity of an alternate catalyst material, Cu-ZSM-5 zeolite, for the removal of NO from net oxidizing exhaust streams. The improved abatement of NO would lead directly to lower NO_x emissions, to lower production and emissions of CO and hydrocarbons, and to greater fuel efficiency.

1.1 Nitric Oxide, Surface Ozone, Photochemical Smog, and Acid Rain

Nitric Oxide, NO, is one of the seven known (neutral) oxides of nitrogen, the other six being NO₂, N₂O₃, N₂O₄, N₂O₅, and N₂O (nitrous oxide). NO_x generally refers to all of the oxides except N₂O, or, since the other species are not commonly found, just NO and NO₂. N₂O is a naturally occurring product of biological activity and exists in significant concentration in the atmosphere.

The main source of NO_x pollution is from the combustion of fossil fuels and burning of biomass (Bosch and Jansen, 1987). In the combustion process, 90 - 95% of the NO_x formed is NO and most of the rest is NO₂. Fixation of atmospheric nitrogen (thermal NO_x), oxidation of nitrogen in the fuel (fuel NO_x), and oxidation of the combustion intermediate HCN all contribute to NO_x formation, although the thermal process accounts for the greatest part.

Any NO that is released into the atmosphere is almost immediately oxidized to NO₂ with the aid of radiation at a wavelength of 415 nm:



or by ozone:



As is shown in Figure 1.1, a schematic of the atmospheric NO - NO₂ cycle, the NO_x pollution results in the production of toxic ozone (often in excess of the NO_x originally emitted) as well as nitric acid, nitrous acid, and pernitric acid which lead to acid rain. When NO_x and its derivatives combine with airborne

hydrocarbons, various peroxy-nitrates (RCOONO_2 , or PANS), the most common of which is peroxyacetyl nitrate (PAN), are formed; these PANS are the major components of photochemical smog.

1.2 Regulation of NO_x Pollution

In their excellent review of fixed source NO_x pollution and its abatement, Bosch and Janssen point out that the harmful effects of air pollution are not limited to urban areas, but also affect agricultural lands as well as forests and other natural environments (Bosch and Janssen, 1987). The regulation of such environments is not new; in England, one of the first official acts on record is the Assize of the forest (Douglas and Greenaway, 1961). In 1184, Henry II legislated the Forest Law to "ensure preservation of the beasts of the forest" (Warren, 1978). In response to the specific issue of air quality in his European realms, Emperor Frederick II banned the treatment of flax within a radius of one mile of any settlement to prevent "annoyance by dust and bad scent therein" in 1231. Dealing with the problem of smoke, a Royal Proclamation, issued in England in 1306, prohibited craftsmen from using coal in their furnaces under penalty of death (Clarke, 1984). It was not until the 1960's, however, that legislation was enacted to deal with the specific problem of NO_x emissions. California was then, and is now, the world leader in such legislation. Table 1.1 shows recent and future Californian and US Federal emissions standards. Canadian federal standards are expected to fall in line with the U.S. federal standards.

Current gasoline automobiles produce about 2 to 10 grams of NO_x per mile (Cadle *et al.*, 1993), so high levels of conversion of the NO are needed if the standards are to be met.

1.3 NO Production and Abatement

The NO produced in automobile exhaust is a direct function of the air/fuel ratio of the engine feed. A lean feed will produce a net oxidizing exhaust; a rich feed will produce a net reducing exhaust. Figure 1.2 shows measured concentrations

Table 1.1 California and U.S. Federal Automobile Emissions Standards, in Grams per Mile:

Year	Standard	NO _x	HC	CO
1990	U.S.	1.0	0.41	3.4
1993	California	0.40	0.25	3.4
1994	U.S.	0.4	0.25*	3.4
1994	California TLEV	0.40	0.125	3.4
1997	California LEV	0.20	0.075	3.4
2000	California ULEV	0.20	0.040	1.7

* Non-methane HC

TLEV = Transitional low emission vehicles

LEV = Low emission vehicles

ULEV = Ultra low emission vehicles

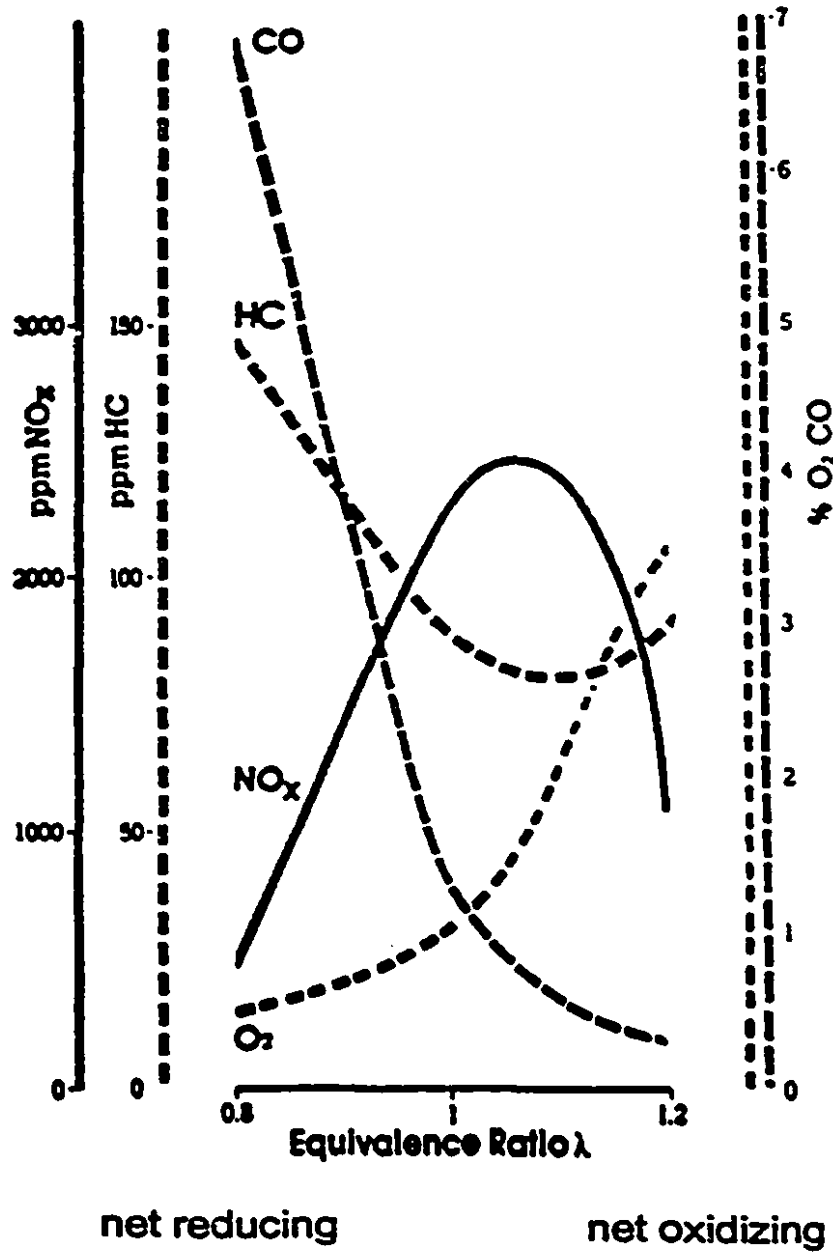


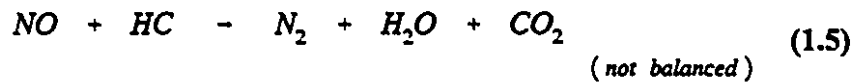
Figure 1.2 Exhaust components concentration as a function of λ (Church *et al.*, 1989)

of the exhaust gas components NO, CO, and HC as a function of the equivalence ratio (or redox ratio), λ , of the exhaust mixture:

$$\lambda = \frac{NO + 2O_2}{CO + (\frac{1}{2}m + 2n)H_mC_n} \quad (1.3)$$

where H_mC_n (HC for short) represents the hydrocarbons left from incompletely burned fuel. Note that a minimum of HC are produced at a λ of 1.15, and that the CO produced is greater than the NO at all points on the curve, even at high values of λ .

The desired reactions for the elimination of NO are the reduction by CO and hydrocarbons and the direct decomposition:



The reduction by CO is the most important reaction for stoichiometric and reducing conditions ($\lambda \leq 1$), since the number of equivalents of HC is much less than that of CO. For net oxidizing mixtures ($\lambda > 1$), the direct decomposition may also play a significant role. To be effective at the high λ 's, the catalyst must be more selective for the oxidation of CO by NO than by O_2 , or be active for the decomposition reaction in the presence of O_2 .

The effectiveness of a typical three-way PGM catalyst is shown in Figure 1.3. As is seen from the figure, the PGM is almost completely ineffective for NO reduction just above the stoichiometric point, so automobiles must be run at λ 's equal to or less than 1, causing a loss of efficiency and an excess of CO and HC pollution.

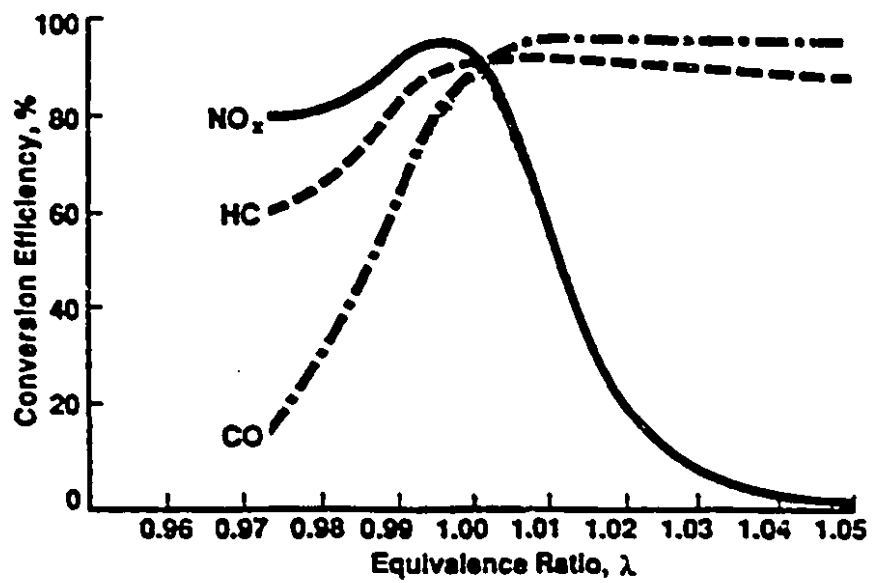


Figure 1.3 Conversion efficiency of a typical PGM three-way catalyst (Church *et al.*, 1989)

1.4 Thermodynamic Considerations

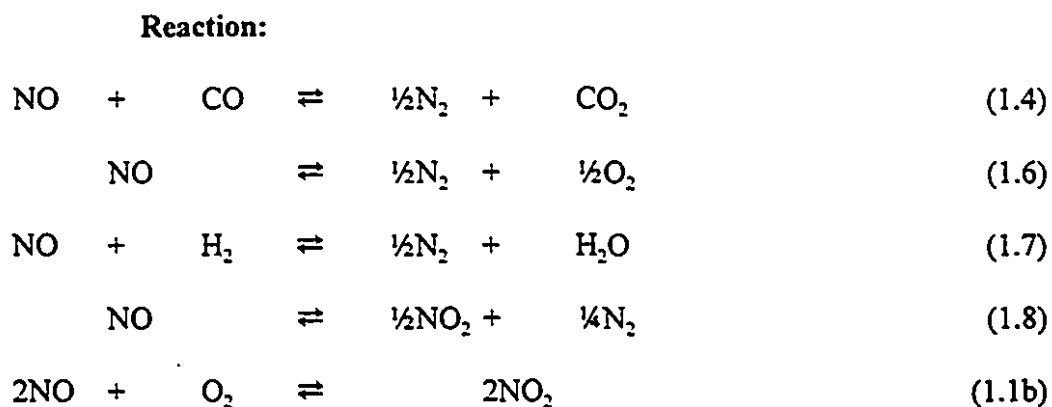
At temperatures below several thousand degrees celsius, NO is thermodynamically unstable with respect to oxygen and nitrogen. Over time, the decomposition reaction (Equation 1.6) will go virtually to completion at the temperatures encountered in this research project (less than 1000°C). The reduction by CO (Equation 1.4), is similarly favoured at such temperatures, and the driving force for the reaction (from a thermodynamic standpoint) is stronger than that for the oxidation of CO by O₂. Likewise, the conversion of NO by H₂ and most hydrocarbons (Equation 1.5) will progress almost to completion at low temperature, if given enough time. Yet, although thermodynamically favoured, these reactions progress slowly, and need for better catalysts is present.

A complication with this reaction system is that while the desirable reactions all have unfavourable kinetics, the oxidation of NO by O₂ to form NO₂ is not slow. Although it is also thermodynamically unstable with respect to its constituent elements, NO₂ has a lower energy of formation at low temperatures, and is thus thermodynamically more favoured than NO. For better comparison, Table 1.2 provides equilibrium data for various reactions at various temperatures.

1.5 Nitric Oxide Reduction and Direct Decomposition Testing Over the Last Two Decades

A wide variety of materials has been tested for activity for both the reduction of NO to N₂ in exhaust gas, and the direct decomposition of NO. In the 1960's and early 70's, research focused on the transition metal oxides alone or supported on Al₂O₃, SiO₂, TiO, and other materials (Hightower and Van Leirsburg, 1975; Amirnazmi *et al.*, 1973). The few catalysts that did show some limited activity for NO reduction or decomposition to N₂ (e.g. nickel and nickel-copper alloys) also showed a strong inhibition by O₂. The platinum group metals gave slightly improved results. In order of increasing activity in exhaust gas (and, also, lower NH₃ formation when used for the reduction of NO in net reducing exhaust) at higher λ's, are Pd, Pt, Rh, Ru, and Ir (Church *et al.*, 1989; Herz *et al.*, 1983; Lester *et al.*,

Table 1.2 Equilibrium Constant, K_p , versus Temperature for Pertinent Reactions:



Equilibrium Constant, K_p , by Reaction Number, and Temperature:

Reaction:	(1.4)	(1.6)	(1.7)	(1.8)	(1.1b)
Temp:					
(°C)					
0	1.7×10^{66}	4.4×10^{16}	1.3×10^{64}	6.8×10^{12}	-
25	-	-	-	-	2.4×10^{12}
93	1.1×10^{48}	1.7×10^{12}	5.0×10^{45}	1.9×10^8	-
127	-	-	-	-	1.8×10^7
371	3.5×10^{34}	4.8×10^6	1.4×10^{22}	1.6×10^4	-
427	-	-	-	-	5.51
627	-	-	-	-	6.29×10^{-2}
649	1.1×10^{25}	3.0×10^4	4.2×10^{12}	7.8×10^1	-
927	8.3×10^{15}	1.9×10^3	2.8×10^7	8.3×10^0	-

(Harrison *et al.*, 1982; Hightower, 1975)

1978). Ru was ruled out because of the toxicity and the volatility of its oxide, and Ir because of its great expense (Kim, 1982). Numerous combinations of PGM mixtures and base or rare earth metal promoters have also been tested, and these mixtures are the basis of current TWC (Muraki *et al.*, 1989, 1986; Adams and Gandhi, 1983; Kim, 1982). In recent years, much research activity has turned to alternate formulations, such as ion exchanged zeolites and related complex compounds.

Numerous zeolite formulations have been tested for the direct decomposition or reduction of NO following the early advances of Iwamoto (Iwamoto *et al.*, 1986-91; Minsono and Kondo, 1991; Tzou *et al.*, 1991; Li and Hall, 1990-91; Held *et al.*, 1990). By far the most active catalyst found was excessively exchanged Cu-ZSM-5 zeolite. The various advances made with Cu-ZSM-5 are reviewed in Chapter 3.

1.6 Cu-ZSM-5 Zeolite Properties and Structure

ZSM-5 is a highly siliceous zeolite which was synthesized and patented by Mobil Corporation in the early 1970's. Its structure was not worked out until the late 1970's when the nature of its crosslinked channels was revealed, as shown in Figure 1.4; the unit cell of the sodium form is $\text{Na}_n\text{Al}_n\text{Si}_{96-n}\text{O}_{192} \sim 16\text{H}_2\text{O}$ where n is less than 27, but typically 3 (Kokotailo *et al.*, 1978). All zeolites are composed of the same building blocks, silicon oxide tetrahedra, where occasionally there rests an aluminum atom in the place of the silica. The aluminum oxide tetrahedra are not isolated, as might be thought, given their low concentration, but typically rest in clusters of two or three, depending on aluminum content (Dijkstra *et al.*, 1991). Each aluminum atom brings a charge imbalance to the silicate framework, and for each one there must be a charge balancing cation.

The channels of the ZSM-5 are small enough for water molecules to enter, so these non-lattice ions can be exchanged in aqueous solution. With the simplified schematic structures shown in Figure 1.5, the exchange of two Na^+ ions with one Cu^{2+} ion is shown. If all of the sodium is exchanged for copper(II) then the catalyst is said to be *100% exchanged*. If more copper were to be introduced into the

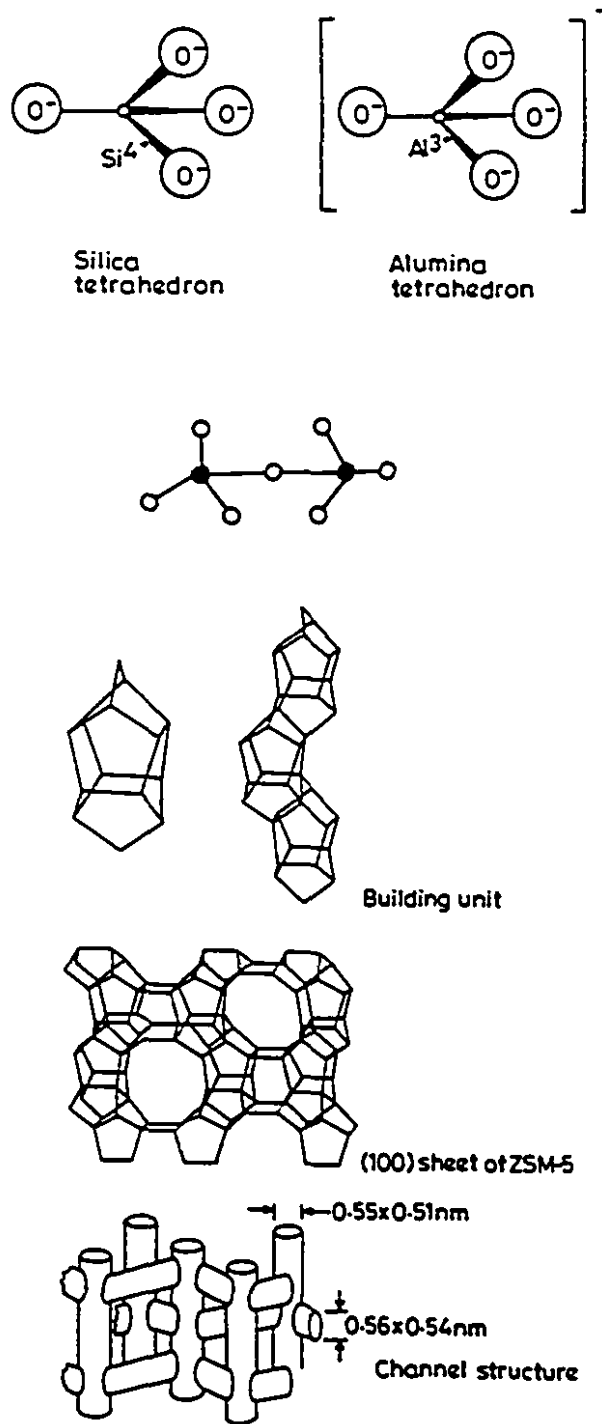
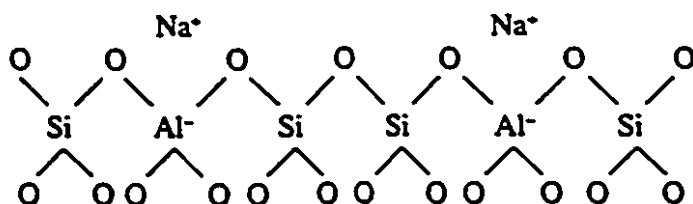


Figure 1.4 Schematic structure of Cu-ZSM-5
(Kokotailo *et al.*, 1978; Bhatia, 1990)

The structure of the sodium form of the zeolite can be represented in a simplified schematic fashion:



If Na⁺ is replaced by Cu²⁺, the structure is:

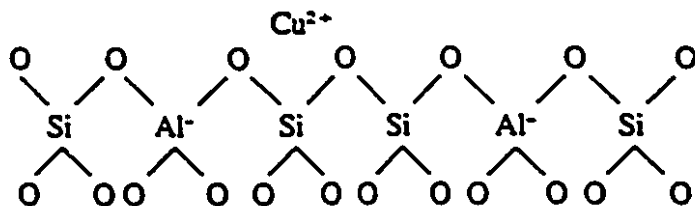


Figure 1.5 Simplified schematic of Na-ZSM-5 and Cu(II)-ZSM-5 (Bhatia, 1990)

zeolite, then it would be *excessively exchanged*. The excess Cu may be the result of the introduction of various copper-hydroxide complexes ($\text{Cu}_2(\text{OH})^{3+}$, $\text{Cu}(\text{OH})^+$, $\text{Cu}_2(\text{OH})_2^{2+}$, $\text{Cu}_3(\text{OH})_2^{4+}$) during the exchange, depending on the pH of the exchange solution (Ohtaki *et al.*, 1972 (from Iwamoto, 1990)).

1.7 Overview of the Thesis

This thesis is composed of seven chapters. Immediately following this one are the objectives and literature review chapters; the review will deal specifically with recent developments in NO decomposition and reduction, and with Cu-ZSM-5. The materials and methods used for this research project are described in Chapters 4 and 5 and the results and discussion are presented in Chapter 6. A summary of the conclusions and recommendations for future work are given in Chapter 7.

Chapter 2

Objectives of the Research

Nitric oxide is a major pollutant which is produced by the combustion of fossil fuels. Upon release into the atmosphere, NO causes nitrogen dioxide and surface ozone pollution and contributes to the formation of photochemical smog and acid rain. The platinum-group metal TWC technology used for the reduction of NO in the exhaust of gasoline automobiles, the largest source of NO, is only effective under conditions which cause inefficient use of the fuel source and, in many cases, generate carbon monoxide and hydrocarbon pollution from the incompletely burned fuel. The standard TWC has a limited lifetime and is susceptible to poisons commonly found in gasoline and motor oils.

Of the large number of compounds tested over the last three decades, only excessively exchanged Cu-ZSM-5 shows potential as catalyst which would allow the engine to be run at under moderately oxidizing conditions, and thus most efficiently, and yet convert the NO by-product into nitrogen. This potential exists because excessively exchanged Cu-ZSM-5 has been shown to be highly active for the direct decomposition of NO in the presence of O₂, and also for its reduction by CO. The aim of this research is to measure the overall activity for the reduction of NO to N₂ by CO in the presence of a small excess of O₂.

2.1 Statement of Objectives

- 1) To evaluate Cu-ZSM-5 for its activity in the overall conversion of NO to N₂ by CO in the presence of varying amounts of O₂, and in particular, in the presence of a moderate excess of O₂, as would be comparable in the exhaust of a gasoline fuelled automobile engine running at its most efficient, namely at λ 's of 1.2 to 1.3.
- 2) To investigate the effect of the equivalence ratio, λ , on the conversion to N₂.
- 3) To investigate the effect of reaction conditions on the catalyst, and its activity over time.
- 4) To compare the activity of the catalyst to that of a modern platinum-group metal three-way catalyst under similar conditions.

Chapter 3

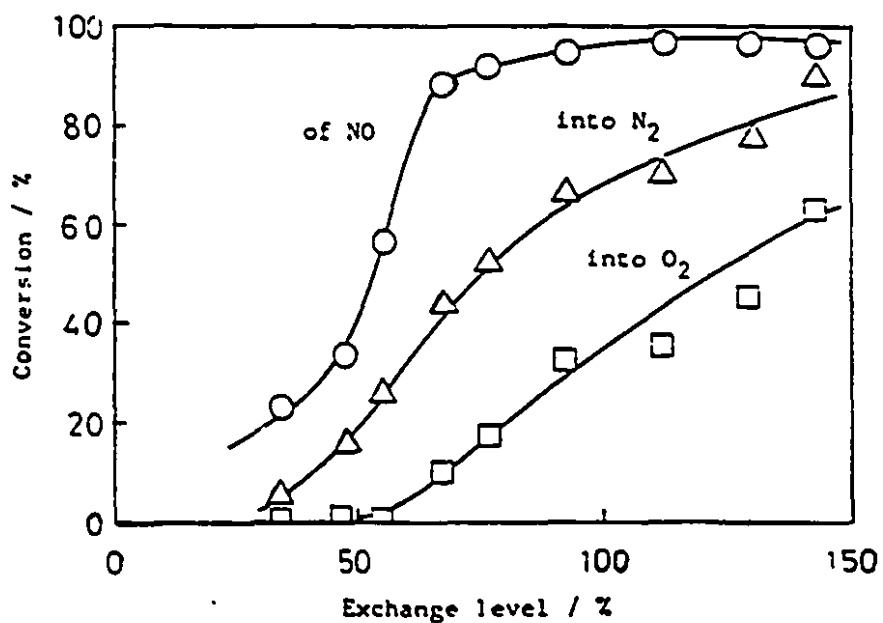
Literature Review

In this chapter a review of recent work concerning the decomposition of NO and the reduction of NO by CO over Cu-ZSM-5 as well as an analysis of the oxidation state of Cu-ZSM-5 under various conditions are presented.

3.1 Conversion of NO to N₂ over Cu-ZSM-5

Iwamoto and co-workers showed that it is the presence of the excess copper that gives Cu-ZSM-5 its activity for the decomposition of NO (Iwamoto *et al.*, 1989). The findings, shown in Figure 3.1, reveal that the conversion is not maximized until an exchange level of at least 146% (Cu-ZSM-5-146 catalyst) is used. The results from the figure also suggest that some of the NO reacted with the O₂ formed by the decomposition, producing NO₂ or other undesirable species. Two years later, Iwamoto and co-workers published an ion-exchange procedure for Cu-ZSM-5 that gave significantly improved results (Iwamoto *et al.*, 1991). Prior to the development of the method, only copper(II) acetate was found to exchange ZSM-5 above 100%. With the new procedure, copper nitrate could be used, and the exchange time greatly reduced.

The new method involved washing the ZSM-5 in dilute NaNO₃ and stirring the sample in very dilute copper(II) nitrate for 24 hours. Subsequently, NH₄OH solution was added until the pH was raised to 7.5. No Cu(OH)₂ precipitate was observed, even though it would ordinarily be expected in such a solution at that pH.



$T = 723 \text{ K}$, $W/F = 4.0 \text{ g}\cdot\text{s}\cdot\text{cm}^{-3}$, $P_{\text{NO}} = 1.0\%$

Figure 3.1 Correlation between exchange level of copper ions (as Cu^{2+}) and conversion of NO to N_2 and O_2 (Iwamoto *et al.*, 1989)

In 1990, the same group showed that the Cu-ZSM-5 was active for the reduction of NO by CO. Under the conditions of the experiment (the space time at 25°C, W/F, was 0.3 g·s·cm⁻³, where W and F are the mass of catalyst and the flow rate, respectively; the temperature was 400°C; and the feed was 1000 ppm NO in helium), the conversion of NO into N₂ went from 24% to 90% with the addition of an equal amount of CO ($\lambda = 1$), as shown in Table 3.1. With the further addition of 1% O₂ (at $\lambda = 11$, far beyond the stoichiometric point) the activity dropped, and was only significant at temperatures above nearing 400°C. It was, however, much greater than that of the activity when an equal amount of H₂ was used as the reductant, showing that the CO, even in the presence of a great excess of O₂, did significantly improve the conversion (Iwamoto *et al.*, 1990). At about the same time, Li and Hall measured the rate of decomposition of NO over excessively exchanged Cu-ZSM-5 in the presence of O₂, and developed the following rate law:

$$r = \frac{k[NO]}{1 + K[O_2]^{1/2}} \quad (3.1)$$

where r is the turnover rate in units of [s⁻¹·site⁻¹], k is the rate constant in units of [s⁻¹·site⁻¹·(mol/L)⁻¹] and K is the equilibrium constant for the adsorption of O₂ on the catalytic sites in units of [(mol/L)^{-1/2}]. Values of k and K were given for a few temperatures (Li and Hall 1990, 1991):

T (K)	k	K
623	0.95	-
673	1.91	-
723	5.03	157.5
773	7.58	84.2
823	7.43	53.0

The k values were first determined from results of the decomposition of NO over Cu-ZSM-5 in the absence of O₂ and the K values were then fit to the data for the NO decomposition in the presence of O₂.

One problem with the rate expression (Equation. 3.1) is that the values for the oxygen dependency are given only in the temperature region where the Arrhenius plots (in the publication) show mass transfer dependence (above 723 K),

Table 3.1 Decomposition of NO (in Helium) over Cu-ZSM-5: Reported Results:

Experiment	Cu-ZSM-5 Si/Al	Cu-ZSM-5 Ex% Cu	W (g)	F (cm ³ /min) 25°C 1 atm	Space Time W/F (g s cm ⁻³)	Space Velocity (hour ⁻¹)	Temp (K)	pNO (%)	Conv. to N ₂ (%)
I. (1990)	11.7	144	0.5	60	0.5	3600	773	0.495	48.4
I. (1990)	11.7	144	0.5	60	0.5	3600	823	2.05	73
I. (1990)	11.7	152	-	-	0.3	60 000	773	0.1	20
I. (1990)	11.7	152	-	-	0.3	60 000	773	0.1*	90
I. (1990)	11.7	152	-	-	0.3	60 000	773	0.1**	97
I. (1990)	11.7	152	-	-	0.3	60 000	773	0.1***	9
I. (1990)	11.7	152	-	-	0.3	60 000	773	0.1****	2
I. (1989)	11.7	143	-	-	4.0	450	773	1	83
I. (1989)	11.7	142	-	-	4.0	450	723	1	83
I. (1989)	11.7	112	-	-	4.0	450	723	1	70
I. (1986)	25	54	-	-	4.0	450	773	4	60
I. (1986)	25	73	-	-	4.0	450	823	4	78
L. & H. (1990)	26	166	-	-	1	1800	773	4	55

* pNO = 0.1%, pCO = 0.1%

** pNO = 0.1%, pH₂ = 0.1%

*** pNO = 0.1%, pCO = 0.1%, pO₂ = 1%

**** pNO = 0.1%, pH₂ = 0.1%, pO₂ = 1%

I. = Iwamoto *et al.*,

L. & H. = Li and Hall

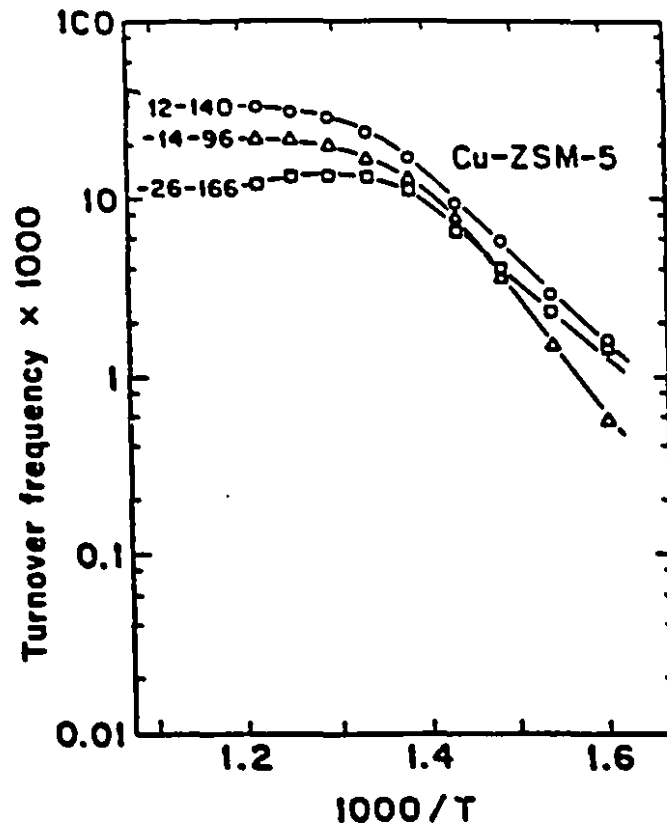


Figure 3.2 Arrhenius plots for NO decomposition over Cu-ZSM-5 (4% NO in helium) (Li and Hall, 1991)

as shown in Figure 3.2, thus the rate law does not give the intrinsic rate. A second problem is that the concentration of NO and O₂ are not given at consistent temperatures or pressures; in order to reproduce the rate data given in the paper, the concentration of the former must be entered as at 25°C while that of the latter must be entered at the actual reaction temperature.

Based on the data provided, a better rate law can be found:

$$r = \frac{k_p NO}{1 + K_p O_2^{1/2}} \quad (3.2)$$

where the pressures, as opposed to concentrations, are given in atmospheres, and k_p in $\text{site}^{-1}\cdot\text{sec}^{-1}\cdot\text{atm}^{-1}$, and K_p in $\text{atm}^{-1/2}$:

T (K)	k_p	K_p
623	0.0389	-
673	0.0781	-
723	0.206	20.449
773	0.310	10.573
823	0.304	6.450

From these new k_p values, the frequency factor and activation energy was found:

$$k_p = 58418 \text{ site}^{-1}\cdot\text{s}^{-1}\cdot\text{atm}^{-1} \times e^{\left(\frac{3756 \text{ cal}\cdot\text{mol}^{-1}\cdot\text{K}^{-1}}{RT}\right)} \quad (3.3)$$

Unfortunately, because the information needed for the full rate law was only presented in the mass transfer control temperature region, if physical set-ups other than that of Li and Hall are used to measure the reaction rate, the rate law can only be used to compare rates found for the direct decomposition of NO in the absence of O₂. The limitations of the rate analysis are unfortunate, as the analysis is the most in-depth one given in the recent literature in this field.

In the same work, Li and Hall also observed data that gave Arrhenius plots (Figure 3.2) with inverted slopes at the higher temperatures for Cu-ZSM-5 and other copper-exchanged zeolites. Such slopes have been observed for other reactions over zeolites, and may be the result of unusually high energies of adsorption and the fact that extra steps are introduced in the reaction process (Bhatia, 1990). The standard

Langmuir-Hinshelwood kinetic model involves five steps: transport of reactants from the bulk phase to the active catalyst sites; adsorption; reaction; desorption of the products; and transport of those products back to the bulk gas. On zeolites, however, the additional steps of transport of the adsorbed reactants within the zeolite crystal to the active sites, and after the reaction, transport of the adsorbed products to the surface occur.

It is because of the high activity for both the direct decomposition of NO decomposition in the presence of O₂, and for the reduction by CO that has been reported, that excessively exchanged Cu-ZSM-5 is proposed here as a candidate catalyst for the reduction of NO by CO in the presence of a moderate excess of O₂ ($\lambda = 1$ to 1.3).

3.2 Redox Properties of Cu-ZSM-5

During the course of the experiments made for the present research, the colour of catalyst was observed to change dramatically, depending on the experimental conditions. A search for similar observations from the literature was made, and one paper was found.

Variations in the colour of Cu-ZSM-5-164 as a function of its redox chemistry were reported by Sárkanáy *et al.* in 1992. Temperature programmed reduction (TPR) by H₂ and CO and temperature programmed desorption (TPD) of H₂ were used to change the oxidation state of the Cu in the samples. Freshly prepared Cu-ZSM-5-164 was light green. The reduction by H₂ at elevated temperatures took place in three discrete stages as the temperature was raised, in the end producing a red/purple sample. Outgassing the sample under Ar turned it white/grey. Reducing again with H₂ returned it to red/purple; oxidation under O₂ turned it brown/tan; and re-reduction turned it red/purple again. The reduction of a fresh sample under CO left it white with red and not red/purple, although further reduction by H₂ did turn it red/purple, suggesting that addition of protons may be needed to cause total reduction. By the various results, Sárkanáy proposed the following redox processes:

With H₂:



With CO:



In Ar:



* The value is 293 K in the paper, but it seems to be an error, based on the figures therein.

From the results in the H₂ TPD experiments the authors were able to make a rough estimate of the Cu distribution of the fresh Cu-ZSM-5-164: [Cu-O-Cu]²⁺ = 35%, CuO = 25%, and Cu²⁺ = 40%. From this distribution, the degree of exchange can be estimated: Counting one Cu in each [Cu-O-Cu]²⁺ ion as *excessive* and one as if it were an *exchanged* Cu²⁺; the Cu in the CuO as *excessive*; and the Cu²⁺ as *exchanged*, and taking the exchange ration as that of all of the Cu atoms present over just the *exchanged* ones, the exchange ratio would be 174% (100% / (½*35% + 40%) = 1.74). The value is close to the actual value of 164% (a relative difference of 6%), so the estimated distribution is reasonable. It may be that the CuO came from neutral Cu(OH)₂⁰ impregnated in the catalyst during the exchange procedure (and not exchanged as such), and the [Cu-O-Cu]²⁺ came from Cu₂(OH)₂²⁺ ions which exchanged onto the ZSM-5; with both complexes loosing water upon drying. Whatever the process, most researchers agree that there is extra-lattice oxygen in the excessively exchanged Cu-ZSM-5.

Chapter 4

Materials and Methods

4.1 Catalyst Material and Gas Supplies

Two batches of ZSM-5 were obtained for use in the experiments. A sample of Cu-ZSM-5 in the form of a fine powder was donated by Allied Signal. Pelletized Na-ZSM-5 was donated by Mobil Corporation on the condition that no characterization analyses would be performed on the material. For use as a control, Degussa Canada donated a finished three-way catalyst (alumina-supported platinum-group metal on a ceramic honeycomb monolith) as ready for insertion into the catalytic converter unit of a small automobile.

The feed gasses used were of high quality, with the exception of the CO and of the NO used in the NO/Ar mix; significant levels of N₂ were found in these sources. Table 4.1 shows the source and grade of the gasses used.

4.2 Pelletization of the Allied Signal Cu-ZSM-5 Powder

For the reaction studies a fixed bed reactor was used, so the catalyst powder had to be put in the form of small pellets or some other small shape. The powder would otherwise be elutriated by the reaction gas or cause a large pressure drop across the reactor bed. Because large pellets tend to have problems of considerable internal heat and mass transfer resistances and cause wall effects such as uneven gas flow (channelling) through the catalyst bed causing significant deviation from ideal

Table 4.1 The Gasses Used for the Feed Supply:

Gas	Grade	Purity	Supplier
He	High	99.995%	Matheson
Ar	Ultra High	99.999%	Matheson
O ₂	Ultra High	99.98%	Liquid Air
CO	Ultra High	99.9%	Liquid Air
4.98% NO in Ar mixed from:			Matheson
NO	C.P.	99.0%	
Ar	Ultra High	99.999%	

plug flow, a pellet size of at most 1/15 of the tube diameter is commonly recommended. Direct pelletization and extrusion were investigated as possible means for the production of small pellets.

4.2.1 Direct Pelletization of the Cu-ZSM-5

Two sizes of plunger and die ($\frac{1}{4}$ and $\frac{1}{8}$ inch diameter) were already available for pressing the pellets; however, previous experience with the dies suggested that abrasive crystals would tend to jam the plungers, especially with the smaller size. A quick test verified the problem, and a new die and plunger set was machined from stainless alloy and then hardened. The larger $\frac{1}{4}$ inch size was made, as that size had jammed less often. A Buehler hydraulic press was used to press the pellets.

The initial results showed the powder to be so abrasive that even the new mechanism jammed easily, so smaller die and plungers were not made. A large number of pellets were pressed using forces of 50 to 3000 lbs (0.222 to 13.5 kN). There was little variation in the product quality; the pellets tended to chip or break into thin layers and powder upon handling. The addition of a small amount of water aided the pelletization procedure and the damp pellets could be handled without breakage, but, when dried, they fell apart as before. Calcination of the dried pellets at 700°C overnight gave no noticeable improvement.

Various binding agents were considered, including organic substances that would have to be burned off before the use of the pellets. These were rejected because the burning process might affect the catalyst material or leave unwanted residues. Instead, montmorillonite clay, often used to bind zeolites pellets for use as cracking catalysts, was chosen. The clay is generally used in amounts of 10 to 30%, but in a cracker and regenerator system the pellets undergo severe mechanical treatment, much more so than would occur in the tube reactor studies; therefore, the montmorillonite (#K-10, 0.85 μm particles) was mixed with the zeolite powder in a 10% mixture. The mix was sieved through a number 155 screen (115 mesh; 125 μm openings) to eliminate any zeolite lumps. Pellets were prepared as before with both dry and damp feed. With the binder, the product was more durable, but not

considerably so. The pellets were about 3/16 of an inch thick and had a density of 1.3 g/cm³.

4.2.2 Pelletization by Extrusion of Cu-ZSM-5 Paste

The pelletization results were very poor, so extrusion of a paste was investigated. A 10% montmorillonite-zeolite mixture was used. After sieving, it was mixed with de-ionized water to form a thick paste which was extruded using a 1 mm die and hydraulic press at pressures of 15 to 1000 psi (0.1 - 6 MPa). The spaghetti-like strands of extruded material were cut into 2 mm lengths and dried at ambient conditions for two hours and then in a drying oven at 115°C for 12 hours. The extruded pellets were found to have superior handling qualities than the pressed ones. Before use, the pellets were heated to 600 - 700°C to drive off any adsorbed gasses or moisture.

4.3 Ion Exchange of ZSM-5 Pellets

The pellets from Mobil were ion-exchanged in using a procedure based on that of Iwamoto *et al.* (1989, 1990). Batches of 15 g of ZSM-5 were washed 3 times in 500 cm³ 1 M NaNO₃ for a total of 10 hours. The pellets were then stirred in 700 cm³ of 12 mM Cu(NO₃)₂, the exchange solution, for 24 hours. This exchange step was repeated twice. At the end of the final exchange dilute NH₃OH was added dropwise to bring the pH up to 7.5. After further stirring, the zeolite was rinsed in deionized distilled water and dried overnight at 115°C. Before and after each exchange step the solution was sampled for measurement of the Cu and Na content by atomic absorption spectroscopy. This procedure is a more thorough version of Iwamoto's exchange method, designed to ensure a very high level of ion exchange.

4.4 Catalyst Characterization

4.4.1 X-Ray Crystallography

Powder X-ray diffraction was used to characterize the bulk composition of the Allied Signal Cu-ZSM-5 powder in its raw form and from experimental samples.

By agreement with Mobil Corp. the ZSM-5 obtained from them was not analyzed. A Rigaku Rotaflex Ru-200 BH system using a rotating anode X-ray generator with a copper target and a standard theta 2-theta diffractometer was used to generate the diffraction pattern. The generator was operated at 50 kV and 150 mA and the scanning rate was 20 steps per minute with a 0.05 degree step size over a 2-theta angle of 5 to 32 or more. The raw Cu-ZSM-5 was supplied as a fine powder and the extrudate samples were crushed by hand directly onto the glass sample plate.

The diffractometer measures the intensity of the x-ray signal as a function of the diffraction angle. Based on the angles giving peak intensity and the strength of the incident ray, a relative intensity *versus* 'd -space' table is generated using the Bragg Equation. The results from any crystal compound are unique to that compound, directly dependent on the crystal spacing within the solid. Major peak d-spacing and relative intensity tables of many compounds are registered with the US Joint Committee on Powder Diffraction Standards (JCPDS). The observed patterns were compared with selected file data from the JCPDS database using standard software.

Besides verifying the presence of specific crystalline compounds, the X-ray diffraction patterns were also used to compare the crystal quality of the samples. A perfect crystal sample will yield a pattern with sharp peaks at precise locations, whereas a somewhat amorphous sample will have very low broad peaks, over a high baseline signal.

4.4.2 Chemical Analysis

Several Cu-ZSM-5 samples were analyzed by the Centre de Recherches Minerales Service du Laboratoire d'analyse du Ministere de l'Energie et des Ressources (Mines) Quebec. The samples were digested in hydrofluoric acid and LiBO_2 (for Si) and analyzed for Al, Cu, Na, and Si using standard atomic absorption techniques.

4.4.3 Surface Area, Porosity, and Pore Volume Distribution Analysis

The surface area of the alumina-based PGM catalyst was measured with a Micromeritics Flowsorb 5200 Surface Area Analyzer using the standard single-point BET method. Such a measurement on the ZSM-5 could not, however, be considered equivalent; the open cage-and-channel structure of the zeolite allows the N_2 access to virtually all of the material of the compound, whereas the surface area, as measured by the BET method, of a regular solid is dependant on the porosity and particle size, as well as chemical composition. In the case of the zeolite the results are often not reproducible because many compounds, including water, remain on the sample at very high temperatures and affect the adsorption of N_2 .

Before the measurement, the 0.1 to 1 gram samples were placed in a sample holder and heated at length at 300°C under the nitrogen/helium mixture of the analyzer exit stream to de-gas any volatile components on the solids. Beginning after several hours, the samples were weighed (under the nitrogen/helium) each hour until a constant weight was achieved. After the final de-gassing period, the sample was moved into the test position and cooled in a liquid N_2 bath. When adsorption of N_2 from the gas stream was complete, the sample was immersed in a water bath at 25°C . The measured amount of N_2 desorbed off of the sample was used to calculate the surface area.

The calculations were based on the assumption of an exact molecular size of N_2 in the adsorbed phase and the blanketing of the samples by a monolayer of N_2 under the measurement conditions. Replicate measurements for each sample were performed, and the agreement was within 2 to 3%, depending on the sample size. The analyzer was calibrated and zeroed before every individual measurement.

The same device was also used to measure the porosity and pore volume distribution of the Degussa catalyst using multi-point analyses. Research grade nitrogen and helium were mixed in various ratios using two Tylan model FC-260 mass flow controllers.

4.5 Wet Chemical Analysis

To monitor the exchange process, the exchange solutions were analyzed for Cu and Na. The samples were diluted with de-ionized or HPLC grade water to levels appropriate for measurement. A Thermo Jarell Ash model Smith-Hieftje 11 spectrometer was used to perform the measurement. Copper and Sodium hollow cathode tubes were used. The spectrometer was calibrated after every five samples. The error associated with the measurements is typically much less than 5%.

4.6 Experimental Setup

A schematic of the experimental system used for the activity measurements is shown in Figure 4.1. The feed gasses were metered and mixed and passed by a pressure gauge and on to the reactor. After passing through a cold trap, the product gas was sampled for analysis.

A more detailed diagram is presented in Figure 4.2. Ports for sampling the gas streams for gas chromatographic analysis were located at the feed component sources and directly upstream and downstream of the reactor, and downstream of the NO₂ trap. The feed gasses were delivered at pressures of 20 psig. Three Tylan FC-260 and mass flow controllers were used to set and measure the flow rates of the NO-Ar mix, O₂, and CO. The mass flow controllers were in turn set by high precision analog controllers, and the flow displayed on a digital readout. The flow rate of the diluent (helium or pure argon) stream was measured by a Tylan model FC-280 mass flow controller, and was set by a Matheson size 1 High Accuracy needle valve. All of the feed streams were also routed through rotameters (Matheson sizes 600 - 604) with HA1 needle valves which could be used in the event of a failure of the Tylan units. The calibration data for the flow devices are located in Appendix A. The NO-Ar mix, the mixed feed gas and the reactor effluent were carried in 316 stainless steel tubing.

The reactor, shown in Figure 4.3, was a 65 cm long 22.5 mm I.D. quartz tube. The catalyst bed was located in the middle of the tube where the temperature

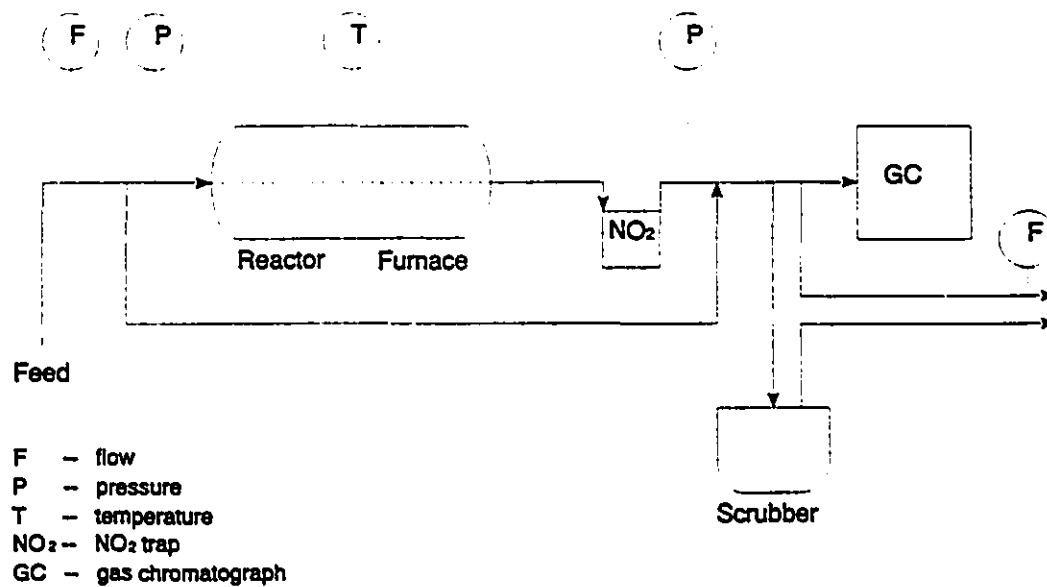


Figure 4.1 Schematic diagram of the experimental setup

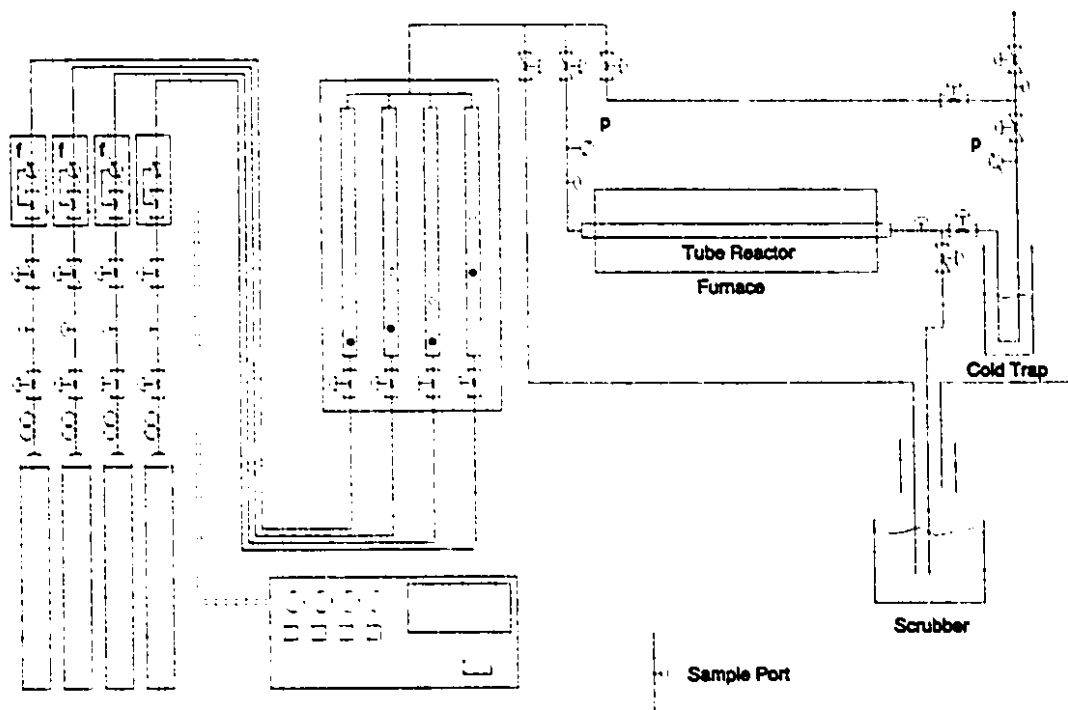


Figure 4.2 Diagram of the gas handling system, showing the mass flow controllers, rotameters, and sample ports

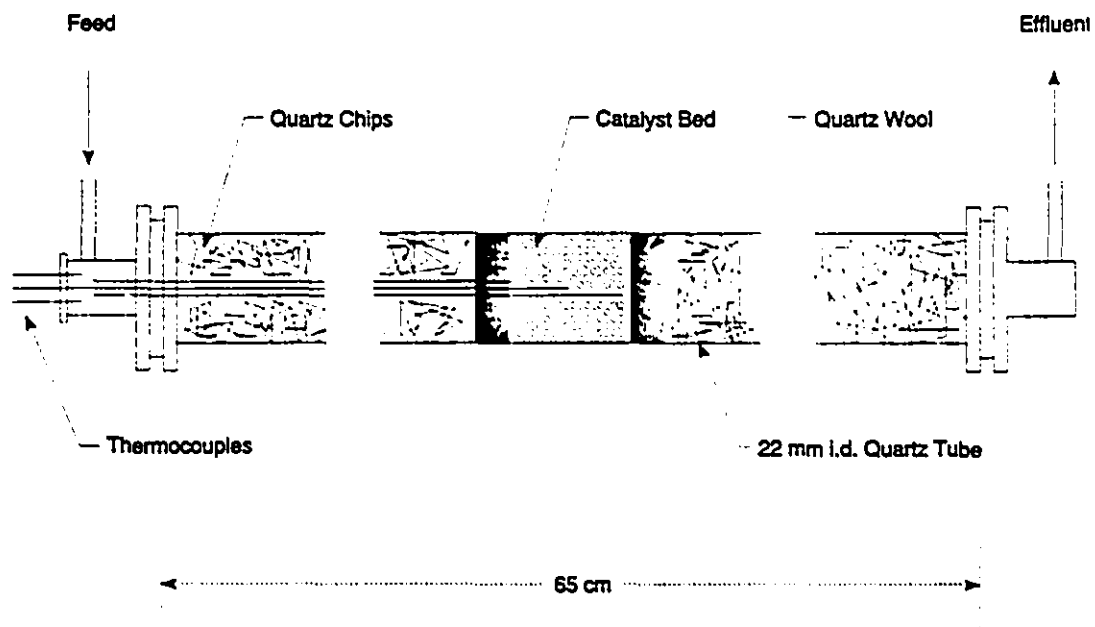


Figure 4.3 The tube reactor with the catalyst bed

was kept uniform by a Lindberg model 1500 "Heavi-Duty" tubular furnace. Upstream of the catalyst bed the tube was filled with small quartz chips to improve mixing and pre-heating of the reactant gas as well as to lower the void volume of the reactor. The catalyst bed was held in place by plugs of quartz wool. A flange and gasket connection was used to fasten the reactor to stainless steel end-caps. The total volume of the reactor, end-caps, and tubing between the feed and exit sample ports, excluding the volume of the chips, wool, and catalyst pellets, was approximately 375 cm³.

The temperature of the catalyst bed was measured by three chromel-alumel type K thermocouples supplied by Thermo Electric Corp. An Omega model 650 digital temperature gauge was used to continuously display the temperature of the thermocouples. To check the temperature profile of the catalyst bed, the thermocouples were positioned near the centre-line at the beginning, in the middle, and at the end of the bed.

When not being measured, the product gasses were diverted through a scrubber containing 20% NaOH. The off-gasses were then exhausted through a fume hood to the outside air. Prior to sampling, the product gasses were diverted through a u-tube immersed in a dry ice slurry to trap any NO₂ that may have formed. The product gasses then passed by the product sample port and the exit flow was measured with a bubble flow meter. All stages of the gas handling system upstream of the product sample port were either stainless steel or were shielded to ensure that no external light could enter the system and promote the oxidation of NO by O₂.

4.7 Description of a Typical Experimental Run

The catalyst was prepared, by ion exchange in the case of the pellets from Mobil, or by extrusion in the case of the Cu-ZSM-5 powder from Allied Signal, as described above. A fresh plug of quartz wool was inserted in the reactor and packed flat. The catalyst sample was loaded and a second plug of quartz was added. The conditioning gas (either dry air, a mix of carbon monoxide in helium, or pure

helium) flow rate was fixed and the furnace set at the conditioning temperature. When the conditioning was complete the temperature was reset to the experimental level. As the temperature stabilized, the feed gas mixture was set by the mass flow controllers and/or needle valves. With the addition of each component the total flow rate was verified by bubble flowmeter.

Prior to the gas analyses, the dry ice in the GC cold bath was refreshed and the GC columns conditioned with a few preliminary feed injections. Once the reactor temperature stabilized, a feed or product stream sample was taken every ½ hour, the length of time needed for each GC analysis. When the temperature was constant and the product analyses yielded integrated peak areas consistent within 5%, steady state was indicated. After the steady state measurements were taken a new target temperature was selected and the furnace adjusted. Although it could be measured accurately by the thermocouples, the final stabilized temperature of the reactor could be only loosely predicted when adjusting the furnace setting.

At the end of an experimental run, the flow rates were verified again and only the diluent flow was left on. The furnace was shut off, and the reactor let to cool to room temperature before the catalyst was removed for analysis. In some cases the catalyst pellets were removed individually using a suction device, so that pellets from different locations within the bed could be analyzed.

4.8 Data Evaluation

At steady state the rate of production of species *i* is given by

$$r_i = F_i^p - F_i^f \quad (4.1)$$

where F_i^f and F_i^p are the molar flow rates of *i* in the feed and product streams. The rate of production of species *i*, per unit of mass of catalyst is given by

$$r_{im} = \frac{(F_i^p - F_i^f)}{m} \quad (4.2)$$

where *m* is the mass of the catalyst. The rates per unit volume (r_{iv}) and per unit surface area (r_{is}) of the catalyst can be defined likewise. The turnover frequency

(TOF), is defined as the rate of reaction of NO to form N (i.e. $\frac{1}{2}N_2$), per mole of active metal (Cu) in the catalyst bed

$$TOF = \frac{2 (F_{N_2}^p - F_{N_2}^f)}{n_a} \quad (4.3)$$

where n_a is the total number of moles of active metal. The factor 2 in the numerator reflects the conversion of two NO molecules to form one N_2 . The TOF is commonly used for activity and kinetic measurements when it is likely that the amount of active metal ingredient present is a more important indicator of activity than the surface area of the catalyst or total mass of the catalyst. This is often the case for ion exchanged zeolites where different exchange levels and different Si/Al ratios directly vary the amount of exchanged metal.

From the rates of production of each species, the yield can be calculated:

$$Y_{N_2} = \frac{2 r_{N_2}}{r_{NO}} \quad (4.4)$$

$$Y_{NO_2} = \frac{r_{NO_2}}{r_{NO}} \quad (4.5)$$

For the purposes of this work, x_{NO} is defined as the total steady state conversion of NO and x_{N_2} as the steady state conversion of NO to N_2 :

$$x_{NO} = \frac{F_{NO}^f - F_{NO}^p}{F_{NO}^f} \quad (4.6)$$

$$x_{N_2} = x_{NO} * Y_{N_2} \quad (4.7)$$

$$\therefore x_{N_2} = \frac{2 (F_{N_2}^p - F_{N_2}^f)}{F_{NO}^f} \quad (4.8)$$

From the mass flow controller data and the volumetric flow data the molar flow rate of each feed component was known and the flow rate of each component relative to that of argon calculated. From the GC analyses of the feed gas these relative rates were verified for those species which could be measured quantitatively (Chapter 5).

Since Ar is inert, its molar flow rate in the feed and product streams was the same. The molar flow rate of each element was, of course, also conserved. From the analysis of the product stream, sampled after the removal of the NO_2 , the rate of production of N_2 and CO_2 was easily calculated. When NO could be measured quantitatively, the conversion of NO was determined and, from the elemental balance, the net rate of production of the other oxides of nitrogen (as NO_2) could also be calculated.

In theory, the mass balances could be closed by converting the calculated product stream flow rate to a volumetric figure and comparing it to the measured flow rate. In practice, however, even in the case of high conversions of NO and CO, the change in overall flow rate was very small at only a few per cent since the inert components of the mixture (argon and helium) made up 83 to 93% of the flow.

Several problems were encountered in the course of formalizing the GC analysis. In particular, difficulties in measuring the N_2 , O_2 , and NO levels in the sampled gas hampered the work. Because of these difficulties, further discussion of the data interpretation will be presented after the discussion of the GC analysis in Chapter 5.

4.9 Reactor Flow Characterization

In order to determine the deviation of the gas flow through the reactor from the ideal plug flow model, the residence time distribution of the reactor was measured. A steady flow of helium was replaced by a step change to argon and the response measured at the product sample port. The reactor was packed with the heating chips, quartz wool plugs, and 7.5 grams of low surface area pellets and heated to 500°C . The flow rate was set at $95 \text{ cm}^3/\text{min}$ (at 25°C) of helium which

was replaced with argon at time zero. Samples of the exit gas were taken every 40 seconds and analyzed by GC until the argon level stabilized.

Chapter 5

Gas Analysis

A significant amount of the work in this research project involved the selection and development of the analytical tools used to determine the compositions of reaction gas mixtures. Several gas chromatograph columns and programs were tested for use, and the method presented inherent difficulties which had to be overcome. The most important of these difficulties were the inability to accurately measure the NO and O₂ levels within gas samples, and the persistence of N₂ contamination in the samples. In this chapter an over-view of the gas analysis is given, the difficulties encountered are discussed, and the equations for the calculation of x_{NO} and x_{N_2} are developed.

5.1 Introduction

In the work reviewed for the gas analysis (Appendix D) the use of mass spectroscopy, chemiluminescence spectroscopy, and, for O₂ analysis, paramagnetic susceptibility revealed clear advantages over GC; however, none of these techniques were available for the present investigation. Wet chemical methods were ruled out on the basis of reliability and time.

After extensive testing, a GC configuration that could separate and measure CO, CO₂, N₂, and Ar quantitatively and O₂ and NO qualitatively was found. NO₂ in the effluent stream was trapped out prior to the product gas sampling during all experiments, and was not measured. Had O₂, NO, or NO₂ been quantitatively

measured, enough information would have been available to completely characterise the gas streams. Fortunately, for the purposes of this investigation, only the extent of the conversion of NO to N (i.e. $\frac{1}{2}N_2$) and of CO to CO_2 were of primary importance, and these extents could be determined accurately.

5.2 The NO_2 Trap

Because the GC with the thermal conductivity detector (TCD) and potentially useful columns was available and in the lab, it was obvious that the research should begin with this tool. Ideally, chemiluminescence spectroscopy and paramagnetic susceptibility, which would have measured the NO_x and O_2 , would have been employed in tandem with the GC; however, the GC had to take the burden of the entire analysis, and that presented a difficulty because of the NO_2 .

As expected, when the final GC method was determined, the NO_2 could not be measured and therefore had to be trapped out. The NO_2 was condensed (m.p. $-9^\circ C$, b.p. $21.2^\circ C$) in a cold trap upstream of the product sample port. The procedure used by Li and Hall (1990, 1991), that of transferring trap with the condensed NO_2 (N_2O_4) to a vacuum system, to measure the NO_2 production was not employed. This would have been time consuming due to the low gas flow rates (and hence, low formation rate of NO_2) and to the necessity of extra safety precautions and, more importantly, the results would have been in doubt. A marked oxidation and crud build-up was noted in the stainless steel reactor end-cap downstream of the reactor. Since this was not the case upstream, it had to have been due to the formation and reaction of a corrosive component not present in the feed stream. Most likely this product was NO_2 . Because of these reactions, the NO_2 collected in the cold trap would not have given a complete measure of the NO_2 produced.

5.3 The Analysis by Gas Chromatography

5.3.1 Description of the Sampling System and Analysis Hardware

Shown in Figure 4.2, the gas handling system was equipped with three sampling ports about the reactor, and at the gas supply cylinders. During the experiments the reactor feed was sampled directly upstream of the reactor. The effluent was sampled either directly at the exit of the reactor or after the gas passed through the dry ice slurry cold trap to remove any NO_2 formed. The sample ports were $\frac{1}{4}$ inch (6.35 mm) Swagelock "T" joints with a standard $\frac{1}{4}$ inch GC septum fastened in one of the connection openings. The sampling syringes were gastight Hamilton 1800 series (10 and 100 μL) or gastight Precision Sampling Corporation "Pressure Lock" series (500 and 1000 μL). The GC was a Hewlett Packard model 5890 with a TCD operating at high sensitivity. To obtain optimal sensitivity/separation the reference gas flow rate was set at 30 cm^3/min and the carrier gas at 20 cm^3/min . The injection port was not directly heated and generally equilibrated to 45°C. As shown in Figure 5.1, the GC was fitted with an actuated Valco four port bypass valve to allow for programmed bypass of the second of the two columns. During use, the second column was extended from the GC with lengths of 1/16 inch (1.59 mm) o.d stainless steel tubing and immersed in a dry ice/acetone slurry. Both columns were standard $\frac{1}{8}$ inch (3.18 mm) o.d. stainless steel with 80/100 mesh packings. The primary column was 8 feet long, with Porapak Q packing and was maintained at 30°C, while the secondary column was 12 feet of Porapak QS which was immersed continuously in the slurry at -79°C.

During a run, the bypass valve was activated after all of the gasses except CO_2 (N_2 , O_2 , Ar, CO and NO) had passed through the first column. The CO_2 eluted and passed directly to the detector, after which the bypass valve was returned to the off position and the N_2 , O_2 , Ar, CO and NO came off of the second column and were measured. Sample chromatograms are shown in Figures 5.2 and 5.3; the calibration factors are given in Appendix B. The selection of the columns, and the determination of the column temperatures and the program timing are presented in Appendix E.

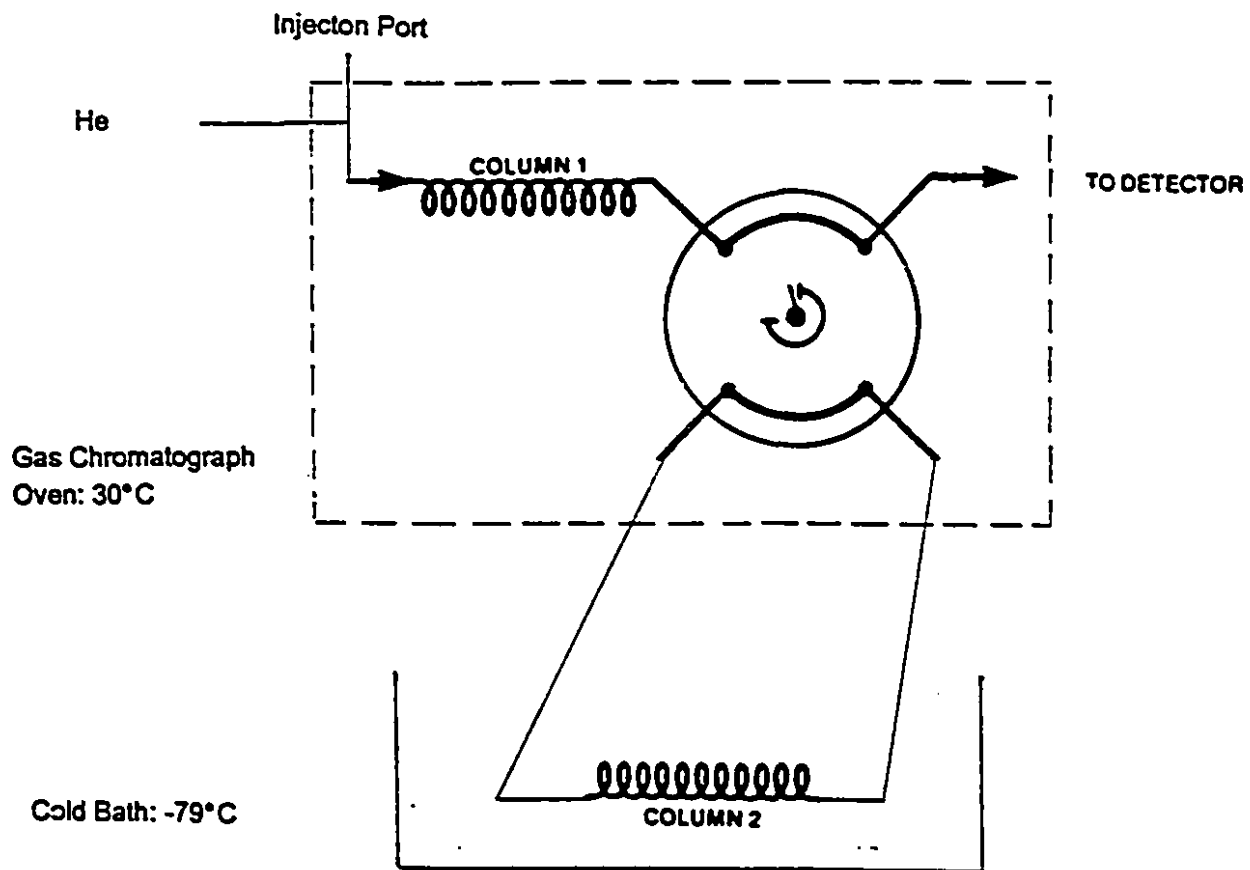


Figure 5.1 The gas chromatograph with the bypass valve activated

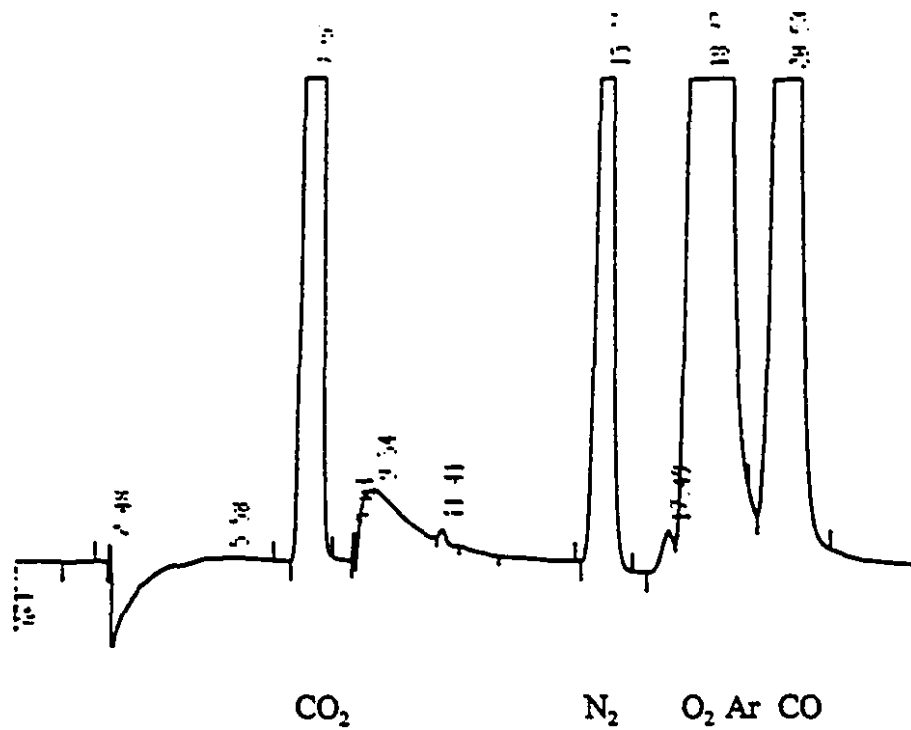


Figure 5.2 A typical chromatogram showing the CO₂, N₂, O₂, Ar, and CO peaks. A chromatogram with an NO peak is shown in Figure 5.3

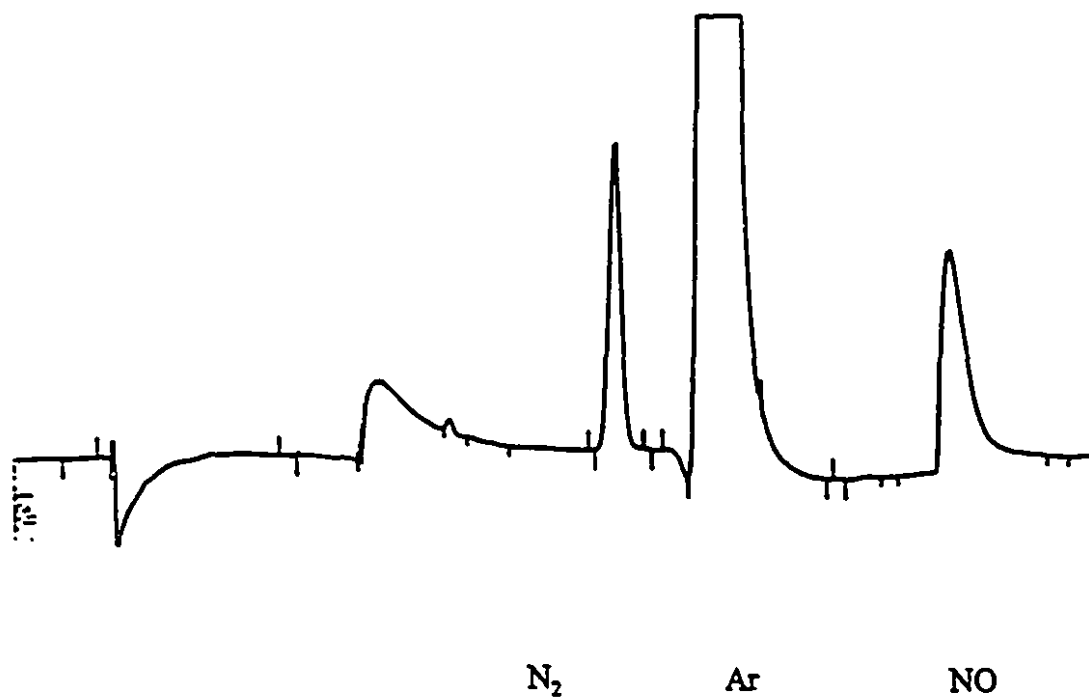


Figure 5.3 Typical chromatogram of a mixture of N_2 , Ar, and NO

5.3.2 GC Preparation and Gas Sampling Procedure

Before each experiment, the injector septa were replaced and the columns were cleaned with a thermal cycle. The columns were then primed with three NO containing feed gas injections. Periodically, the dry ice in the slurry was refreshed or stirred to maintain the proper cooling of the second column, which tended to get warmer if the slurry was not stirred. To minimize the amount of N₂ (or air) co-injected with each sample, a few precautions were taken from the outset of the research. The syringe was flushed three or more times with the gas to be sampled before each injection and a large amount of sample (eg. 100 μl) was taken into the syringe, allowed to equilibrate for several seconds, and purged down to the appropriate level (usually 80 μl) before removing the syringe from the sampled stream. By this means the contents of the syringe were at the same or greater pressure than ambient when the needle was removed from the gas stream. The plungers of all syringes used were replaced on a regular basis. These precautions ensured that little or no air was accidentally brought into the system as a part of the bulk sample. The remaining cause for the contamination was air diffusing into the syringe needle during transport to the GC, or adsorbing on the needle surface and desorbing in the pure helium carrier gas of the GC. To minimize any diffusion, the time from sampling to injection was kept to a minimum and was relatively constant at less than two seconds.

To prevent light from catalyzing the oxidation of NO by O₂ in the glass syringe, the syringe barrel was covered so that no light could enter the sample chamber. The volume of the sample was determined using an external scale to measure the extension of the plunger handle. Because all of the results were normalized against the internal standard, Ar, the size of each experimental sample did not have to be the same; nonetheless, in most experiments, the injections were generally kept to within less than a 1% variation in volume (as calculated from the Ar peak size).

5.3.3 Description of the GC Analysis, by Component, in Order of Measurement

- CO₂: Last gas off of the Porapak Q column, it was measured directly at about 7 minutes. The peak was isolated, gave a linear response by sample size, and was reproducible.
- N₂: It gave a linear response and was sharp, isolated, and reproducible. An ever-present problem was the existence of N₂ from the ambient air being introduced with the sample and measured. The retention time of N₂ on the primary column was about 2.5 minutes. The total retention time was about 15 minutes, depending on the exact temperature of the QS column in the dry ice slurry. The analysis of the N₂ will be discussed further in Section 5.4.3.
- O₂: By itself, oxygen gave a linear and reproducible response. Contamination from air was less of a problem than with N₂, as was expected, since the ambient concentration is ¼ that of N₂. The retention time was about 16 minutes. The peak was situated very close to the Ar peak, which if large tended to be preceded by a slight decrease in the detector response. Comparison of the chromatograms in Figures 5.2 and 5.3, with O₂ and without O₂, respectively, in which this signal depression can clearly be seen. As a result of the depression, smaller amounts of O₂ tended to be under-measured in the presence of Ar. Large O₂ peaks had the tendency to merge with and run up the leading edge of the Ar peak, with a less predictable effect. When NO was present, the O₂ also reacted with it in some stage of the analytical system so the measured amount was even less indicative of the original sample O₂ concentration.
- Ar: The retention time was about 17 minutes. In the majority of the experiments the Ar was, by far, in the highest concentration (typically 38%), with the exception of helium which could not be measured directly. Being of much larger size, its measurement was little affected by interference from the O₂ peak. When the Ar peak was larger than in the usual case, *i.e.* from a sample with larger than the 38% Ar in a typical 80 µL injection, it met the

conditions determined by the integrator for it to be measured as a solvent peak. In this case the CO peak, if present, was measured as if riding over the tail of the Ar peak, as estimated by the integrator. For most of the work, however, the peak was of the typical size or less and ended at the valley point before the start of the CO peak.

- CO: The CO peak came at about 19 minutes, was sharp, was reproducible, and gave a linear response.
- NO: The retention time was about 24 minutes. The peak was low, broad, and often tailed badly. Though the porous polymers were thought to mitigate these occurrences (as compared with the Molecular Sieves), severe and unreproducible tailing as well as reactions involving O₂ sometimes occurred. The TCD signal response was significantly less than for the other gasses, and a non-linear area to mole response was found. When O₂ was present in the sampled stream, the procedure failed to quantitatively measure the NO content of the sample because of the reaction of NO with O₂, or the disproportionation of NO in the presence of O₂, in the syringe or the GC itself.

5.4 Interpretation of the GC Area Results: Calculation of the Composition of the Gas Streams and Conversions

The experimental feed gas mixture contained either argon alone or helium with argon as the inert diluent. Since the carrier gas used in the GC was helium, the argon could be used as an internal standard. Variation in the size of individual injections as well as differences in the molar flow rates of individual components in the product streams and the total molar flow rate were compensated for by comparing all of the measured gas amounts to the measured Ar. The molar flow rate differences were caused by both reactions of individual components as well as the trapping of the NO₂. Because these differences resulted in a change in the total molar flow rate, they also resulted in a change of the concentrations of the other components. After measuring the amounts (in moles) of each gas in a sample and

accounting for any N₂ contamination, these amounts were all divided by the amount of Ar in the sample. Since Ar is inert, the results were normalized and made the direct comparison of samples of different sizes, different streams, (feed, product, and reactor exit) and different experiments possible.

The peak areas generated by the integration of the TCD signal were converted into the measured quantities, expressed in moles, m_i^s for gas i sampled from stream s , using the GC calibration factors. However, the *measured amounts* for N₂, O₂, and NO were not the same as the *actual sampled amounts* in the syringe, n_i^s , because of the complications in the analysis of these gasses, as will be discussed in following sections. For the other gasses, the relative molar flow rates and component mole fractions in each stream are compared easily, since, in general:

$$\frac{F_i^s}{F_{Ar}^s} = \frac{y_i^s}{y_{Ar}^s} = \frac{n_i^s}{n_{Ar}^s} \quad (5.1)$$

(for all i)

Because it is inert, F_{Ar} is the same for all streams. Also:

$$m_i^s = n_i^s \quad (i \neq N_2, O_2, NO) \quad (5.2)$$

For example, by combining Equations 5.1, and 5.2, the conversion of CO is obtained from the measured amounts of CO:

$$x_{CO} = \frac{F_{CO}^f - F_{CO}^p}{F_{CO}^f} \quad (5.3)$$

$$\therefore x_{CO} = 1 - \frac{\frac{m_{CO}^p}{m_{Ar}^p}}{\frac{m_{CO}^f}{m_{Ar}^f}} \quad (5.4)$$

Due to complications, the calculations were not as simple for N_2 , O_2 or NO. The difficulties involved in the NO analysis were the reaction of NO with O_2 in the syringe or GC, the excessive tailing of the NO peak, the low detector response to NO, and a tendency for the NO to permanently adsorb on the column, especially during the early parts of an experiment. With the O_2 analysis, there was the reaction with NO and the interference from the Ar peak, and with the N_2 analysis the problems of large feed impurities and co-injection of ambient N_2 into the GC along with the gas samples existed. The analysis and calculations for these gasses are taken up in the next three sections.

5.4.1 The Analysis of NO and Calculation of x_{NO}

The poor quality of the NO peak made the calibration of the GC and the subsequent analysis of samples for NO difficult. A quadratic fit of the NO *versus* TCD area response was made in the absence of O_2 ; the calibration results are presented in Appendix B. As noted above, a consistent pattern of column loading emerged. When acquiring data at a given injection size, successive samples tended to yield a higher response signal from the TCD, probably due to adsorption of NO on the GC column. After several injections, the column became saturated, or "loaded," with NO, and the measured values tended to become closer together, with a final value being reached asymptotically after more injections. When the results agreed to within a few percent the value was deemed to be final and the point was used as a datum on the calibration curve (Appendix B). Countering the loading effect was a tendency for the peak to tail excessively, forming flatter smaller peaks that were integrated more erratically after a number of injections. These competing history effects lead to increases and decreases in the TCD response at different times. Thermally cleaning the column after each sample failed to give more reproducible results and would have been impractical. Pre-conditioning the column with NO before each experiment was tested in order to lessen the loading effect but, predictably, it exacerbated the flattening/tailing effect. In the end a compromise was

achieved: At the beginning of each experiment a series of three feed injections was made to prime the packing prior to making any product analyses.

The problem of NO reacting in the presence of O₂ in the analytical process is suggested by the experimental results shown in Figure 5.4. A series of feed and product injections from a low temperature experiment where the feed mixture contained 2% NO, 4% O₂, and 10% CO are compared. The measured quantities of the three gasses are shown relative to the measured quantity of Ar from each sample. The plot shows that the feed O₂ was not being measured in full, and that the feed NO, as measured directly by the chromatogram NO peak, was actually *less* than the product NO. The product samples had almost no O₂ because of the oxidation of CO by O₂ taking place in the reactor. From the NO measured in the product samples, where there is no O₂, it is clear that little conversion of NO had taken place. In contrast, the feed samples show both a loss of O₂ and a loss of NO, indicating that the oxidation of NO was taking place in the GC system. It can also be seen that much of the NO survived its passage through the gas handling system and the reactor, even in the presence of the O₂, and it was being measured in the product stream, where little O₂ was present. Therefore when the feed stream was sampled the NO - O₂ reaction must have taken place in the sampling syringe or at an early stage in the GC before significant separation of the gasses had taken place. No indication of NO₂ appeared on the feed chromatograms because any that formed would have been trapped on the column at -79°C, since its boiling point is about 30°C.

Because of the reaction between NO and O₂, the NO content in a sample could not be measured quantitatively by GC, in presence of O₂. However, in the experiments where helium was used as the diluent, an exact measure of the feed concentration of NO could be calculated from the Ar measurement since the NO was supplied as a mixture of 4.98% NO in Ar:

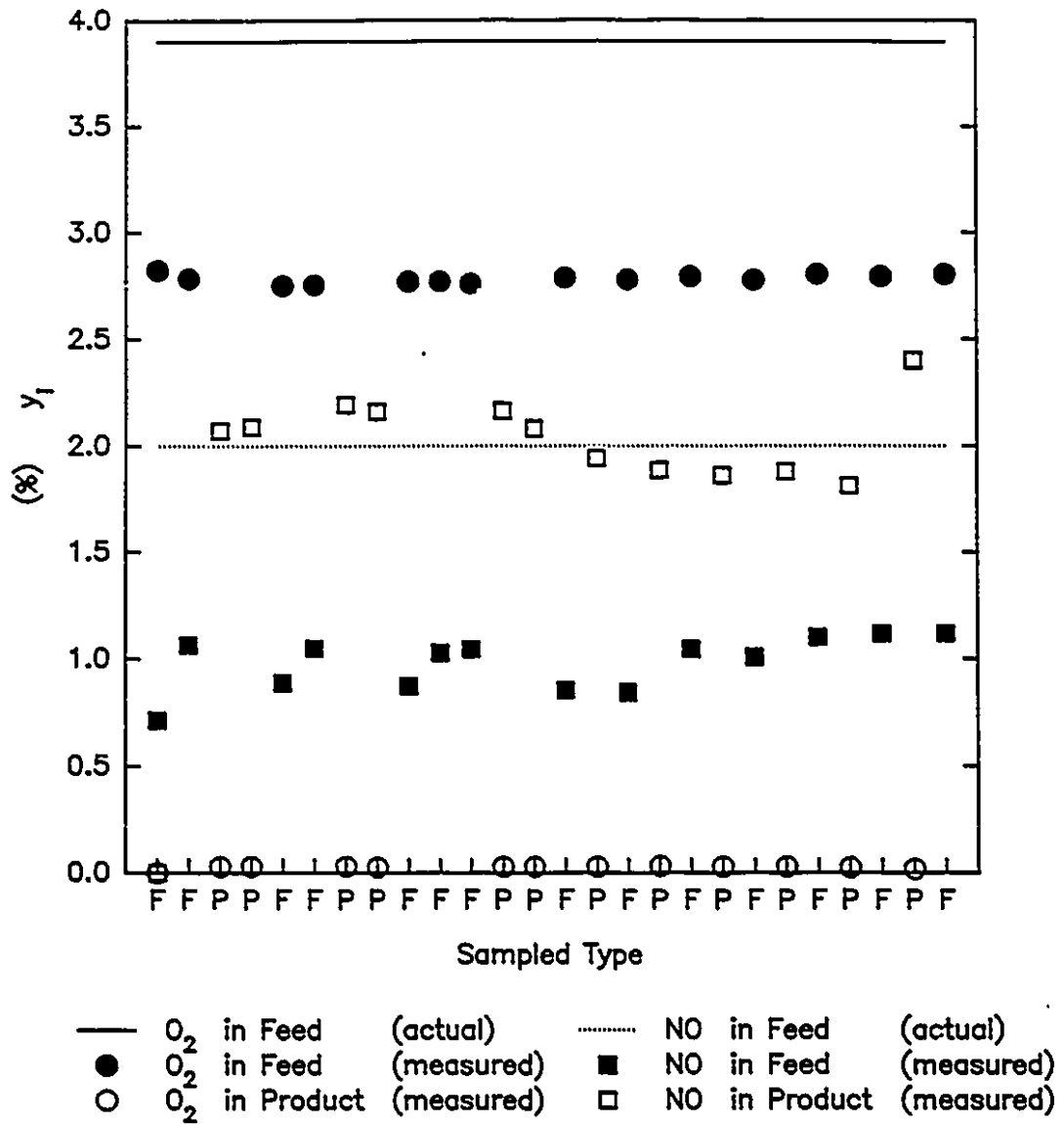


Figure 5.4 Measured and Actual NO and O_2 in one experiment, product normalized by Ar ($y_i^P \cdot y_{Ar}^f / y_{Ar}^P$) (10% CO, 2% NO, 4% O_2)

$$\frac{y_{NO}^f}{y_{Ar}^f} = \frac{0.0498}{0.9502} \quad (5.5)$$

Therefore, by Equations 5.1 and 5.2,

$$n_{NO}^f = 0.0524 * m_{Ar}^f \quad (5.6)$$

In those experiments where Ar was used as the only diluent, the additional Ar had to be accounted based on the measured flow rates of both the NO/Ar and pure Ar streams.

Under the specific conditions of low levels of O₂ in the feed and a low production of O₂ from NO decomposition, an accurate measurement of the NO in the product stream could be made. Experiments measuring the progress of the NO reduction by CO in net reducing conditions fit these criteria. In these cases, the NO area results were converted to mole amounts based on the calibration curve and these mole amounts, while themselves inaccurate, could be used for accurate relative comparison. Based on this conversion, the calculation of the NO conversion, x_{NO}, is developed in Appendix G:

$$F_{NO}^p = \frac{m_{NO}^p}{m_{Ar}^p} * \left(\frac{m_{NO}^f}{m_{Ar}^p} \right)^{-1} * 0.0524 * F_{Ar} \quad (5.7)$$

5.4.2 The O₂ Analysis

There were many problems with the measurement of the sample O₂ content, so only a simple analysis was made and the data obtained were used qualitatively. As has been mentioned, the proximity of the O₂ peak to the leading edge of the Ar peak, the sometimes incomplete separation of these gasses, the depression of the TCD response immediately preceding the Ar peak (*c.f.* Figures 5.2 and 5.3), and the propensity of the NO and O₂ to react in the analysis system all reduced the accuracy of the O₂ measurement. As with N₂, co-injected O₂ was found in the samples, but it was a considerably lower amount, and under the circumstances, not worth

accounting for. In the few experiments where neither Ar nor NO were present, the O₂ measurements were found to be quantitative. In all cases, the peak area found was converted directly to a mole amount using the linear calibration function.

A solution to these problems would have been to have an O₂ analyzer. Alternatively, adding a second bypass valve to allow for the insertion of the short molecular sieve column (also at -79°C) for the O₂-Ar-CO separation would have taken care of the poor O₂-Ar resolution. The CO would be included because of its proximity to the Ar peak. The NO would bypass the MS5A, thus avoiding the tailing and reactions problem associated with its use for separations of NO.

5.4.3 The N₂ Analysis and Calculation of x_{N₂}

The calibration of the GC for N₂ gave an excellent linear response and was very reproducible over the lifetime of the project; however a problem with the analysis existed in all cases. It was brought to light when, in samples expected to contain little or no N₂, higher than expected results were observed. Clearly, N₂ was contaminating the system, and most likely it was from at least one of three possible sources: It entered the gas handling system at the exit and diffused upstream to the sample ports; it was an extraordinarily large impurity in one or more of the feed gas streams; or it was brought into the process with the sampling or injection procedure. A fourth possibility was that the N₂ was formed by the reaction of NO in some upper part of the gas handling system.

As shown in Appendix G, the N₂ came from both feed impurities and co-injection of ambient N₂ with the gas samples, and both sources had to be accounted in calculating the conversion of NO to N₂, x_{N₂}:

$$x_{N_2} = \left(\frac{m_{N_2}^p - \bar{k}_{N_2}^f}{m_{Ar}^p} - \frac{m_{CO}^f * r_{N_2}^{CO} + m_{Ar}^f * r_{N_2}^{Ar}}{m_{Ar}^f} \right) * 19.02 \quad (5.8)$$

where $\bar{k}_{N_2}^f$ is the average amount of co-injected N₂ in the feed samples and

$\frac{I_{N_2}}{I_i}$ is the ratio of N_2 to gas i in the supply cylinder for gas i . The values of $K_{N_2}^i$ and $\frac{I_{N_2}}{I_i}$ can be determined from the calibration data and experimental results as shown in Appendix G.

Chapter 6

Results and Discussion

This chapter is divided into five sections. The first section discusses the results of the preliminary experimentation, including tests to see if the Cu-ZSM-5 samples were active for the direct decomposition of NO as reported in the literature. The second section presents the results of the experiments measuring the activity of the catalyst for the reduction of NO by CO, in the ratio typical of slightly oxidizing exhaust gas, in the presence of varying amounts of O₂. A comparison of the activity of the fresh Cu-ZSM-5 to that of a standard platinum-group metal three-way catalyst is made, and an analysis of the results obtained with used Cu-ZSM-5 samples is given. For both the preliminary decomposition experiments and the reduction experiments, the activity is defined as x_{N_2} , the overall conversion of NO to N (*i.e.* ½N₂). In the third section the conversion of CO in mixtures with and without O₂ or NO is presented and analyzed. The fourth and fifth sections present the results of characterization studies of virgin and used Cu-ZSM-5, and a review of the colours of the Cu-ZSM-5 observed during the experimentation is given, with a comparison of observations from the literature.

6.1 Preliminary Experiments

6.1.1 Characterization of the Reactor

The gas flow in the reactor at 500°C was characterized by measuring the residence time distribution using the method described in Section 4.9. The space

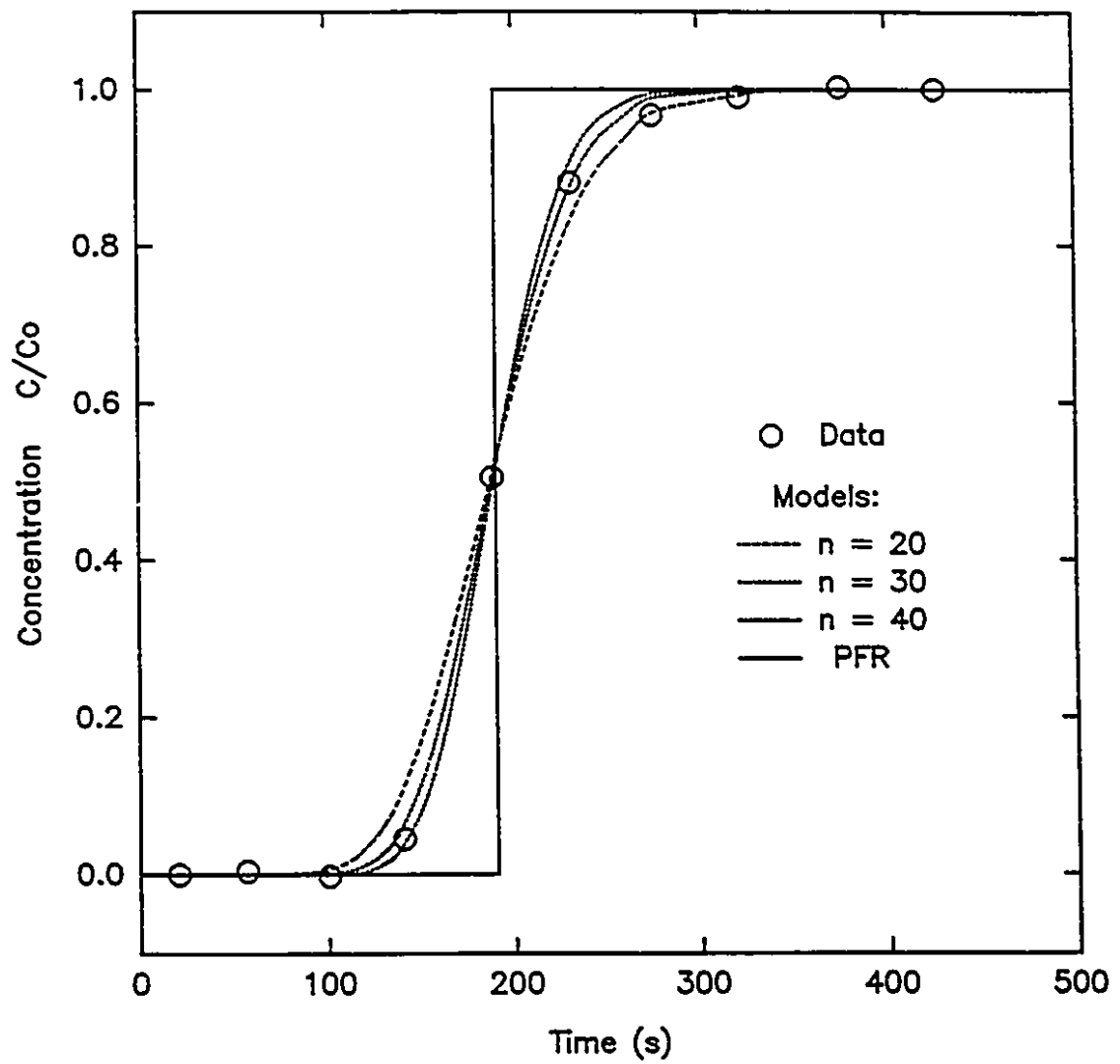


Figure 6.1 Residence Time Distribution: Concentration of Argon in Reactor Effluent after a Step Input Change, and Model Results

time calculated for the reactor volume of 247 cm³ plus the tubing and end-caps volume of 127 cm³ is 234 seconds at 25°C. A plot of the ratio of the argon exit concentration C and the inlet concentration C₀ over time is shown in Figure 6.1. Also shown are the C/C₀ ratios for the series-of-stirred-tanks models that best fit the data. For these models it is supposed that the flow passes through n ideal stirred tanks of equal size and a fixed total volume. A low number of tanks represents a high degree of back-mixing; a high number of tanks represents a low degree of back-mixing. The response for an ideal plug flow reactor (PFR) can be modeled by an infinite number of tanks having the same total volume as the PFR. The C/C₀ response for the series of tanks is given by:

$$\frac{C}{C_0} = 1 - e^{-n \frac{\theta}{\bar{\theta}}} * \sum_0^{n-1} \frac{1}{m!} (n \frac{\theta}{\bar{\theta}})^m \quad (6.1)$$

where n is the number of tanks and $\theta/\bar{\theta}$ is the ratio of the time over the average residence time.

The model fits the data well when a mean residence time of 190 seconds and a total of 30 stirred tanks is used. When compared to the calculated residence time of 234 seconds (at 25°C), the model residence time is reasonable: The higher temperature in the part of the reactor that is heated (to 773 K from 298 K) and the volume taken by the quartz materials and the catalyst bed all serve to reduce the actual mean residence time. The high number of stirred tanks indicates that the flow of the system as a whole behaves much closer to that of an ideal PFR than a highly mixed reactor.

6.1.2 Determination of Homogeneous Reaction Products

To determine if there were any homogeneous reaction products the rate of decomposition of 2% NO and reduction of 2% NO by 10% CO were measured. The reactor was loaded with quartz chips and quartz wool but no catalyst was used. The rate was measured at temperatures up to 550°C; and the feed rate was

60 cm³/min (25°C). No change in the gas composition nor reaction products were observed.

Under similar conditions the rate of reaction between 4% O₂ and 10% CO (in helium) was also measured. Figure 6.2 shows the oxidation of CO at steady state for various temperatures at a feed rate of 95 cm³/min. The reaction is significant but does not go to completion below 600°C.

The homogeneous oxidation of NO by O₂ could not be measured directly because NO reacted with O₂ in the analytical train. However, evidence presented in the discussion of the GC analysis of NO and O₂ in Chapter 4 shows that little or no reaction between the two gasses was taking place in the feed lines or reactor. This is consistent with the results of others who determined that there was no high temperature reaction of NO with O₂ in similar experiments (Li and Hall, 1990). Because precautions were taken to shield the apparatus from external radiation, the low temperature homogenous oxidation was kept to a minimum at all stages of the system.

A check to see if any of the components in the product stream (N₂, O₂, CO, NO and CO₂) reacted with condensed NO₂ (N₂O₄) in the cold trap was made. Product gas was sampled immediately before and after the cold trap, and the GC analysis revealed no difference.

6.1.3 Preliminary Experiments for Catalytic Activity

The ZSM-5 from Mobil was tested for its activity in NO decomposition and NO reduction by CO. The pellets were exchanged according to the procedure described in Section 4.2. The product (Cu-ZSM-5-M) was light blue after the exchange, and became light green after the activation under helium at 600°C for 12 hours.

The Cu-ZSM-5 from Allied Signal (Cu-ZSM-5-AS) was mixed with montmorillonite binding agent, extruded, and pelletized according to the procedure described in Section 4.1.2. The activities for NO reduction and decomposition were

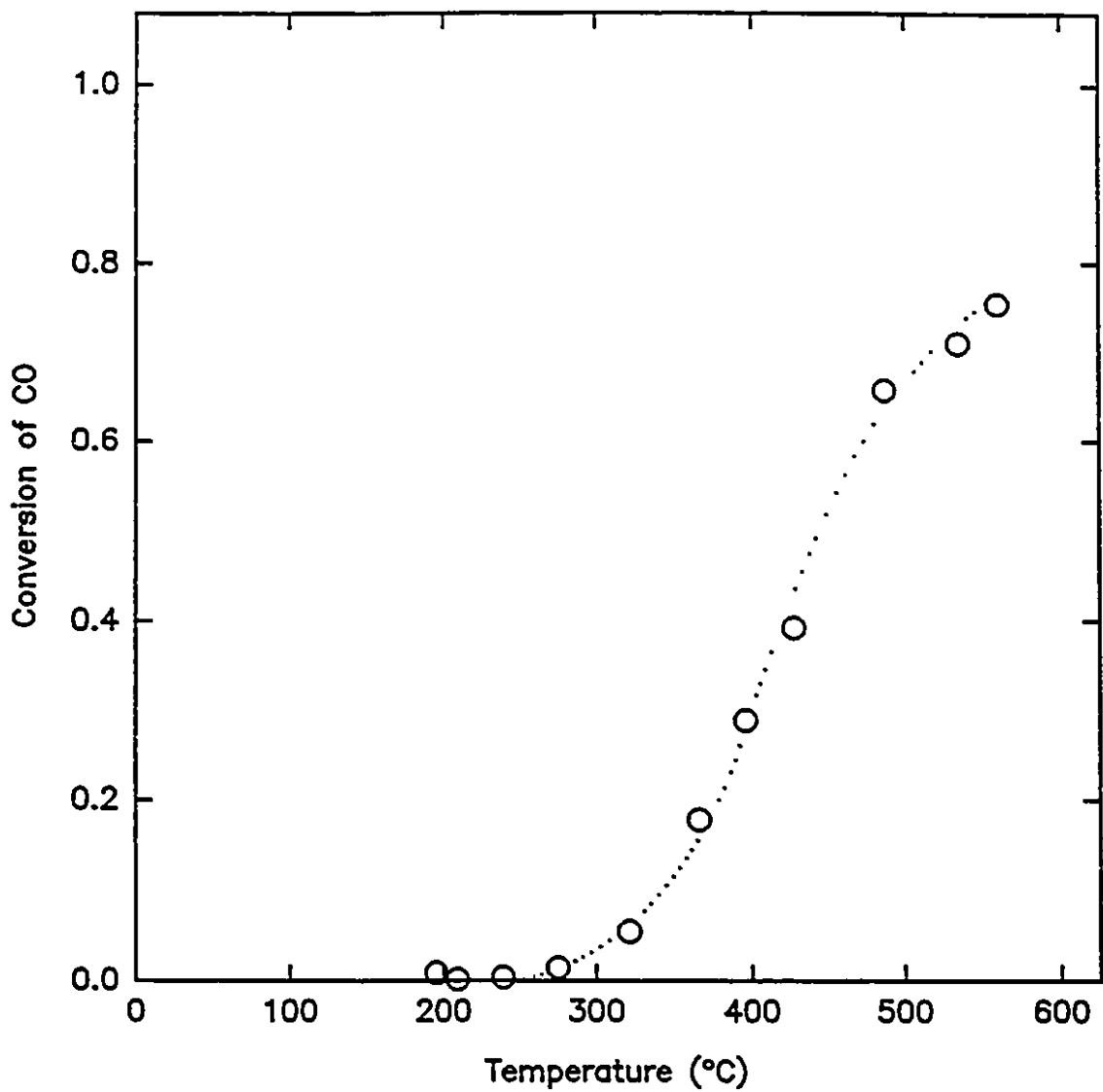


Figure 6.2 Homogeneous steady state oxidation of CO by O₂ at different temperatures
(Feed: 10% CO, 4% O₂, balance Ar and He)

measured in two experiments each. The reduction activity of the montmorillonite binder was also tested.

6.1.3.1 Catalytic Activity of the Cu-ZSM-5-M

In the decomposition experiments the reactor was loaded with 5 grams of catalyst, the flow rate was 410 cm³/min at 25°C (W/F = 0.73 g·s·cm⁻³), the temperature of the catalyst bed was 550°C, and the feed gas was 2% NO in Ar. No conversion of NO to N₂ was observed; for similar conditions Iwamoto observed a conversion of 73% (Iwamoto *et al.*, 1990).

The failure of the catalyst was most likely due to either a failure of the ion exchange procedure or because the zeolite may have had a very high Si/Al ratio. The ion exchange may have failed due to a poor rate of ion transfer through the solid pellets; in addition, any binding agent present may have further hampered the exchange process. If the sample had a high Si/Al ratio, up to 100 or more as compared to the more typical value of 24 to 26, it would have resulted in a very low copper content even at high exchange levels.

The activity for the reduction of 2% NO by 10% CO over the catalyst was measured under similar conditions and was also found to be negligible. Because of the poor performance of the exchanged pellets, and because it had been agreed with Mobil that no chemical characterization of the ZSM-5-M would be made, the issue of the low activity was not pursued further. It was assumed that there was a flaw in either the material or that the pellets could not be exchanged easily. The focus of the research shifted to the powdered Cu-ZSM-5 from Allied Signal (Cu-ZSM-5-AS).

6.1.3.2 Catalytic Activity of the Cu-ZSM-5-AS

A 90% Cu-ZSM-5, 10% montmorillonite mixture was prepared according to the method described in Section 4.1.2. Four preliminary experiments were made using the same sample of catalyst. Those experiments measured the activity for the reduction of NO by CO and for the direct decomposition of NO at 550°C, and at 535°C. In the first two experiments, at 550°C, the sample size used for the gas

analyses was 100 μL , and, for the experiments at 535°C, a sample size of 15 μL was used.

The reactor was loaded with 6 g of catalyst which was activated under Ar for 12 hours at 600°C. For the decomposition experiments the feed consisted of 2% NO and 98% Ar, while for the reduction experiments the feed contained 2% NO, 10% CO, and the balance Ar. The space velocity (calculated at 25°C) was 450 hour^{-1} . Figure 6.3 shows the conversion to N_2 of 60% and 55% measured in the two decomposition experiments, respectively. The catalyst is slightly less active than that used by Iwamoto, as observed in his experiments (Iwamoto *et al.*, 1989, 1986; refer to Table 3.1). As one might expect, there appears to be a slight dependence on temperature; however, the results at 535°C are less precise and are likely less accurate because the gas sample size used was very small. Shown in Figure 6.4, the conversion to N_2 obtained in the reduction experiments was 100% and 77%. In both figures, error bars of the 95% confidence interval of the mean of the three or four data points taken for each steady state have been included.

6.1.3.3 Activity for NO Reduction of the Montmorillonite

The binder used in the preparation of the catalyst pellets was tested for its reduction activity at 535°C. Six grams of pellets were extruded and activated under helium at 600°C for 12 hours. As before, the feed was 2% NO and 10% CO and the space velocity (at 25°C) was 450 hour^{-1} . No conversion or reaction products were observed.

6.1.3.4 Dependence of Activity on Reaction Time

The time dependence of the activity of the catalyst in the preliminary reduction and decomposition experiments was examined. Figure 6.5 shows the activity in each of the decomposition experiments as a function of the time after the steady state reaction temperature had been reached, and Figure 6.6 shows the results for the NO reduction experiments. The initial age of the catalyst, measured in total

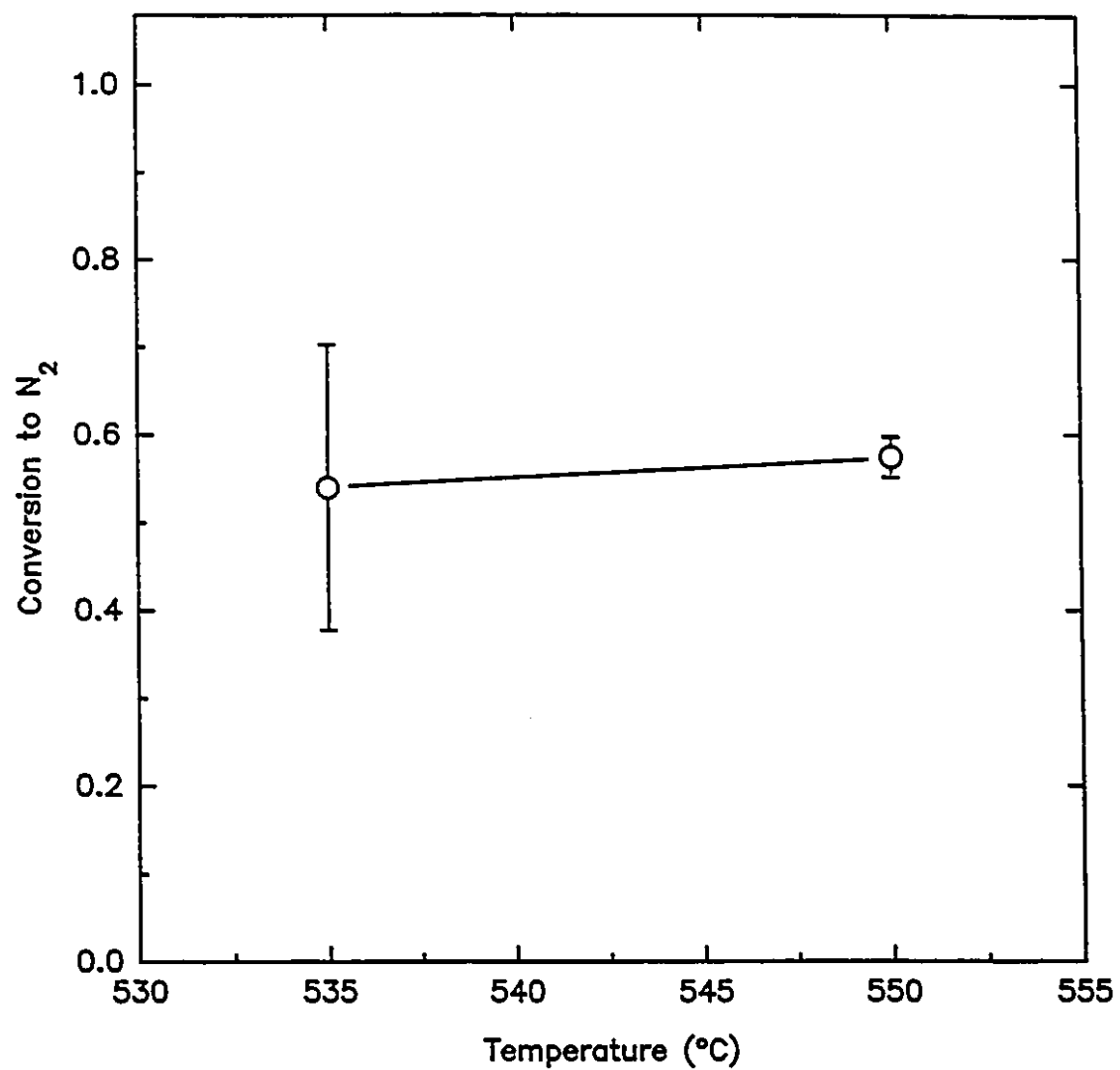


Figure 6.3 Activity of Cu-ZSM-5-AS for the decomposition of NO.
(Feed: 2% NO, balance Ar)

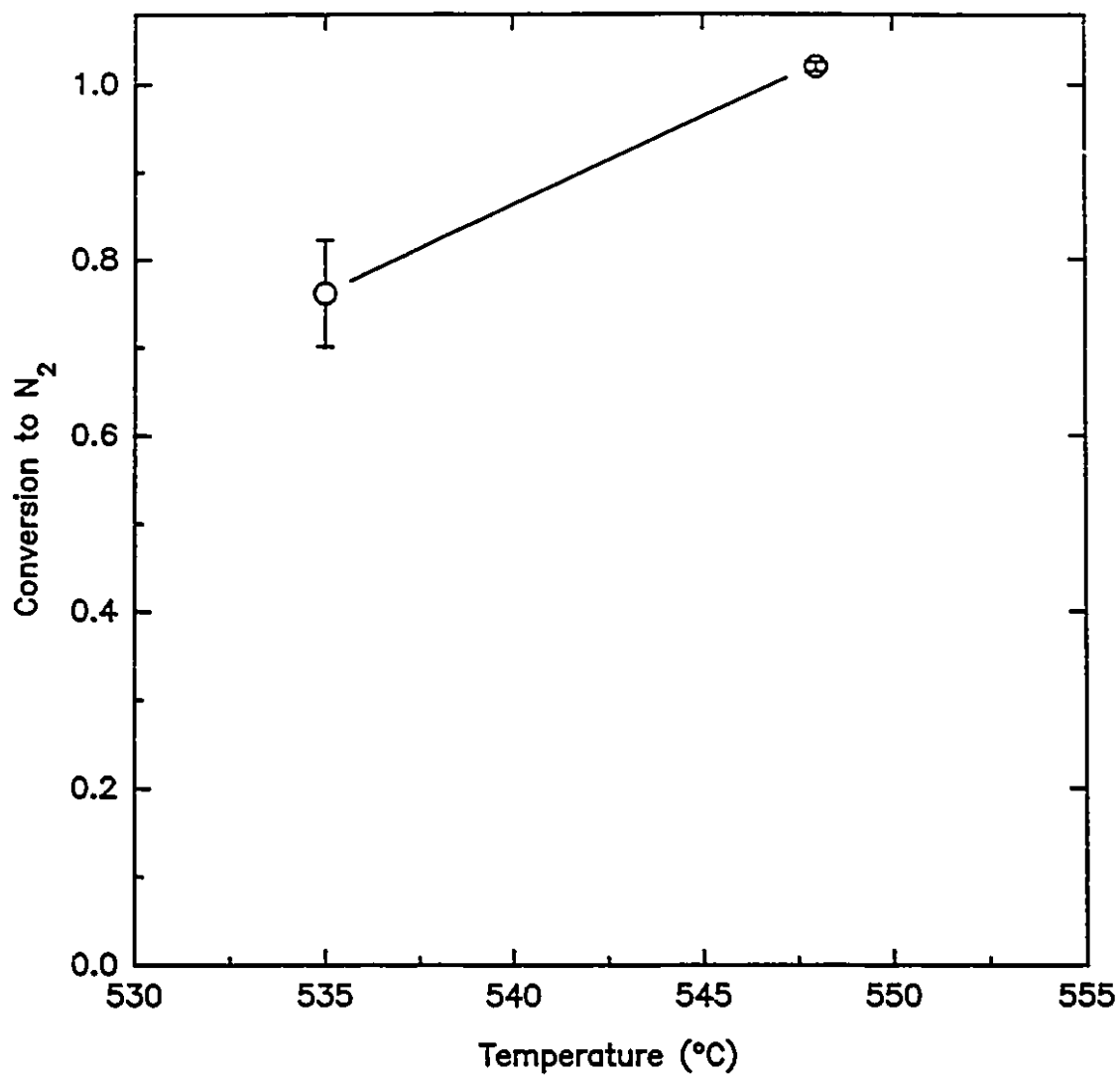


Figure 6.4 Activity of Cu-ZSM-5-AS for reduction of NO
(Feed: 10% CO, 2% NO, balance Ar)

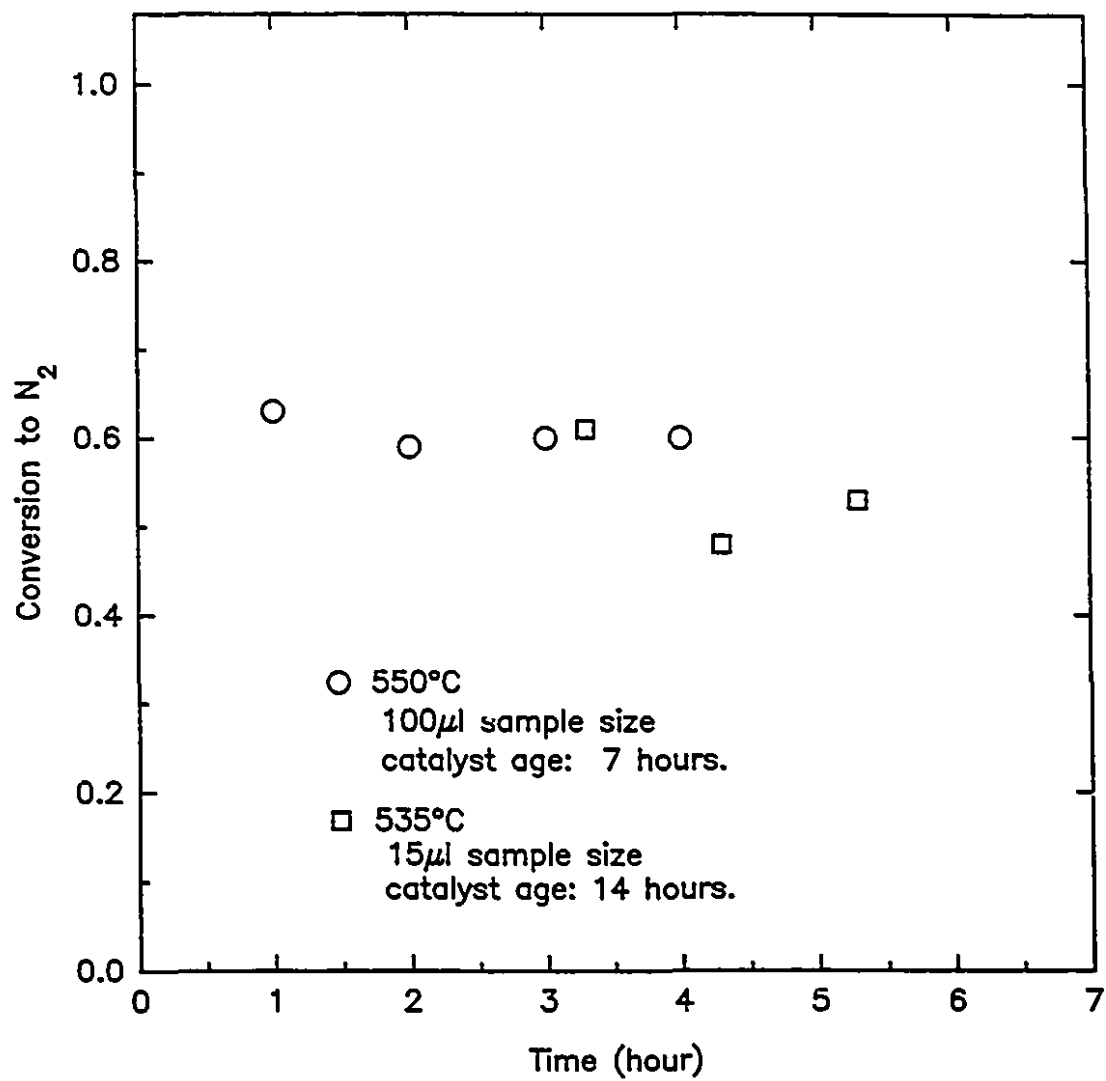


Figure 6.5 Decomposition activity as a function of time
(Feed: 2% NO, 98% Ar)

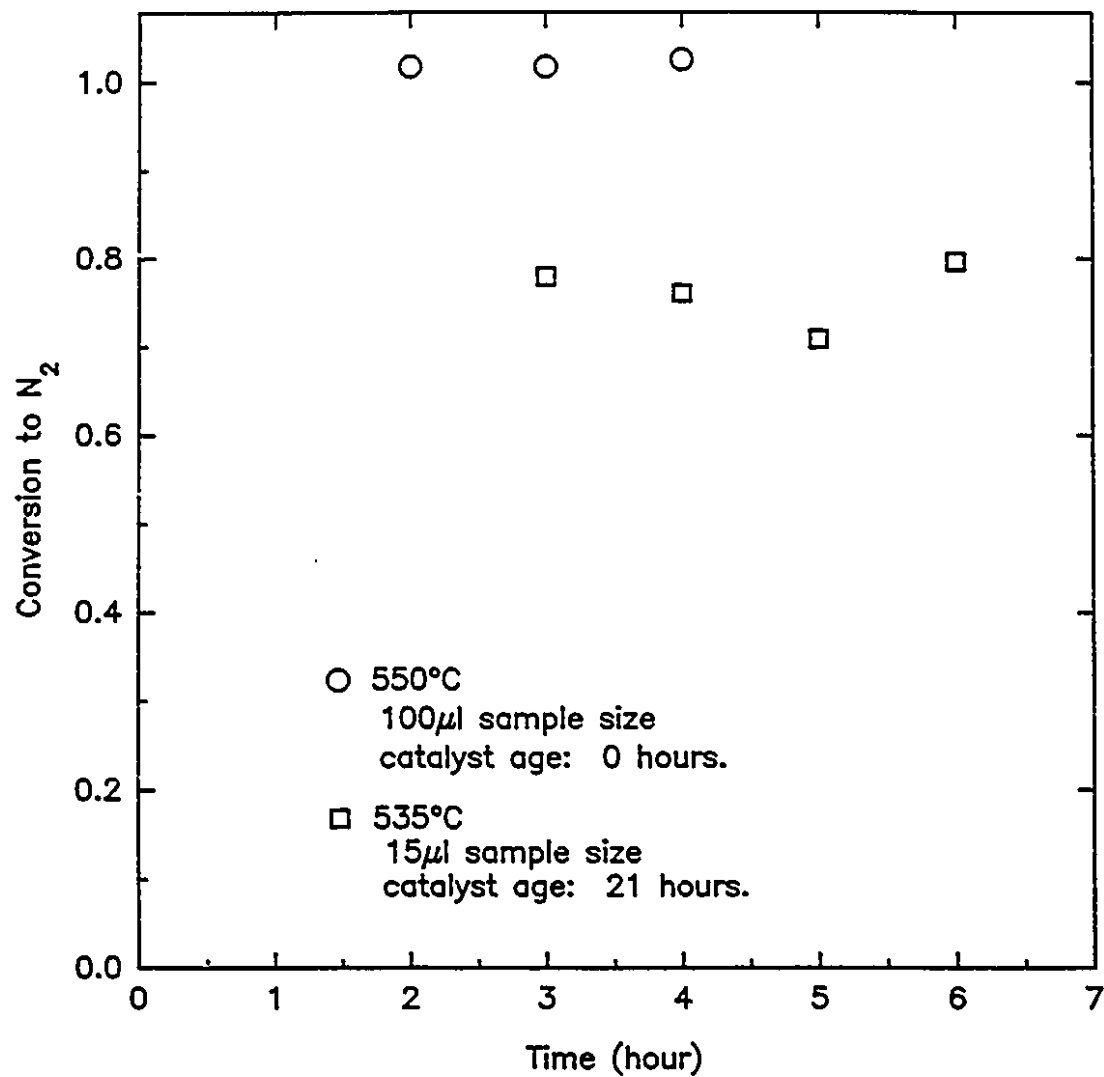


Figure 6.6 Reduction activity as a function of time
(Feed: 10% CO, 2% NO, balance Ar)

hours spent exposed to NO at or above 200°C in previous experiments is provided in both figures.

For the decomposition experiments, at 550°C (with the large sample size), the conversions obtained after 1 hour agree to within 2% and were deemed steady state values. These results are consistent with those of Iwamoto (1989) who found that, under similar conditions, steady state was reached in just over one hour. Because of the very small sample size, the results taken at 535°C are too scattered for any conclusions regarding time dependence to be drawn; however, the data were taken starting at a reaction time of three hours so it can be assumed that steady state had been reached. All of the points were used in obtaining the mean value shown in Figure 6.4.

For the reduction experiments (CO + NO) there is no dependence on reaction time. However, the drop in activity from 100% to 77% between these experiments could be attributable to the drop in reaction temperature (15°C) or, perhaps, to aging of the catalyst in the intervening experiments. Based on the results presented below, the catalyst age of 21 hours may have been sufficient to cause deactivation of the catalyst.

6.1.4 Test for External Diffusion Control

To see if the intrinsic activity of the catalyst pellets was being measured, the effect of changing the external film diffusion resistance was investigated. For a fixed temperature and catalyst loading, the external mass transfer resistance is affected by both the overall gas flow rate and the properties of the gas mixture. Therefore, two approaches in changing the mass transfer coefficient could have been taken. One was to adjust both the flow rate and the catalyst loading while keeping the ratio of the two constant, and the other was to change the diluent gas being used. Because of limitations of the gas delivery system, only the second approach was taken.

For a reaction that is controlled by the external diffusion rate of reactant species i , the observed rate is directly related to the mass transfer coefficient, k_m :

$$r_i = k_m (C_{ib} - C_{is}) \quad (6.2)$$

where r_i is the rate of reaction of species i and C_{ib} and C_{is} are the concentrations of i in the bulk gas and at the surface of the pellet. The integrated form of the mass balance of species i for a plug flow reactor is given by:

$$\frac{1}{C_{if}} \frac{M}{Q_f} = - \int_0^x \frac{1}{r_i} dx \quad (6.3)$$

where Q_f is the total volumetric feed rate, C_{if} is the feed concentration of i , x is the conversion of species i , and M is the mass of the catalyst. If all other parameters are held constant while the inert diluent is changed, then any change in conversion must be due to a change in k_m .

Two short NO reduction experiments were run back to back under identical conditions, except that the diluents used were argon and helium, respectively. Because argon is ten times denser than helium under the same conditions, the diffusivity of all of the reactant gasses changes greatly when the switch is made. Furthermore, there is a change in the inertial and viscous forces which determine the gas flow near the pellets. With the switch from argon to helium, k_m was predicted to rise by a factor of 1.4 (see Appendix C). However, the change in conversion was negligible (only 1%), suggesting the diffusion resistance was insignificant.

6.2 Reduction of NO by CO in the Presence of O₂

The effect of the O₂ concentration on the activity for the reduction of NO to N₂ by CO at various temperatures was measured. Extruded pellets were made from the Allied Signal Cu-ZSM-5 powder as described in Section 4.1.2. No binding agent was used (all further references to "the catalyst" or Cu-ZSM-5 will refer to this catalyst unless stated). A series of experiments was run under the conditions listed in Table 6.1, and the experimental procedure described in Section 4.6 was

Table 6.1 Experimental Conditions for Measuring the Activity for the Reduction of NO by CO in the Presence of O₂:

Fixed Parameters:

Partial Pressure NO:	2%
Partial Pressure CO:	10%
Total Pressure:	1 atmosphere
Catalyst Loading:	7.5 g
Catalyst Composition:	100% Cu-ZSM-5 extrudate pellets (1 mm o.d.). From Allied Signal powder. Platinum-group metal supported on alumina, on ceramic monolith. From Degussa Canada.
Total Flow Rate:	94.6 cm ³ /min (25°C and 1 atm)

Variables:

Partial Pressure O ₂ :	0 - 5.3%
Temperature:	100 - 600°C (373 - 873K)
Catalyst conditioning:	He (or Ar), or 20% CO in He (or Ar), or 20% O ₂ in N ₂

Dependant Parameters:

λ :	0.2 - 1.3
Space Velocity:	450 hour ⁻¹ (25°C)
Space Time (W/F):	4.8 g-s/cm ³

followed. For the purpose of comparison, the activity of a platinum-group-metal three-way catalyst was evaluated under the same conditions.

6.2.1 Reduction Activity of Fresh Cu-ZSM-5

Figures 6.7 to 6.9 show the activity, defined as the conversion of NO to $\frac{1}{2}\text{N}_2$ (Equation 4.7) at steady state, at various temperatures for different values of λ , the equivalence ratio. Curves and arrows have been added to the figures to highlight the trends, rather than to indicate a model. In each of Figures 6.7 and 6.8, two trends are clearly evident. The curves labelled H represent the trends observed when the steady state temperature was approached from a higher temperature and the curves labelled L represent the trends observed when the steady state was approached from a lower temperature. In Figure 6.9, only the H curve is shown for the case of $\lambda = 1.3$. Figure 6.10 is a composite of the trends observed.

The multiple steady states indicated by the presence of the H and L hysteresis loop may result from a few different factors. Two possible explanations are proposed. The first, presented in more detail in Appendix C, is based on external heat and mass transfer considerations. With exothermic heterogeneous reactions the heat liberated by the reaction is a sigmoidal function of the temperature of the catalyst pellet, whereas the heat transferred from the pellet to the surrounding bulk gas is (approximately) a linear function of the temperature difference between the pellet surface and the bulk gas. As a result, in some cases, there are multiple stable steady states for the heat and mass balances for a given bulk temperature. For each such steady state, the pellet surface temperature, reaction rate and conversion is different.

The stable steady state at the lower pellet temperature is generally in the reaction-controlled regime, where the mass transfer resistance is low and does not limit the overall reaction rate; the higher stable steady state is in the diffusion-controlled regime, where the overall rate is limited by the supply of reactants to the pellet surface. This analysis is consistent with the earlier findings, where the mass transfer resistance was determined to be negligible, since those results were obtained

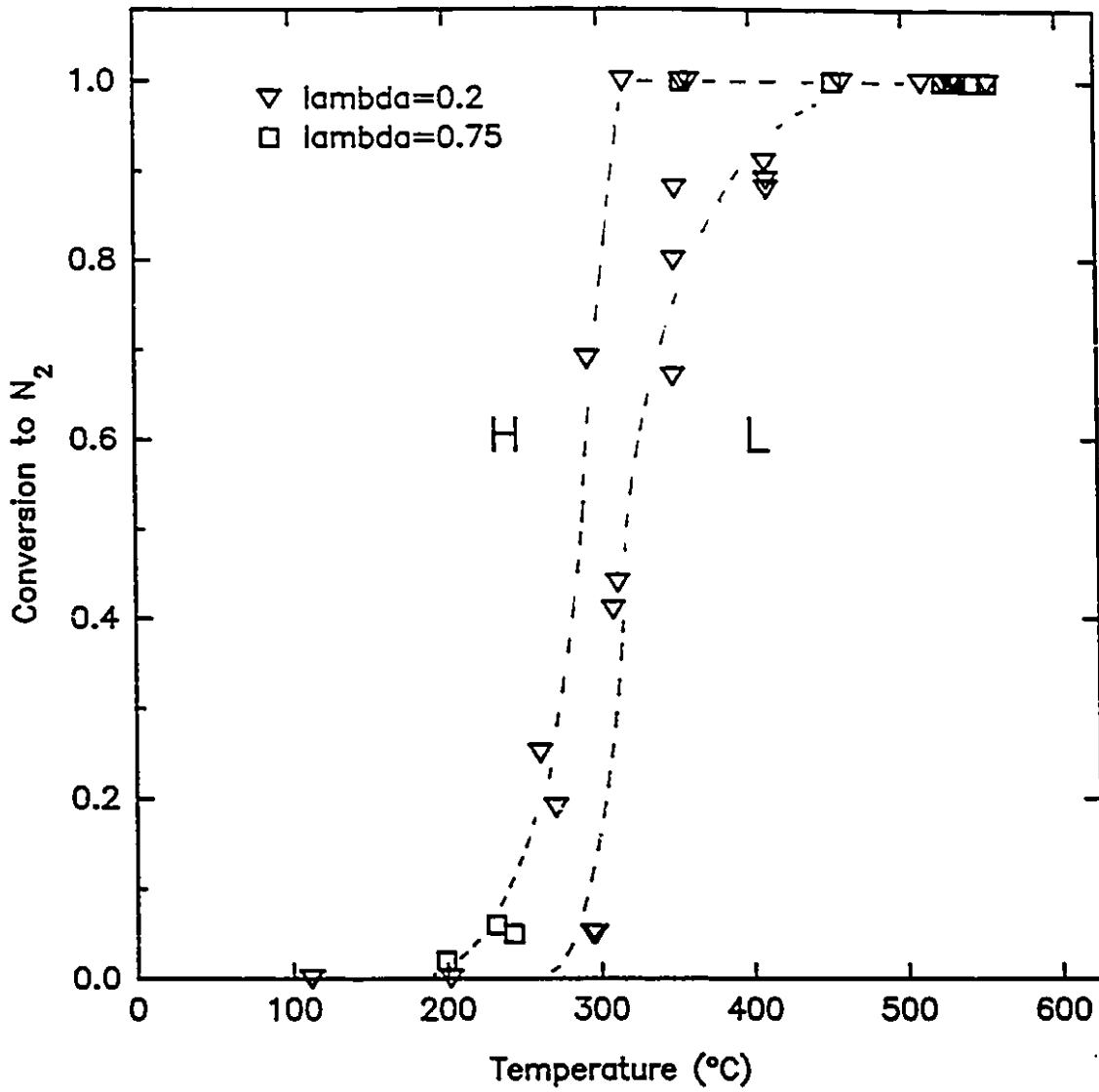


Figure 6.7 Reduction activity at $\lambda < 1$
 ($\lambda = 0.2$; 10% CO, 2% NO, 0% O_2)
 ($\lambda = 0.75$; 10% CO, 2% NO, 2.75% O_2)

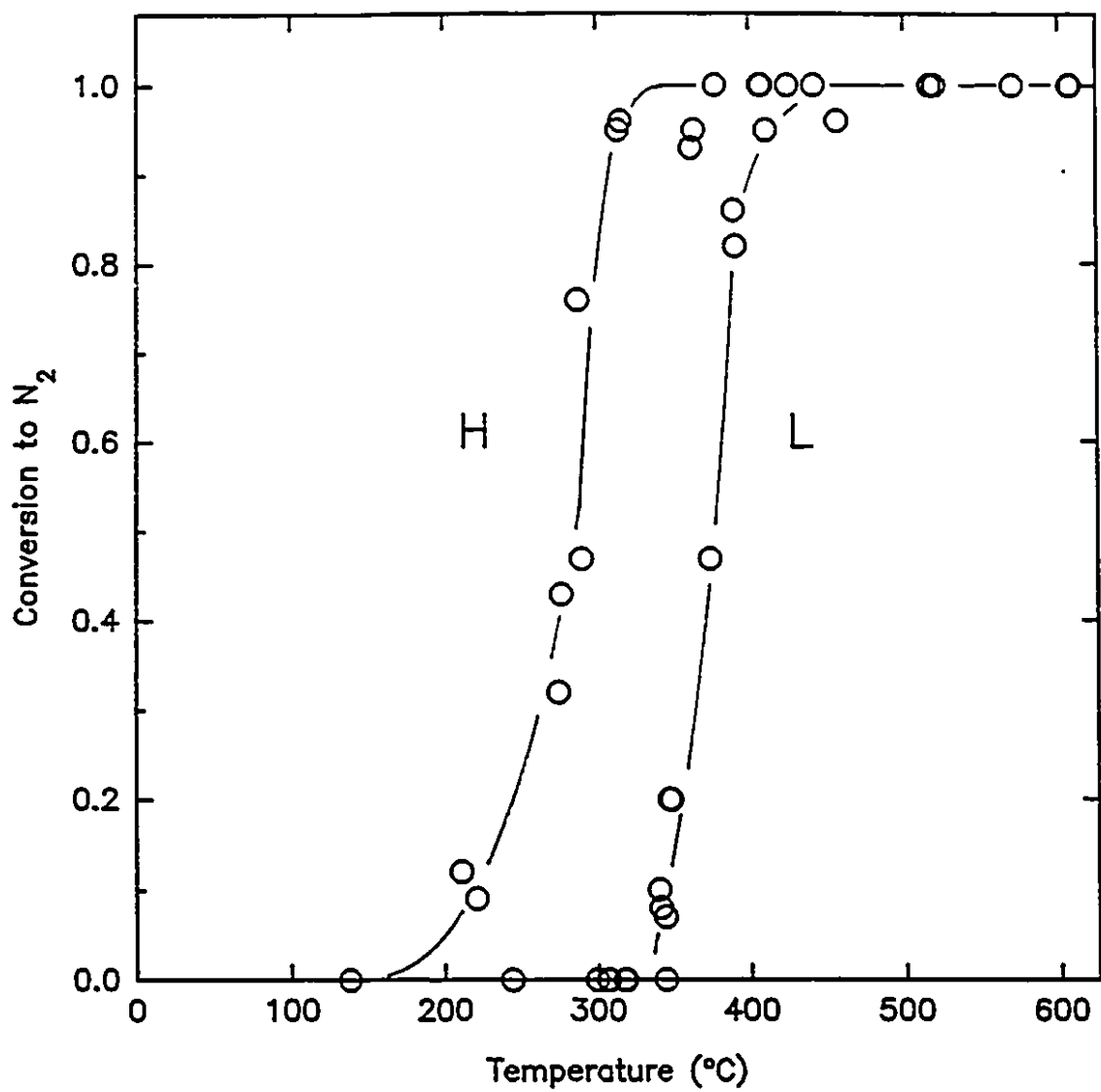


Figure 6.8 Reduction activity at $\lambda = 1$
 (Feed: 10% CO, 2% NO, 4% O_2 , balance inert)

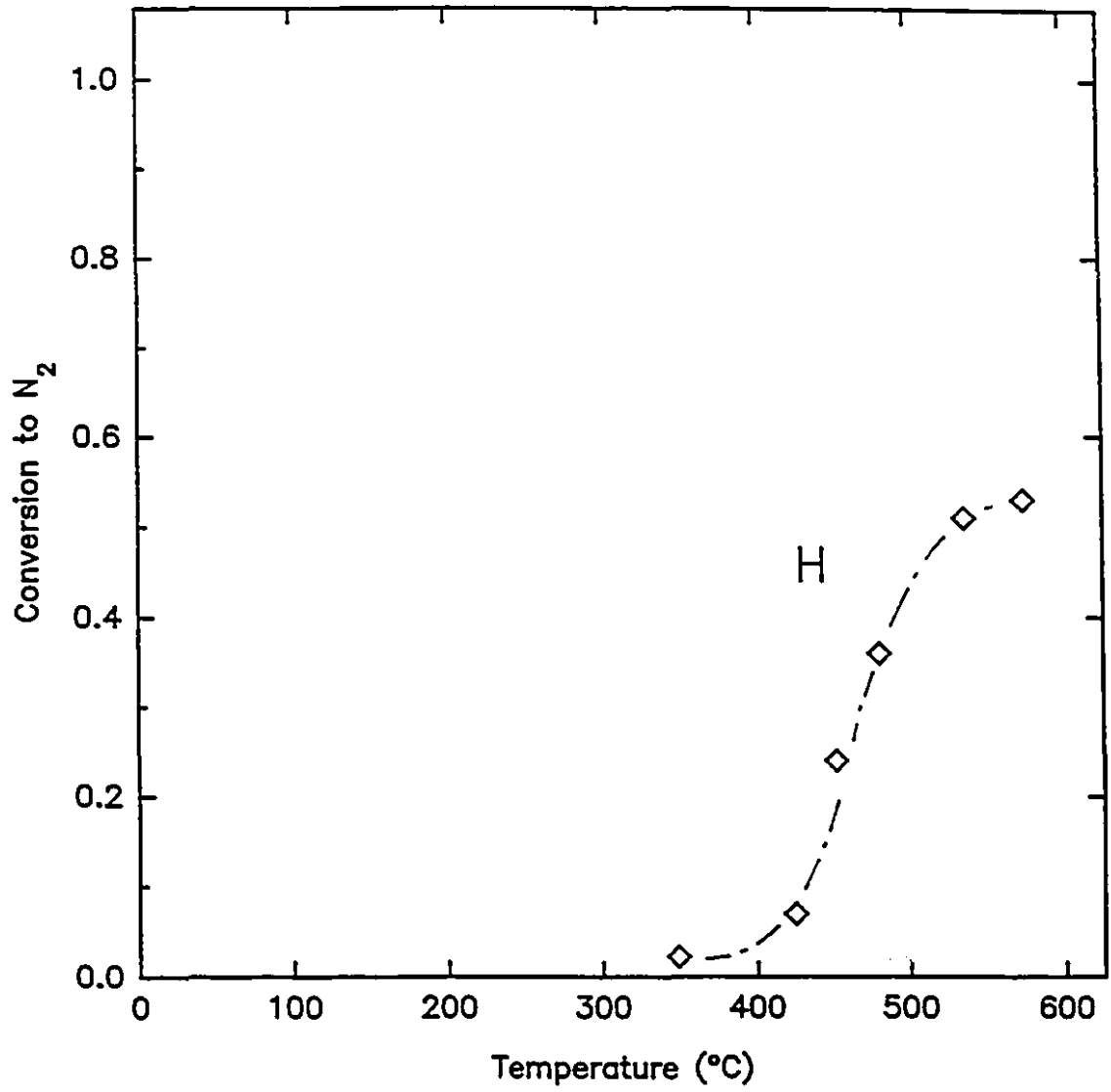


Figure 6.9 Reduction activity at $\lambda = 1.3$
(Feed: 10% CO, 2% NO, 5.5% O₂, balance inert)

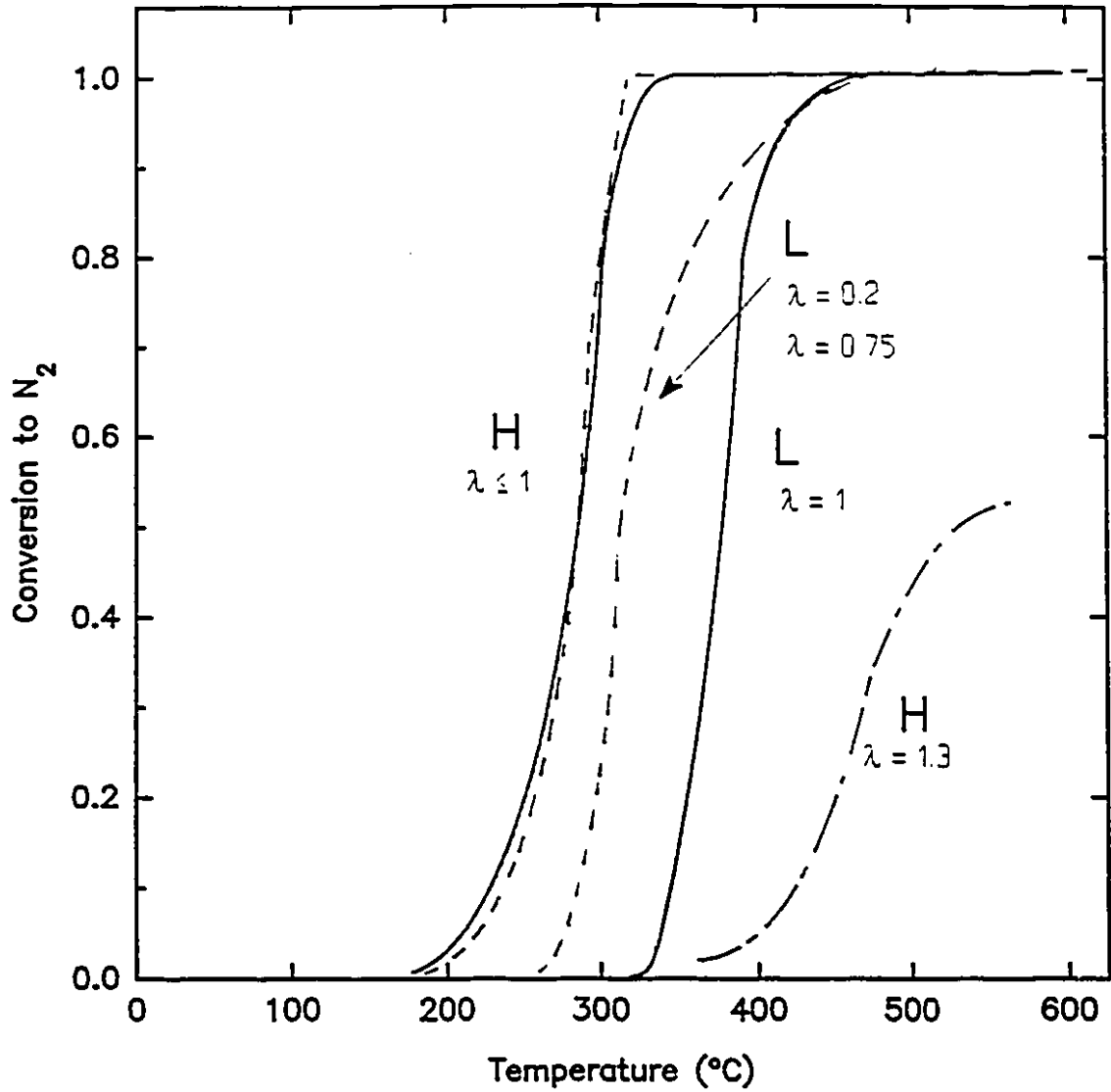


Figure 6.10 Reduction activity trends over Cu-ZSM-5.
 Space velocity = 450 hr^{-1}
 Space time (W/F) = 4.8 g-s/cm^3

by turning up the reactor to a set level, which would then leave the system at the lower stable pellet surface temperature, that is, on the L curve.

The second possible explanation for the multiple steady states is based on an analysis of internal heat transfer limitations and follows a similar line of reasoning as above. This time, the temperature within the pellet may be higher than the temperature at the outer surface of the pellet, and, as a result, the catalyst material inside the pellet may be more active than that at the surface (in such a case, the pellet effectiveness factor η is greater than 1 -by definition) . The significantly higher internal temperatures result from heat generated by the reaction and a poor heat transfer rate within the catalyst pellet. In some cases, multiple steady states may exist where the effectiveness factor is large enough (Smith 1981). This second analysis is also consistent with the preliminary results.

Whatever the cause of the multiple steady states, it is clear from the steep temperature dependence observed in the figures at $\lambda \leq 1$ (Figures 6.7 and 6.8) that the activation energy for the reaction is high. It is of interest that, as seen in the composite (Figure 6.10), the H curve (scanned downwards in temperature) is in approximately the same location for λ 's equal to and less than 1, but the L curve (scanned upwards in temperature) is shifted to a higher temperature position in the $\lambda = 1$ case. By this result, and more noticeably by the shift in the H curve for $\lambda = 1.3$, it is clear that O_2 inhibits the reduction and/or decomposition when present at high enough concentrations.

Using the H trend curves to interpolate the upper activity values at fixed temperatures, the conversion can be plotted as a function of λ . The "lambda-plot" is shown in Figure 6.11. The plot shows that at temperatures of 400 - 550°C, typical of automobile exhaust catalyst placement, for $\lambda \leq 1$, the activity was ~100%, and at $\lambda = 1.3$ the activity was still considerable, with a conversion of 53% at 550°C. This result appears in great contrast to that from the typical lambda plot for the three way catalyst (TWC) presented in Chapter 1, where the conversion to N_2 was negligible at $\lambda \geq 1.05$. On this basis, the Cu-ZSM-5 catalyst seems to be much more active than the TWC. At a λ of 1.1, where the engine runs efficiently, the conversion over the ZSM-5 is still high, at about 85% at 550°C.

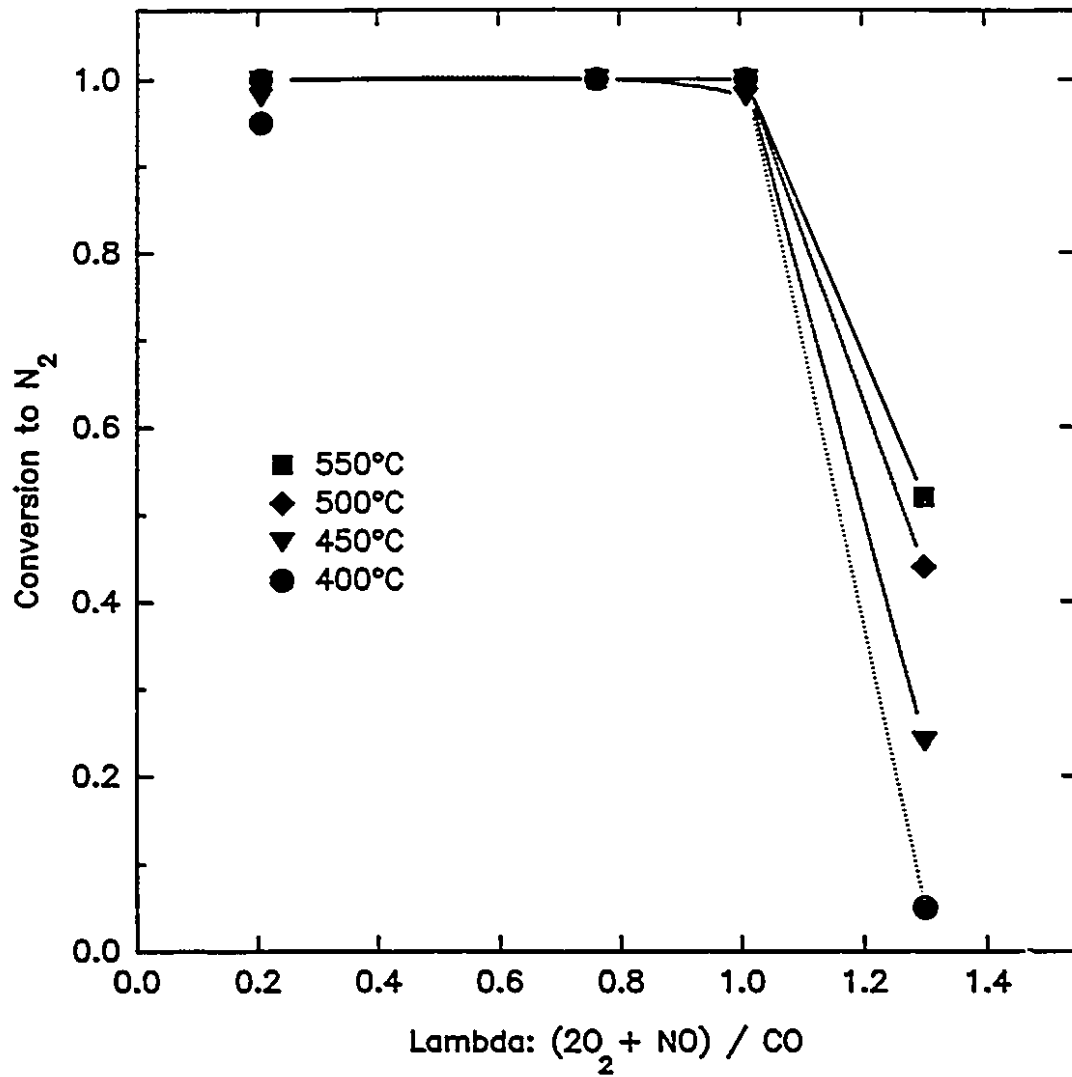


Figure 6.11 Lambda-plot for Cu-ZSM-5: Conversion to N₂ at fixed temperatures for a space velocity of 450 hour⁻¹ (space time of 4.8 g·s/cm³)

6.2.2 Reduction Activity of the Three-Way Catalyst

For a more rigorous comparison of the Cu-ZSM-5 activity and activity of a typical TWC, the activity of a sample of TWC monolith was tested. The bulk density of the Cu-ZSM-5 pellets and the TWC monolith sections was similar, so the comparison was made using the same space velocity, 450 hour⁻¹ (25°C). The surface area of the catalyst was 16.1 m²/g and the porosity was 0.048cm³/g; the pore volume distribution is shown in Figure 6.12. The temperature was held constant at 550°C and the gas mixture adjusted to provide for activity measurement at various values of λ . The steady state results are shown in Figure 6.13 and, for reference, the lambda-curve for the Cu-ZSM-5 at 550°C is reproduced. At λ 's greater than 1, the Cu-ZSM-5 is much more active, and at $\lambda = 1.3$, the activity is almost double that of the TWC.

6.2.3 Reduction Activity of Reused Cu-ZSM-5

When Cu-ZSM-5 catalyst samples were re-used after NO reduction or decomposition experiments, a drop in catalyst activity was observed. This deactivation was noted only after the catalyst had been used for at least 18 to 30 hours. The total time the catalyst spent exposed to the NO-containing feed gas above 200°C (the lowest temperature at which the catalyst was active) was typically 18 hours per experiment. Figure 6.14 shows data obtained using used catalyst samples at $\lambda = 1$. For comparison, the trends observed with fresh catalyst samples is also shown. Figure 6.15 shows data obtained from a used catalyst sample at $\lambda = 1.18$. Data were also obtained with spent catalyst at $\lambda = 0.5$, and are included in Figure 6.16, below. The data shown do not represent steady state values, as the deactivation sometimes occurred at a significant rate between measurements, while at other times a pseudo-steady state was observed, where reproducible product sample analyses were obtained over periods of a few hours. It is clear that the deactivation is significant, and in some cases almost total. Figure 6.16 shows the same lambda-plot as Figure 6.11 before, but the data, or interpolations from the data, of the experiments with used catalysts are also included.

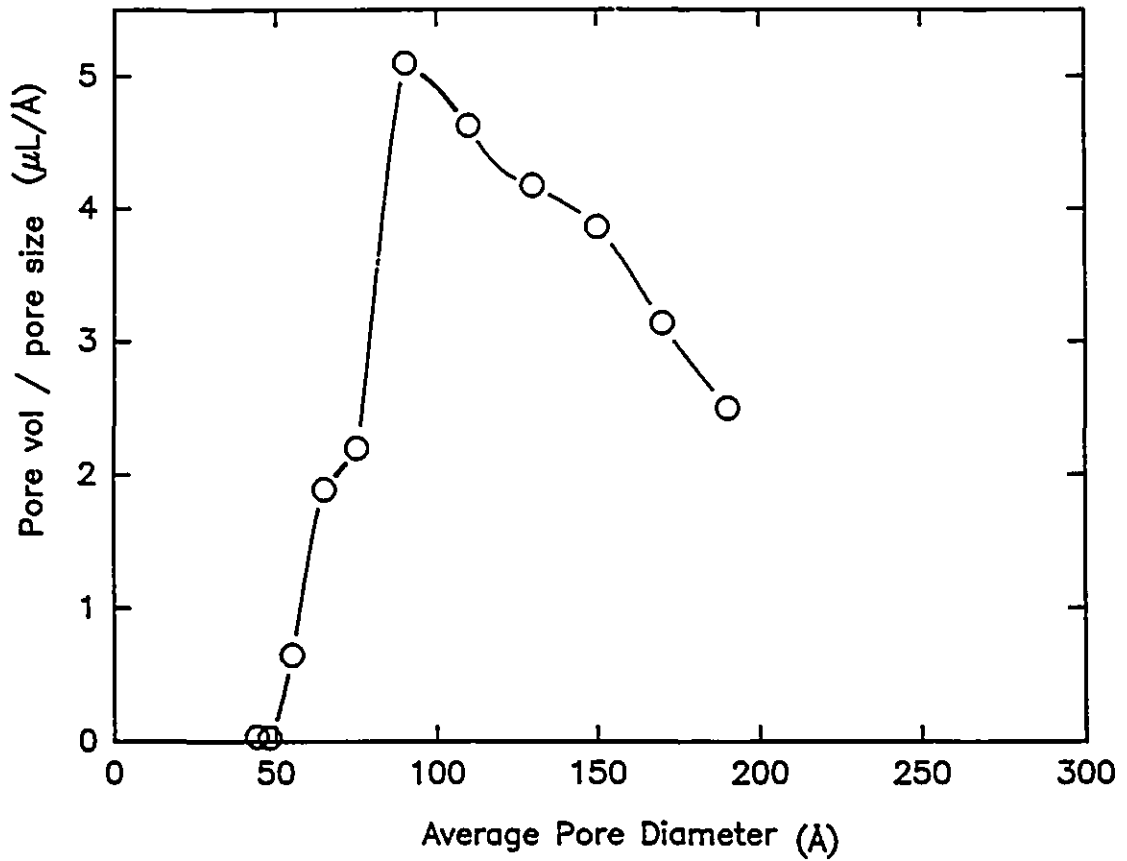


Figure 6.12 Pore volume distribution of the PGM TWC from Degussa

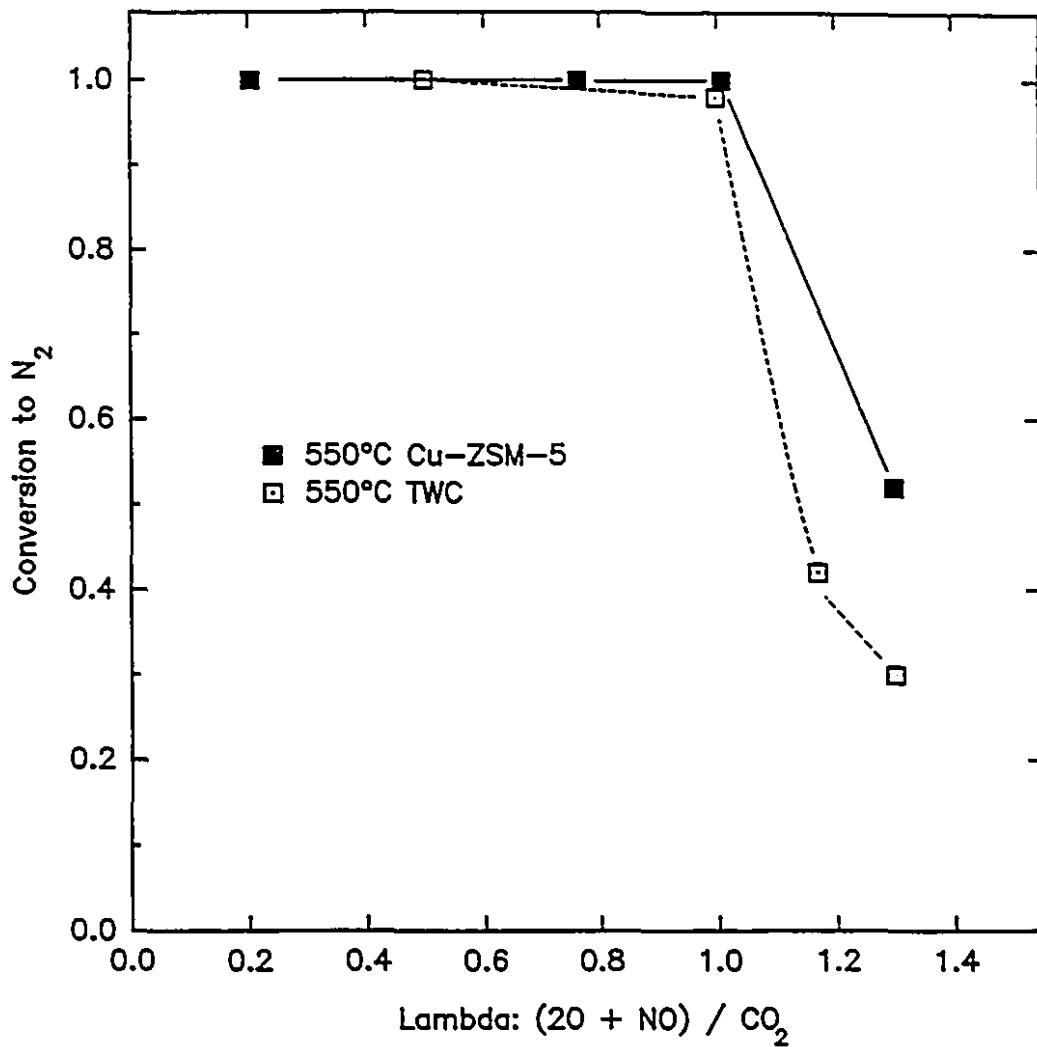


Figure 6.13 Lambda-plot at 550°C for the alumina PGM three-way catalyst from Degussa. For reference, the lambda-plot for the Cu-ZSM-5 at 550°C is shown.

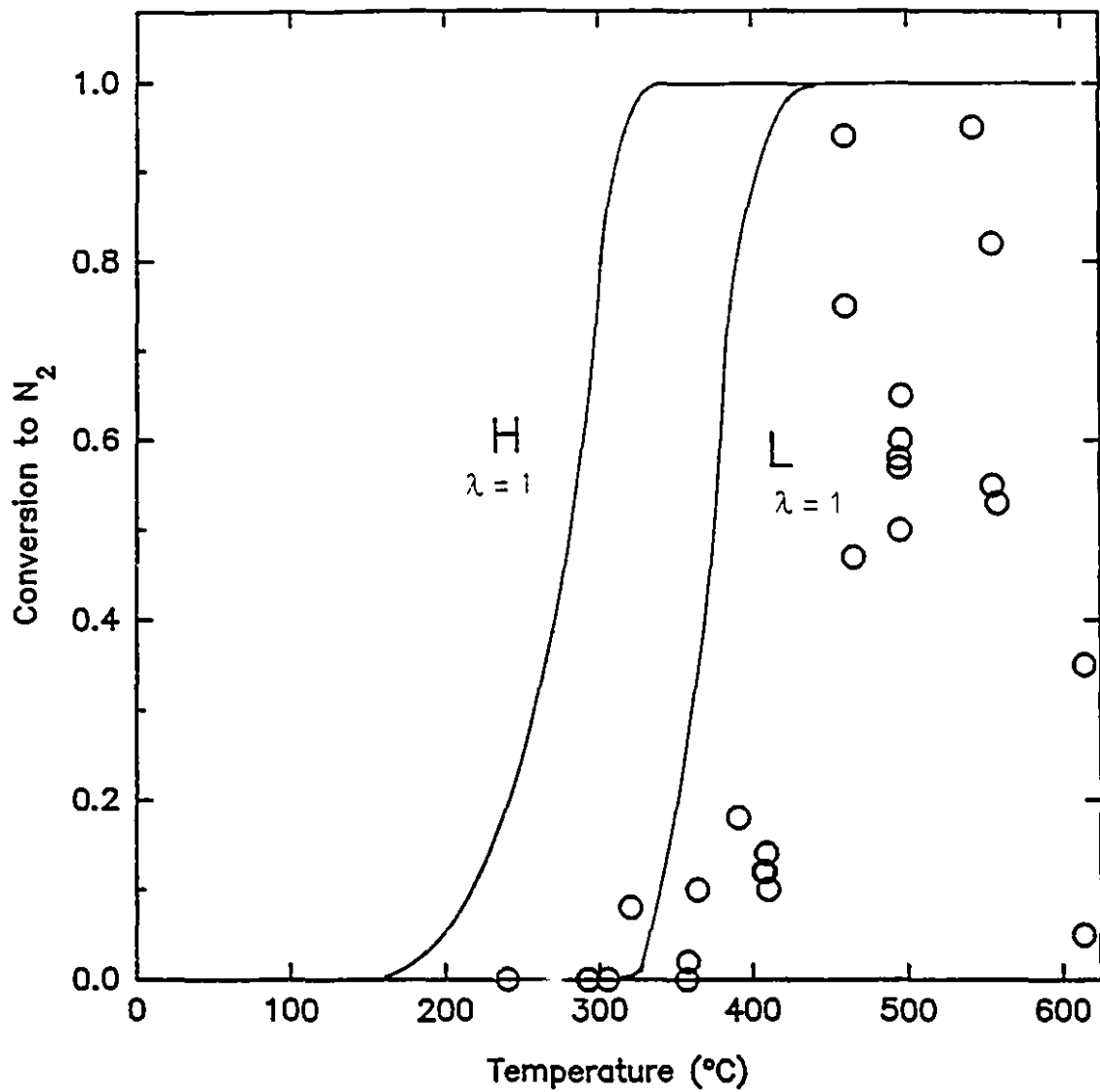


Figure 6.14 Reduction activity of a spent catalyst and trend for new catalyst at $\lambda = 1$. For reference, the trends obtained using the fresh catalyst are shown

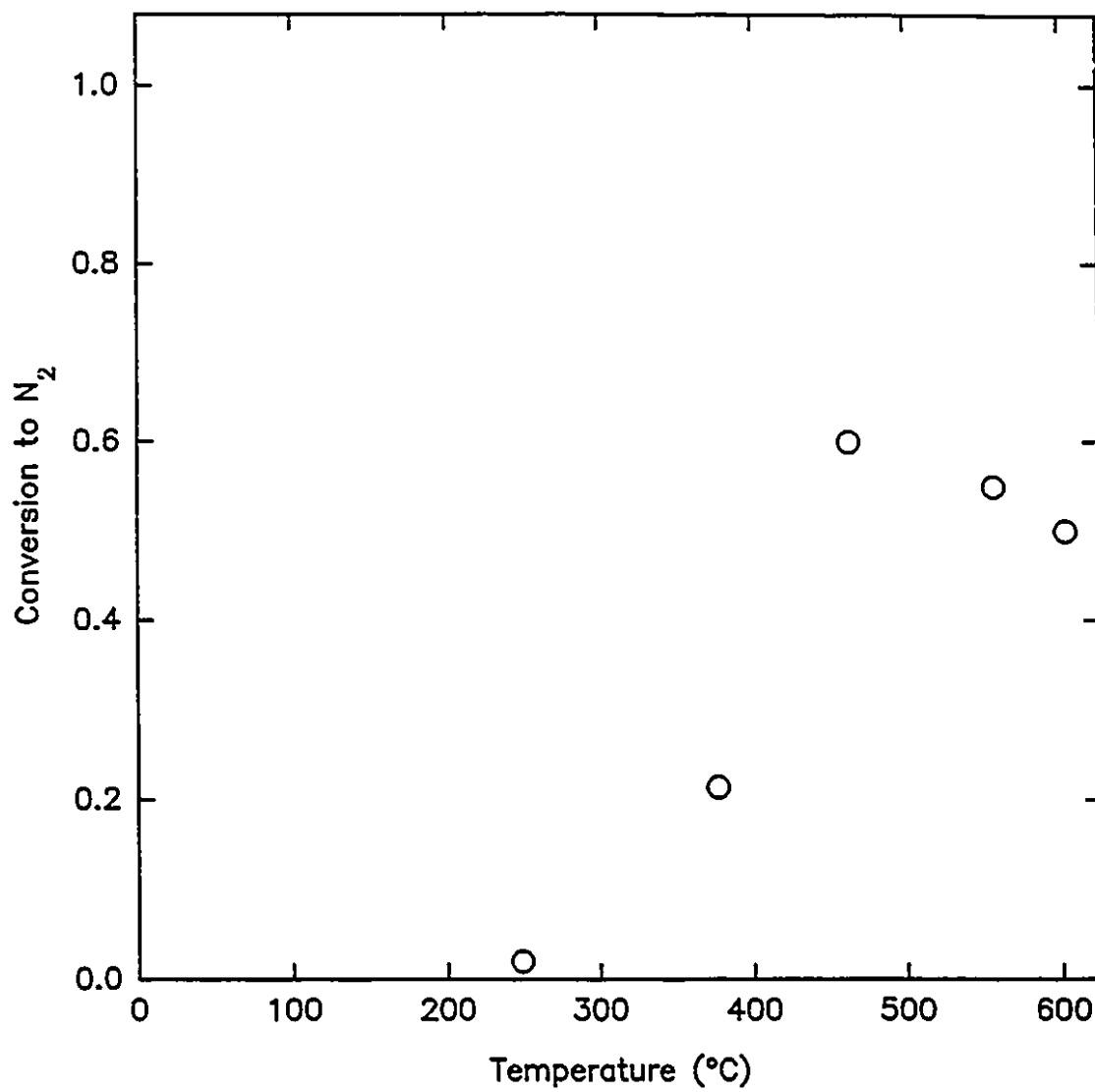


Figure 6.15 Reduction activity for a used catalyst sample at lambda = 1.18

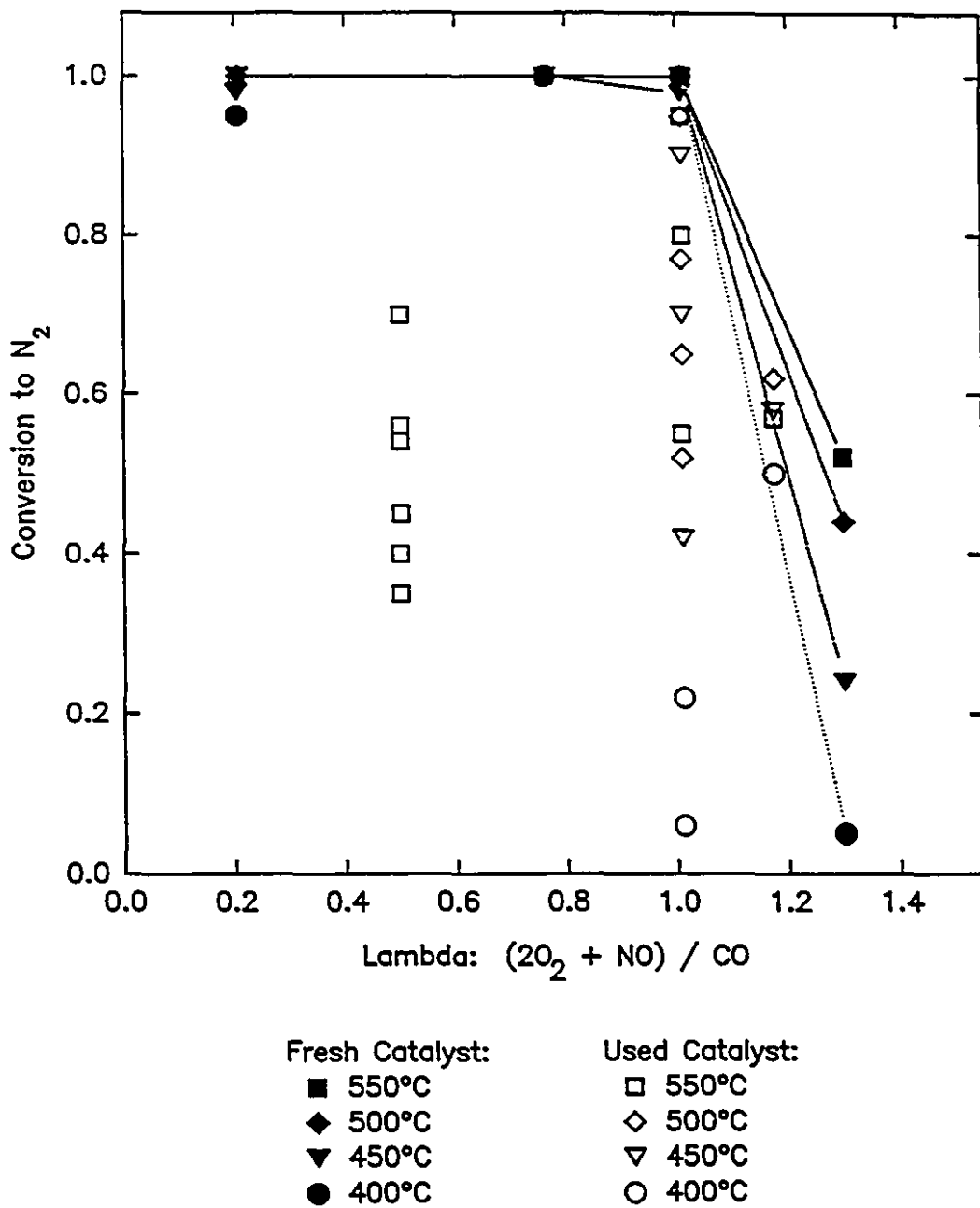


Figure 6.16 Lambda-plot, including results obtained with used catalyst samples

6.2.4 Effect of Regeneration Treatments on the Cu-ZSM-5

Hot gas treatments were investigated as a means of regenerating the spent catalyst. Treatment with pure helium, argon, 20% O₂ in N₂ (dry air), and 20% CO in helium at temperatures of 600°C to 750°C for 12 hour periods were tested, but in each case the catalyst showed no improvement in activity.

6.2.5 Effect of Pretreatment of Cu-ZSM-5 on Reduction Activity

In general, the fresh pellets were conditioned at 600°C for about 12 hours under a flow of pure argon or pure helium to remove any volatile components. To investigate the effect of the pretreatment, in particular to see if it affected the activity or deactivation of the catalysts, two catalysts samples were conditioned for 5 days at 600°C under a flow 20% CO in helium, and dry air, respectively.

The activity of the catalysts was measured at $\lambda = 1$, and the results compared to those originally obtained using catalyst activated overnight under helium. In Figure 6.17, the data from Figure 6.8 are presented again, this time with the pretreatment method indicated. There is a good match to the curves for all of the data; the different conditioning gasses, oxidizing, reducing, and inert, had no effect on the catalyst activity. Given the long time of the treatments, the fact that there was no loss of activity also indicates that the deactivation previously observed was not the result of long-term exposure to net reducing or net oxidizing conditions in general, or to CO or O₂ in particular. Instead, the observed deactivation must have been due to exposure to the NO or to the combination of feed gasses together.

6.2.6 Effect of the Feed Redox Ratio on Cu-ZSM-5 Deactivation

Following the experiments for $\lambda = 0.2$, $\lambda = 1$, and $\lambda = 1.3$, the catalysts were reused for further activity measurement. In all three cases, deactivation was observed within twelve hours of initiation of the second experiment, indicating that the redox nature of the feed gas mixture was not an important factor in the deactivation.

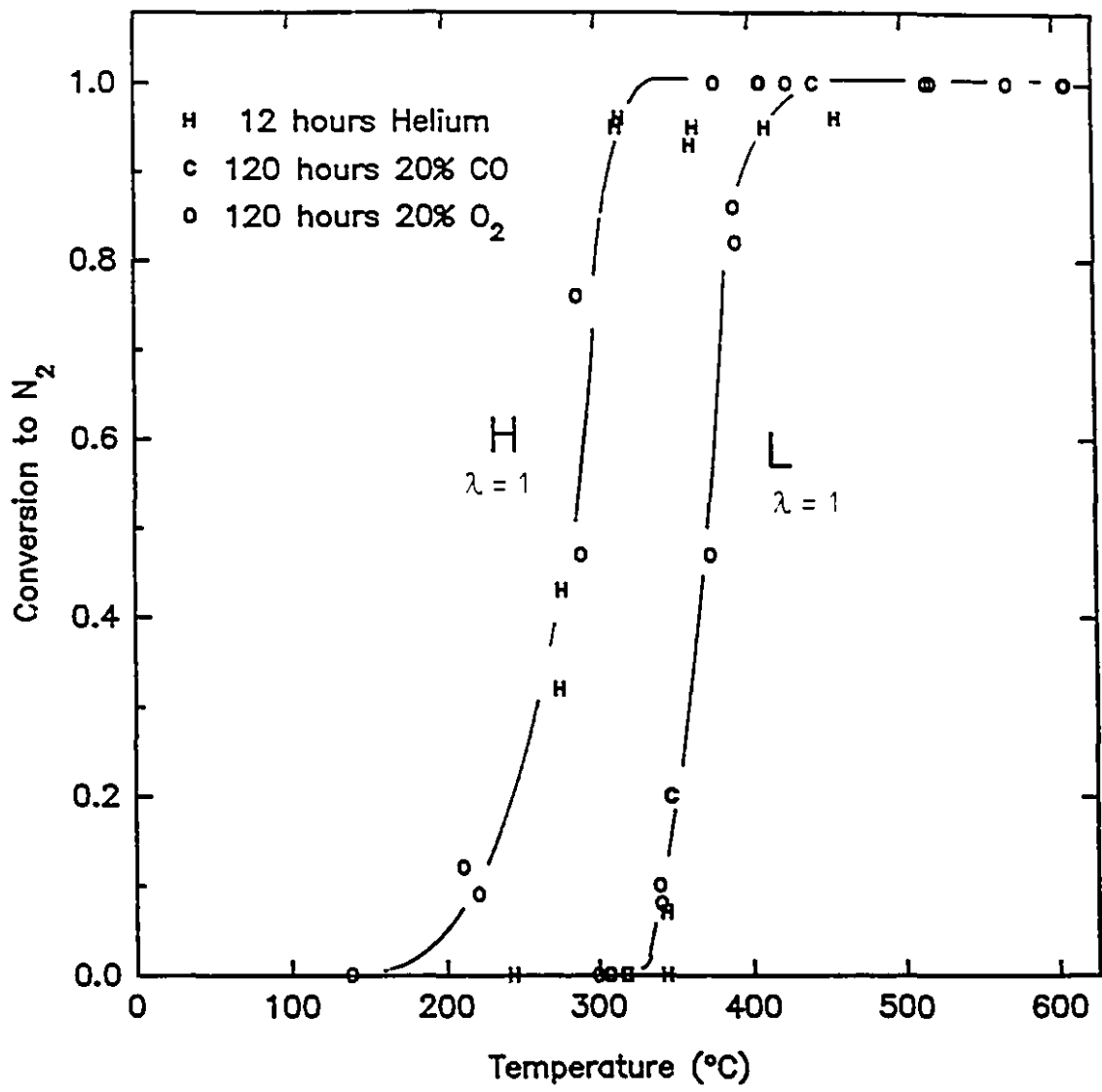


Figure 6.17 Reduction activity at $\lambda = 1$, with pretreatment gas indicated
 (Feed = 2% NO, 4% O₂, 10% CO, balance inert)

6.3 Activity of Cu-ZSM-5 for CO Oxidation

In the above experiments, the feed concentration of CO was 10% and space velocity was 450 hour⁻¹. That these parameters are constant allows the CO oxidation activity to be defined as the conversion of CO to CO₂. The activity for the conversion was measured directly by the CO loss as well as by the production of CO₂. The results were generally as expected; in the absence of O₂, the production of CO₂ was double the production N₂ (refer to Equation 1.4). This being the case, the CO conversion activity for $\lambda = 0.2$ (10% CO, 2% NO, 0% O₂) need not be presented, as it can be determined easily from the data of Figure 6.7. In the presence of both O₂ and NO, the production of CO₂ was equal to the removal of NO and $\frac{1}{2}$ O₂ (when determinable) for $\lambda < 1$ (net reducing), but for $\lambda > 1$ (net oxidizing) the production of CO₂ was slightly less than the removal of O₂ and NO due to the reactions producing NO₂ and, possibly, other nitrogen oxides.

The activity for CO oxidation by O₂ was measured directly in experiments under identical conditions as in the NO activity experiments, but without the NO present. That is, for comparison with the $\lambda = 1$ case (10% CO, 4% O₂, 2% NO, balance inert), the activity for CO oxidation for a 10% CO, 4% O₂, balance inert mixture was measured. Figure 6.18 shows the conversion obtained at various temperatures. In Figure 6.19, this conversion is compared to conversion obtained in the absence of catalyst (originally presented in Figure 6.4) and the conversion obtained for the $\lambda = 1$ experiments. Comparison of the results suggests that the oxidation of CO by O₂ goes almost to completion before there is significant conversion of CO by NO. Therefore, for $\lambda \leq 1$ it is concluded that above 200°C the inhibition of NO conversion activity by O₂ is negligible since the net concentration of O₂ is very small.

Since the CO - O₂ reaction is fast, and, from Figure 6.10, the "H" activity curves (for NO) for the $\lambda < 1$ and $\lambda = 1$ cases are in the same place even though the net CO concentration (CO less 2*O₂) is varied (from 10% at $\lambda = 0.2$ to 2% at $\lambda = 1$), it follows that, for the results on the H trend, the rate of conversion of NO is

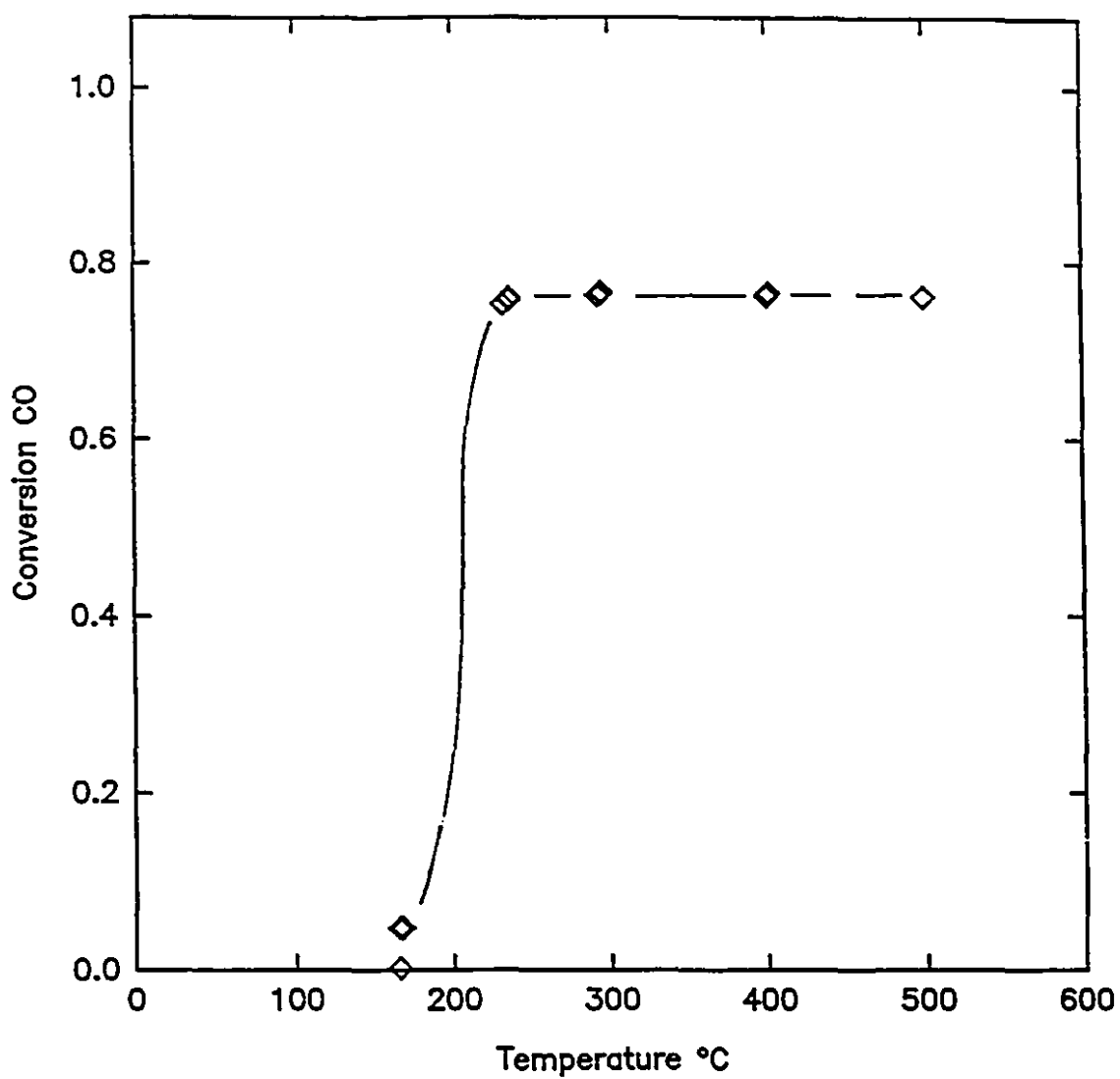
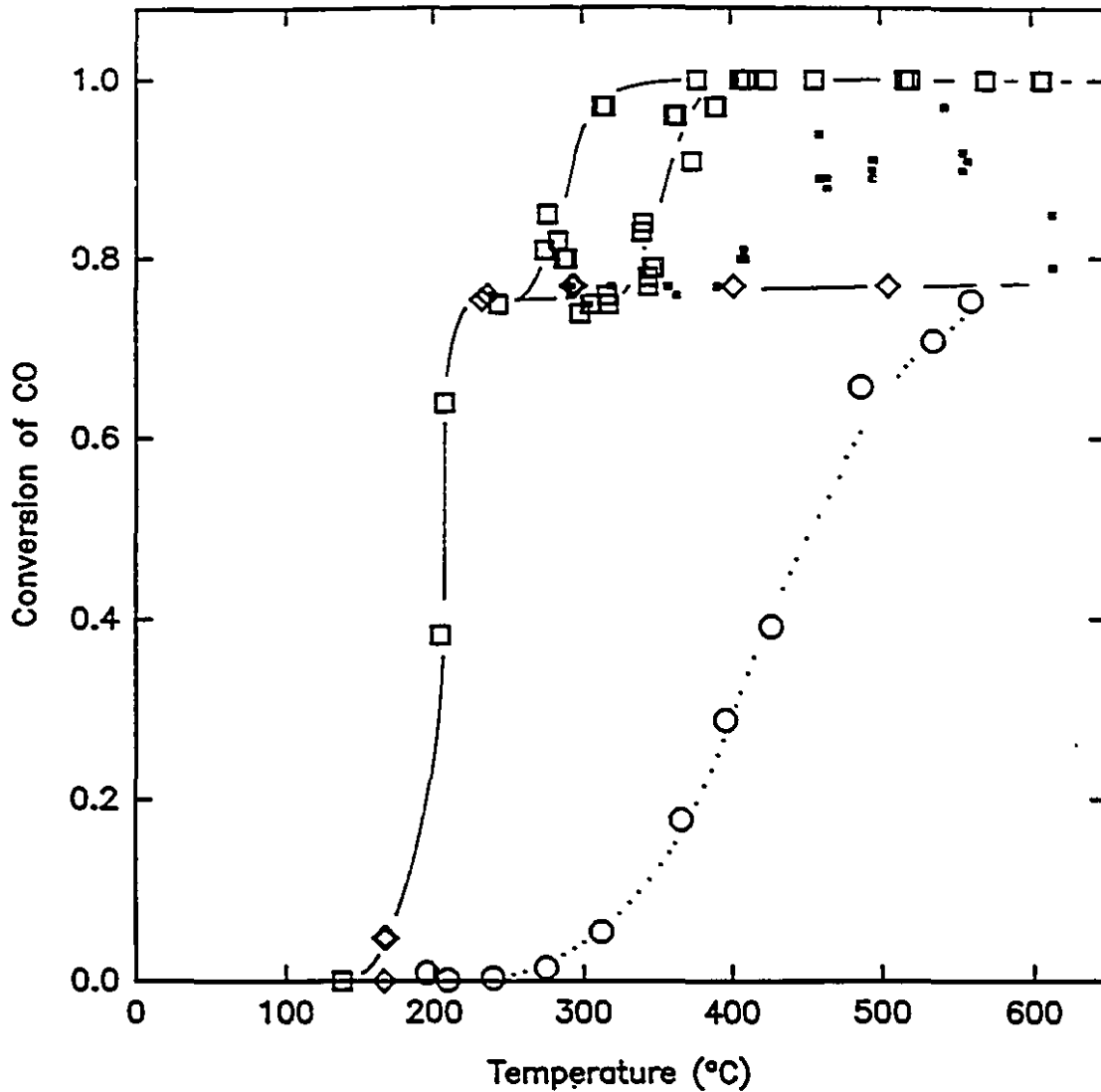


Figure 6.18 Conversion of CO by O₂
(Feed: 10% CO, 4% O₂, balance Ar and He)



- 10% CO, 2% NO, 4% O₂; New Catalyst
- 10% CO, 2% NO, 4% O₂; Deactivated Catalyst
- ◇ 10% CO, 4% O₂; (No NO)
- 10% CO, 4% O₂; (No NO, No Catalyst)

Figure 6.19 CO conversion for comparison with the $\lambda = 1$ case

independent of the CO concentration. In contrast, the location of the L curve varied with the change in the net CO concentration.

The independence of the H curve and dependence of the L curves on the net CO concentration are consistent with the mass-transfer-limitation hypothesis for the multiple steady states of the NO activity presented in Section 6.2.1. For $\lambda \leq 1$, the feed NO concentration is constant at 2%, and NO is the limiting reagent. It is therefore likely that if the reaction is occurring in a diffusion-control regime that the overall rate would be independent of the CO concentration. If the reaction was progressing in the reaction-controlled regime, then it is likely that the CO concentration would affect the rate, and therefore, the location of the L curve.

6.4 Characterization of Virgin and Used Cu-ZSM-5

The Cu-ZSM-5 from Allied Signal was characterized by elemental analysis, and X-ray diffraction. The results obtained using untreated Cu-ZSM-5 powder and oxidized, reduced, and deactivated catalyst samples are compared. The oxidized sample was fresh catalyst conditioned under 20% O₂ for 120 hours at 600°C, the reduced sample under 20% CO for 120 hours at 600°C, and the deactivated catalyst, originally treated under helium for 12 hours, was used in experiments totalling 60 hours at $\lambda = 1$, at 200 to 600°C. In all three cases the conditioning of the catalyst was lengthy: the deactivated catalyst was exposed to reaction conditions for the equivalent of over three full length experiments, and the other samples were conditioned for much longer than the usual 12 hours.

6.4.1 Chemical Analysis of the Cu-ZSM-5

The four samples were analyzed for their Si, Al, and Cu content; the results of the analysis are presented in Table 6.2. The oxidized and reduced samples proved to be virtually identical and the results from the deactivated sample are also very close. Relative to silicon, all three samples showed lower aluminum content compared to the original Cu-ZSM-5. The reduced and deactivated samples also showed a lower copper content, relative to silicon. In both cases, the deactivated

Table 6.2 Elemental Analysis of Cu-ZSM-5 Samples:

	Original	Deactivated	Reduced	Oxidized
Composition:				
by Weight (%)				
Al	1.48	1.41	1.38	1.40
Cu	3.80	3.88	3.74	3.96
Si	38.1	42.5	40.8	41.8
by Atomic Ratio:				
Al	1	1	1	1
Cu	1.09	1.13	1.19	1.20
Si	24.7	29.0	28.4	26.7
Exchange Level (%)	218	226	238	240

sample had larger loss than the other two heat treated samples. The losses also caused a lowering of the exchange level, due to the higher loss of copper. These higher losses are especially significant when the lower average temperature and shorter treatment time of the deactivated sample is considered.

6.4.2 Crystallographic Analysis of the Cu-ZSM-5 by X-ray Diffraction

The X-ray diffraction pattern obtained using the raw Cu-ZSM-5 powder is reproduced in Figures 6.20 and 6.21. Superimposed on the pattern are data indicating the location and relative intensity of major peaks from JCPDS XRD file data that match closely. The data from files 37-359 and 37-361 are from diffraction patterns of H-ZSM-5 and Na-ZSM-5 respectively. The coincidence is excellent. It is of interest that the only area of noticeable difference between the two reference data sets is in the location of the peak at $2\theta \cong 24^\circ$. In the H-ZSM-5, the peak is located about $\frac{1}{3}$ of one degree higher than for the Na-ZSM-5. There is also a slight difference in the location of the same peak in the Cu-ZSM-5 pattern, suggesting the exact location is due to the exchanged cation.

The patterns obtained using the deactivated, oxidized and reduced samples are presented in Figure 6.22 along with the pattern from the original Cu-ZSM-5. As with the elemental analysis, the crystallographic analysis provided clear evidence of a physical change associated with the deactivation. Only the deactivated sample shows a significant deviation from the original. Figure 6.23 shows the patterns of the three samples superimposed over the original Cu-ZSM-5. Figures 6.24 and 6.25 show greater detail of the difference between the original and the deactivated samples. In particular, there is significant relative growth of the peaks at 2θ 's of 7.86, 8.74, and 26.56 ($d_a = 11.24, 10.11, 3.35$) and a relative decrease at 2θ 's of 23.0, 23.2, 23.6, 23.8, 24.3, 24.7, and 29.2 ($d_a = 3.86, 3.82, 3.76, 3.72, 3.65, 3.59,$ and 3.06).

The 2θ angles where changes in relative peak intensity occurred were compared to angle locations from patterns filed with the JCPDS for various forms of silicon oxide and aluminum oxide, but no matches were found. Comparisons were

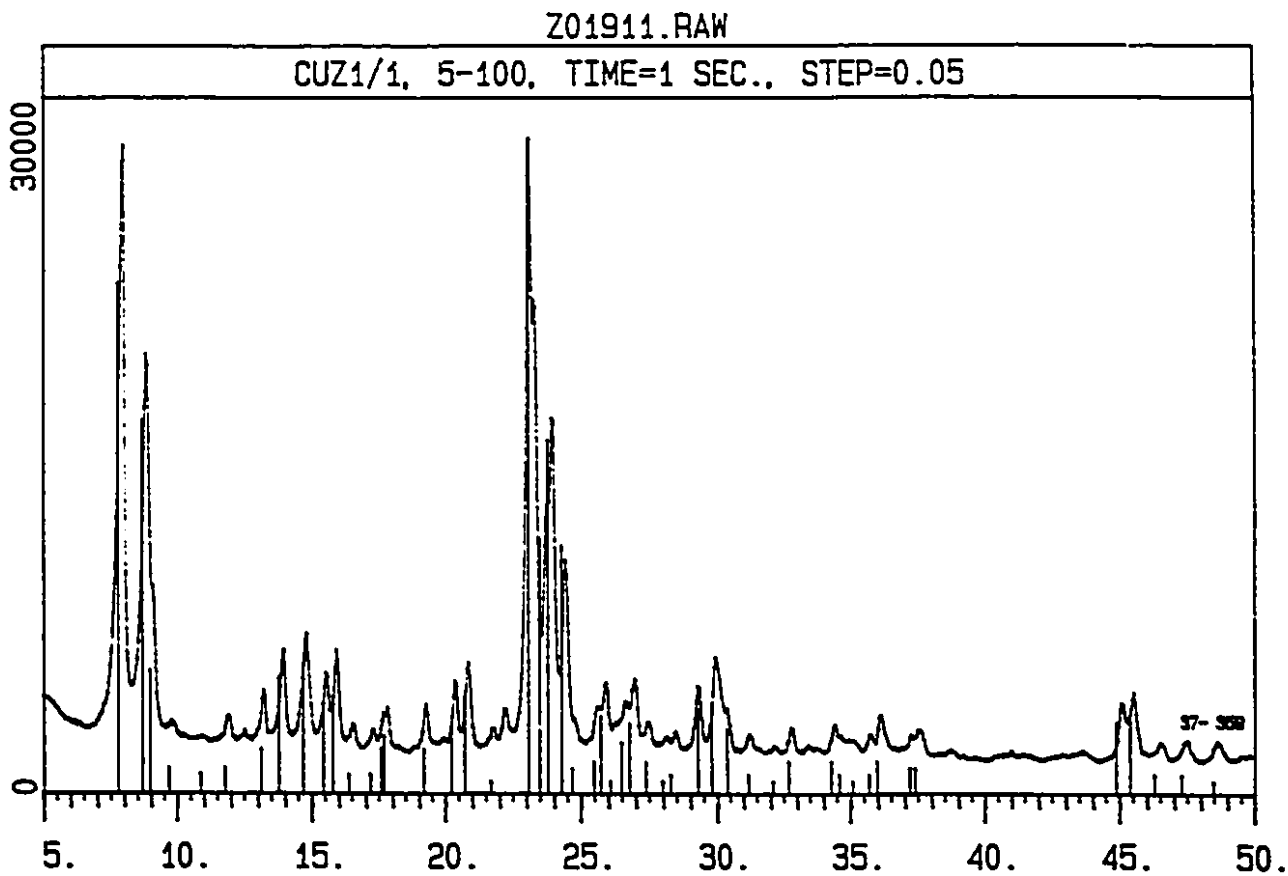


Figure 6.20 X-ray diffraction pattern of virgin Cu-ZSM-5, with H-ZSM-5 reference data

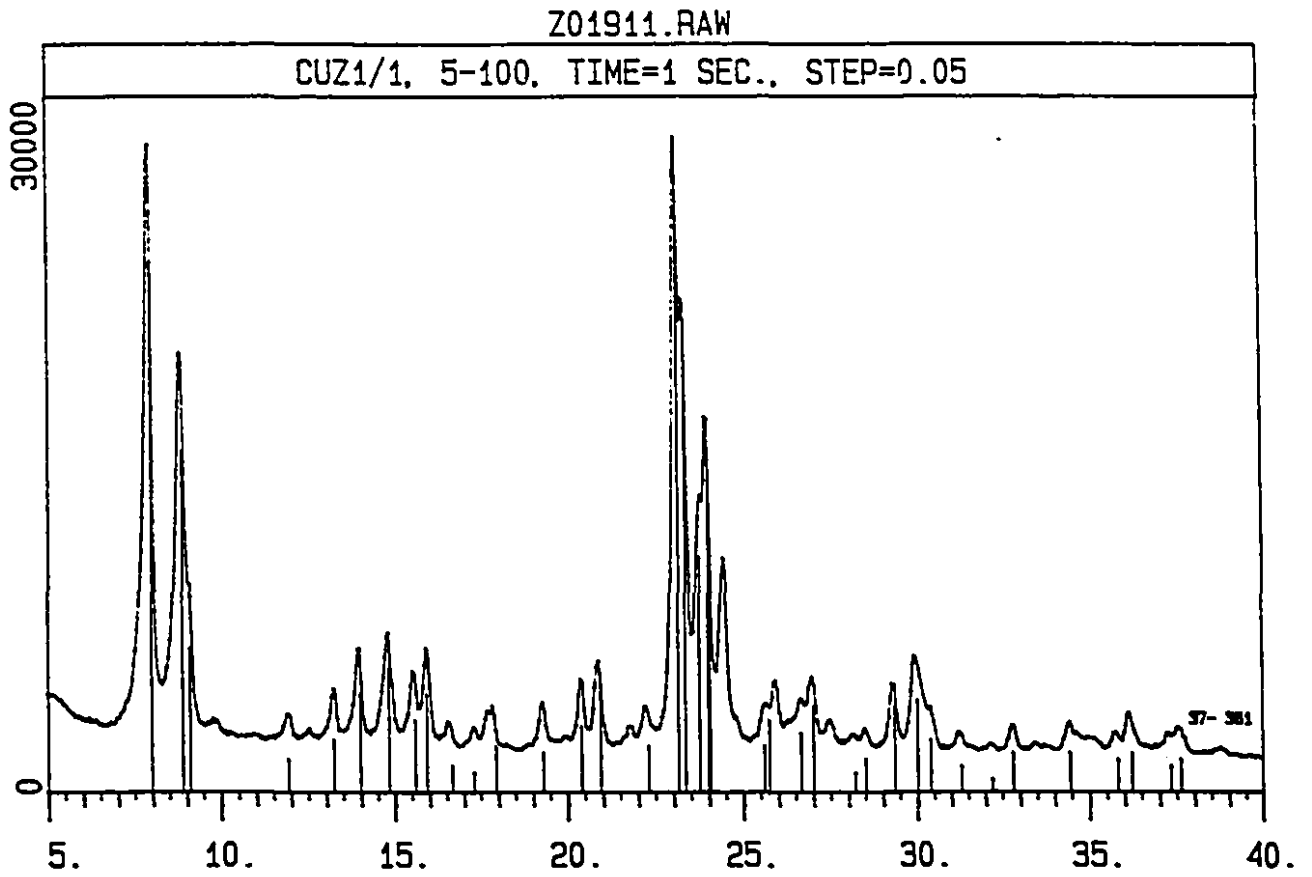


Figure 6.21 X-ray diffraction pattern of virgin Cu-ZSM-5, with Na-ZSM-5 reference data

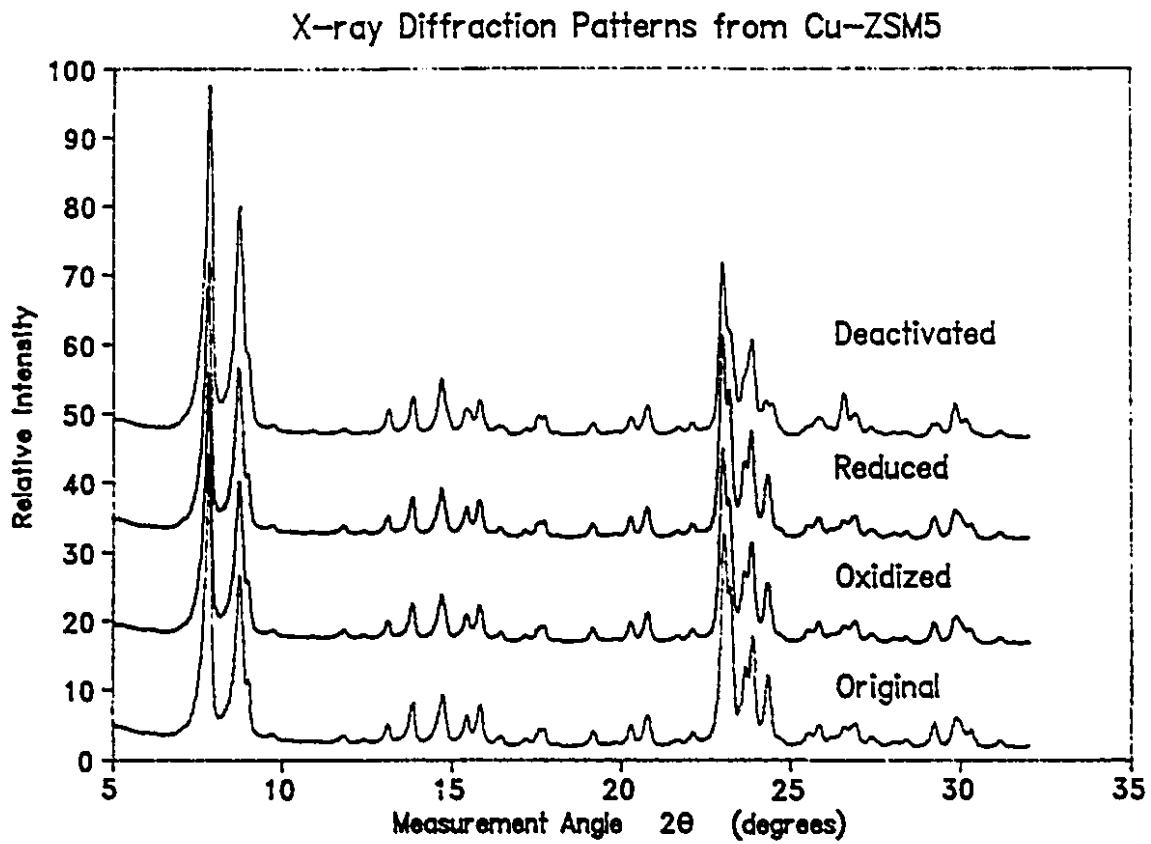


Figure 6.22 X-ray diffraction patterns:
Untreated, reduced, oxidized, and spent Cu-ZSM-5

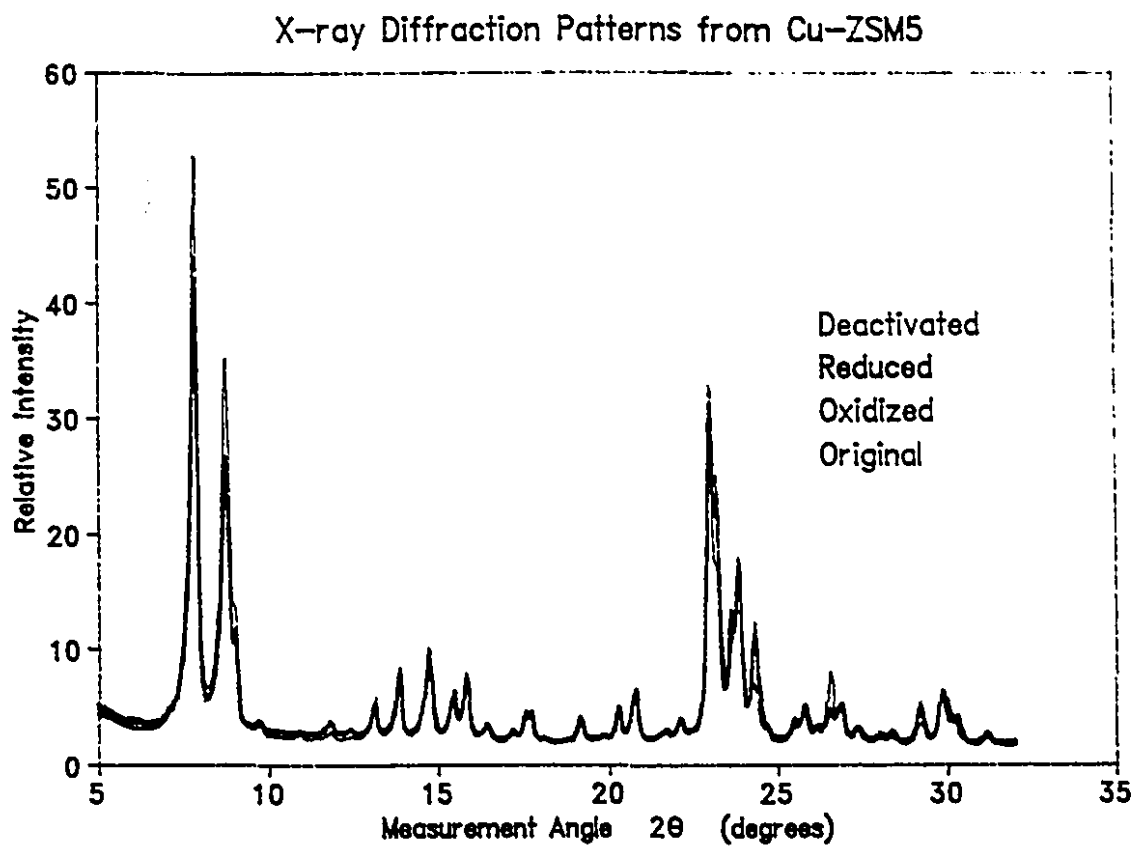


Figure 6.23 X-ray diffraction patterns:
Untreated, reduced, oxidized, and spent Cu-ZSM-5

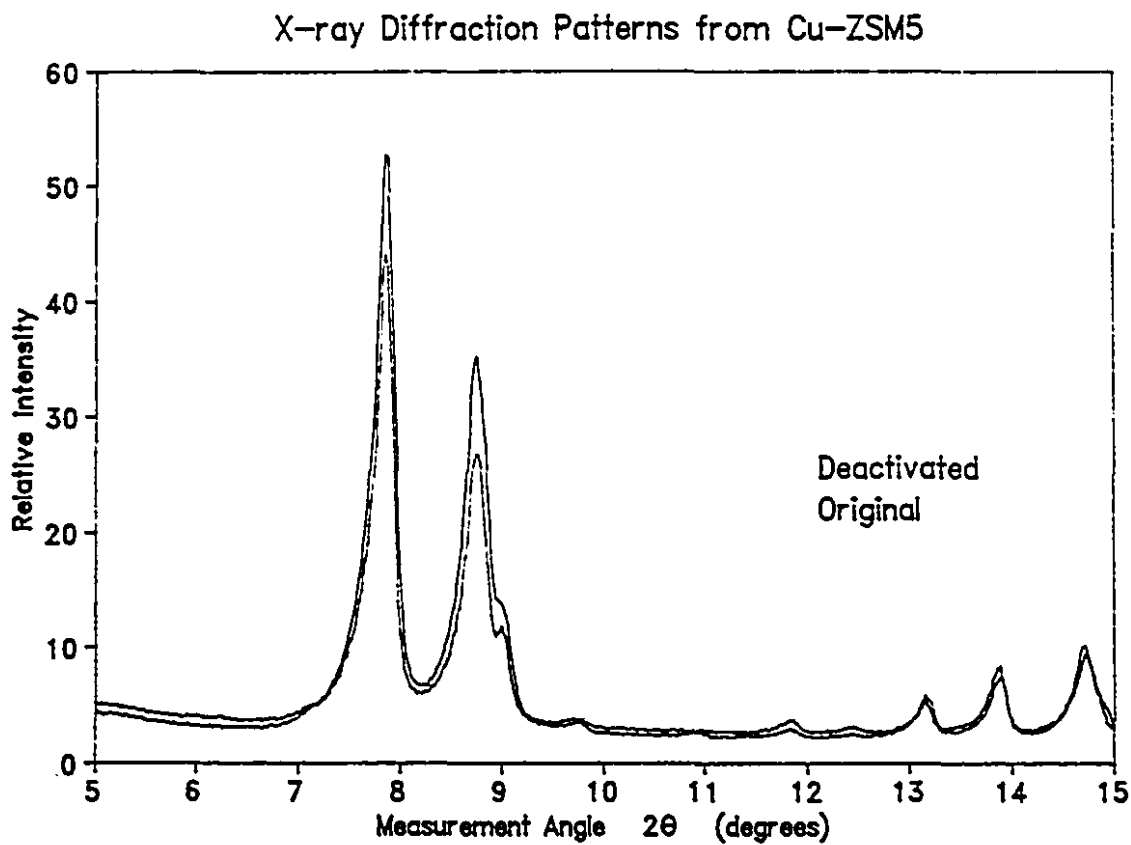


Figure 6.24 Partial x-ray diffraction pattern:
Untreated and Spent Cu-ZSM-5

X-ray Diffraction Patterns from Cu-ZSM5

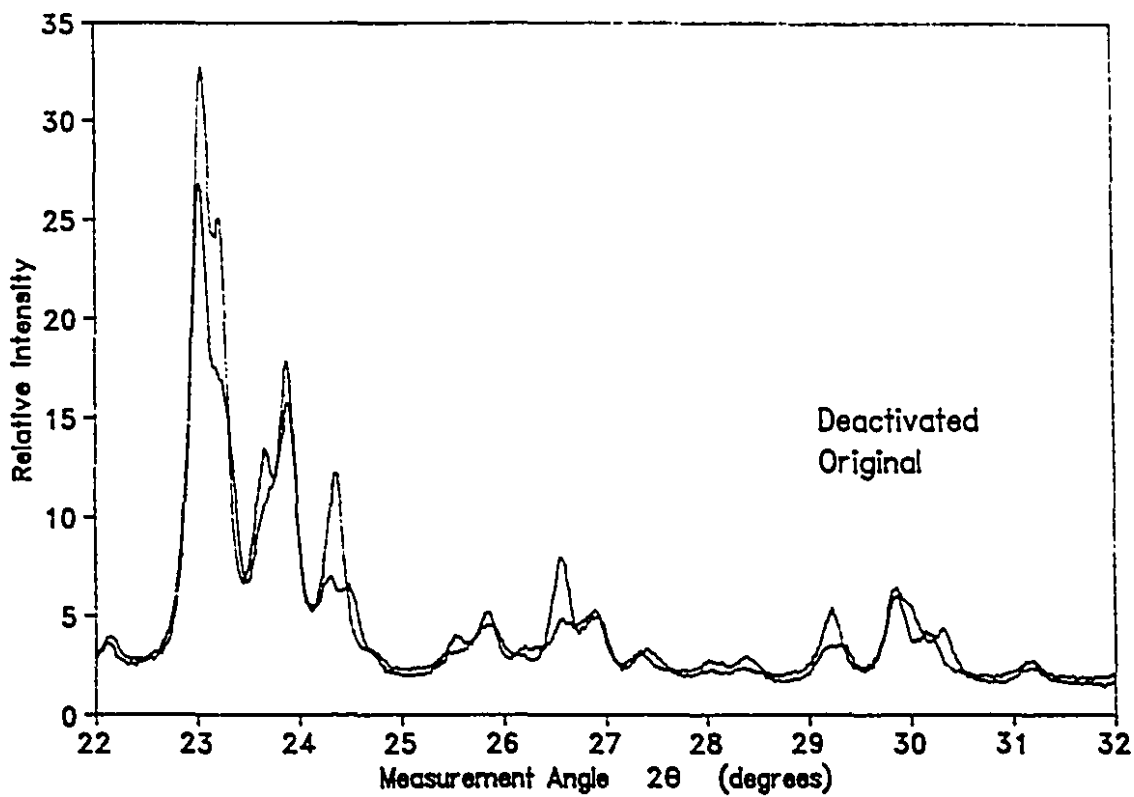


Figure 6.25 Partial x-ray diffraction pattern: Untreated and spent Cu-ZSM-5

also made to file data for the various copper oxides but there were no observed similarities with any of these patterns either.

6.5 Redox State and Observed Colour of the Cu-ZSM-5

In the course of this work, the Cu-ZSM-5 catalyst exhibited a wide variety of colours, which were observed after each experiment. These observations lead to further review of the literature for similar findings. As mentioned in Section 3.2, Sárkanáy *et al.* observed many colours on the Cu-ZSM-5: green; white; red/purple; white/red; and tan, on Cu-ZSM-5 that had been: fresh; degassed (under Ar); reduced under H₂; reduced under CO; and re-oxidized by O₂, respectively (Sárkanáy *et al.*, 1992).

In the current work, the catalyst as fresh, activated under O₂, or treated with pure NO was green; conditioned under helium, it was white or grey upon cooling; conditioned under CO, it was light purple when cooled. After being activated under helium and exposed to reaction mixtures it reached a variety of colours. Table 6.3 lists the colours, observed after the catalyst was cooled, for the various conditioning (activating) and experimental conditions.

When colour divisions were occurred, they were very precise. In the $\lambda = 0.2$ case the division was half way through the catalyst bed, indicating that the oxidizer, NO, was present (in significant amount) until at least this point. The Cu was thus not reduced until the gas is strongly net reducing, since the feed was already net reducing. For the cases of $\lambda > 0.2$ there was less purple. When the catalyst batches were re-used without unloading the reactor, bands of colour (of those listed above) were observed.

Consistent with the results from the tests of the effect of the catalyst conditioning (Section 6.2.5), it was observed that neither the green nor the purple colour was indicative of any change in catalyst activity; in the conditioning tests the catalyst was initially all green, all white, or all purple, and all of the samples showed the same activity. The deactivated samples, however, all were, at least in part, tan or light brown in colour, the colour Sárkanáy *et al.* observed upon re-oxidation of

Table 6.3 Colour of the Cu-ZSM-5 Under Various Conditions:

Feed Gas Composition (per cent)			Lambda	Colours Observed in the Catalyst Bed
NO	CO	O ₂	λ	C A T A L Y S T B E D ← upstream end downstream end →
0	20	0		Purple·Purple·Purple·Purple·Purple·Purple·Purple
0	0	0		¹ Grey·Grey·Grey·Grey·Grey·Grey·Grey·Grey·Grey
0	0	20		² Green·Green·Green·Green·Green·Green·Green·Green
2	10	0	0.2	Green·Green·Green·Green Purple·Purple·Purple
2	10	< 4	< 1	Green·Green·Green·Green·Green Purple·Purple·P
2	10	4	1	³ GG·GG·GG·GG Grey·Grey·Grey·Grey·Grey P
2	10	> 4	> 1	⁴ GT·GT·GT·GT GB·GB·GB·GB·GB·GB P

Colour Codes:

P = Purple
 GG = "Greenish Grey"
 GT = "Greenish Tan"
 GB = "Greyish Brown"

Notes:

1. Activated with pure helium or argon.
2. Samples previously reduced (with CO) became light grey upon re-oxidation by O₂.
3. A very thin band of purple was at the end of the sample beds. Brown, tan, and olive green were sometimes observed, especially after multiple experiments.
4. Specks of purple were observed at the end of the bed, even in the case for $\lambda = 1.3$.

the Cu-ZSM-5. Combined with the stability of activity for the NO decomposition reported in the literature (Iwamoto *et al.*, 1989), this result suggests that it is reduction of the catalyst by CO and subsequent reoxidation that is involved in the deactivation of the catalyst.

In general, the results obtained by Sárkanáy *et al.* were confirmed in this work, except that tan colour obtained upon re-oxidation was only observed with the NO mixtures and not with the re-oxidation by O₂ as Sárkanáy found, and that a wider range of shades was observed in this work than Sárkanáy reported. These discrepancies may be due to a subjective view of the difference between various shades of grey, green, and tan.

Chapter 7

Conclusions and Recommendations

7.1 Conclusions

The objectives of the research project were met, and significant obstacles overcome. An existing gas handling system was substantially modified, with improvements made to the general versatility of use, and to the accurate metering of gas feed mixtures. An analytical system, based on the accurate GC measurement of N_2 , Ar, CO, and CO_2 (and, under reducing conditions, NO) and the qualitative measurement of NO and O_2 was successfully developed. The exact conversion of NO to N_2 , and qualitative conversion of NO to other oxides of nitrogen as NO_2 was measured. The method is more accurate and versatile than other GC methods reported in the literature. An extrusion method for the pelletization of Cu-ZSM-5-218-25 powder was developed, and the activity of the pellets was measured.

The activity of the fresh catalyst was found to be independent of the redox nature of the activating gas. For equivalence ratio's of 1 or less, the activity was found to be 100% for the space velocity tested. The activity of the traditional platinum-group metal three-way catalyst at an equivalence ratio of 1 was essentially the same, at 97%. For equivalence ratios of more than 1, however, the activity of the Cu-ZSM-5 was significantly greater than that of the three-way catalyst; for example, 53% compared to 26% at an equivalence ratio of 1.3.

The Cu-ZSM-5 was found to loose activity after 20 to 30 hours of use, resulting in almost complete deactivation after 60 hours of use. Upon regeneration attempts with Ar, CO, and O_2 , no improvement in activity was found. The

deactivation was accompanied by a loss of both copper and aluminum, changing both the Si/Al and exchange ratios: the fresh Cu-ZSM-5-218-25 became Cu-ZSM-5-226-29. The crystal structure, as observed by x-ray diffraction, of the virgin, oxidized, and reduced Cu-ZSM-5 varied little, but the deactivated Cu-ZSM-5 showed significant differences in the relative size of peaks and in the existence of some peaks, especially in the region about $d_p = 3.6$, where the (Cu²⁺, H⁺, and Na⁺)-ZSM-5 patterns differed significantly. The loss of activity was thus related, at least in part, to a change in the state of the exchanged cation, Cu. Because of the loss of activity of the Cu-ZSM-5, it cannot be recommended for use as an NO reduction catalyst.

7.2 Recommendations for Future Work

Future research in this area should include a search for promoters to improve the stability of the Cu-ZSM-5 formulation, or for compounds similar to Cu-ZSM-5, but with better stability. Further work with the same experimental system should be preceded by physical improvements allowing for the accurate use of high flow rates of mixtures with lower reaction component concentrations to allow for better simulation of exhaust gas. The analytical system should be improved with either the addition of an extra GC column and bypass capability to allow for better separation of oxygen and argon (on a molecular sieve packing), or with separate means for the measurement of nitrogen oxides and oxygen, such as chemiluminescence spectroscopy and paramagnetic susceptibility.

If an improved catalyst formulation is found, intrinsic rate law determination through differential conversion measurements should be made, and activities for the reduction by hydrocarbons typical of exhaust gas should be measured.

Appendix A Mass Flow Controller Calibration

The calibration curves for the mass flow controllers were linear within the range used for the experiments:

S = Setting
R = Display output (reading)
F = Flow rate (cm³/min at 25°C and 1 atmosphere)

MFC 1 FC-260 (#S/N 8082240)

NO/Ar mix:	R	=	0.017333 * F	- 0.00906
	F	=	57.69208 * R	+ 0.5225
	S	=	0.163433 * F	- 4.44531
	F	=	0.163433 * S	+ 0.727852

MFC 2 FC-260 (#S/N 8092011)

O ₂ :	R	=	0.025770 * F	- 0.00325
	F	=	38.80514 * R	+ 0.126232
	S	=	8.596581 * F	- 1.66677
	F	=	0.116325 * S	+ 0.193888

MFC 3 FC-260 (#S/N 8082233)

CO:	R	=	0.030469 * F	- 0.04696
	F	=	32.82060 * R	+ 1.541294
	S	=	10.97515 * F	- 21.322
	F	=	0.096431 * S	+ 1.931606

Ar or He:	R	=	0.022065 * F	- 0.05208
	F	=	45.32090 * R	+ 2.36026
	S	=	7.352113 * F	- 16.5932
	F	=	0.136015 * S	+ 2.256935

MFC 4 FC-280 (#AW 703007)

Ar or He:	R	=	0.006307 * F	- 0.03415
	F	=	158.5505 * R	+ 5.413966

(flow measurement only)

Appendix B Gas Chromatography Calibration

The calibration curves for the mole to area response of the GC detector were linear within the range used for all of the gasses except the NO:

m = moles of gas
a = area under TCD response curve

CO ₂	m	=	6.038e-14*a
N ₂ :	m	=	7.136e-14*a
O ₂ :	m	=	7.675e-14*a
Ar:	m	=	6.833e-14*a
CO:	m	=	7.003e-14*a
NO:	a	=	2.728e19*m ² + 1.489e12*m

With NO, column loading and other effects were observed:
(Hollow points not used for the regression or calibration)

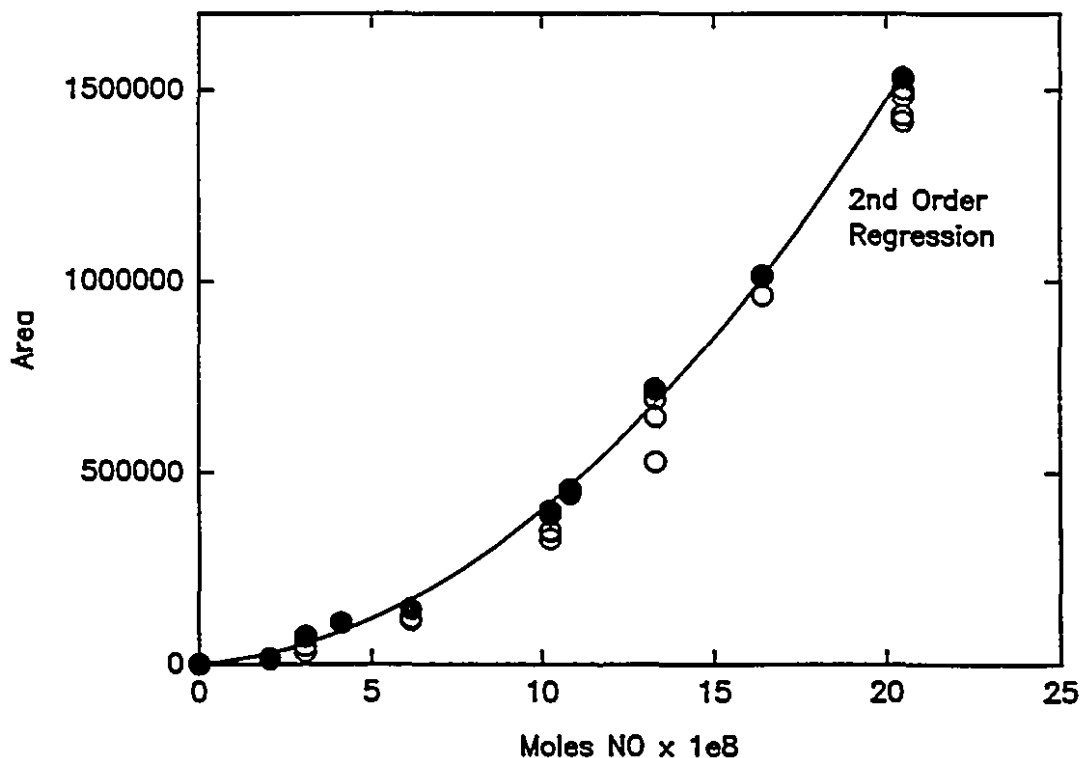


Figure A.1 GC Calibration Curve for NO

Appendix C Test For Mass Transfer Control

The effect of the change in carrier gas can be predicted using correlations presented in Smith (1981) and Geankoplos (1983). The mass transfer coefficient can be estimated from the j factor, which is a function of the Stanton and Schmidt numbers:

$$j_d = \frac{k_m \rho}{G} \frac{a_m}{a_t} \frac{\mu}{\rho D} \quad (\text{A.1})$$

The j -factor can be estimated from the correlation:

$$j_d = \frac{0.455}{\epsilon_B} \left(\frac{d_p G}{\mu} \right)^{-0.407} \quad (\text{A.2})$$

Where:	a_m	=	effective mass transfer area of pellet
	a_t	=	total external area of pellet
	D	=	molecular diffusivity of the species being transferred
	d_p	=	effective diameter of the pellet
	G	=	mass velocity ($G=\rho u$), where u =superficial velocity
	k_m	=	mass transfer coefficient
	ϵ_B	=	void fraction of the catalyst bed
	μ	=	viscosity of the gas
	ρ	=	density of the gas

Combining the equations and solving for k_m :

$$k_m = \frac{0.455}{\epsilon_B} \frac{a_t}{a_m} d_p^{-0.407} G^{0.593} \mu^{-0.2597} \rho^{-0.3333} D^{0.6667} \quad (\text{A.3})$$

Therefore, if all else is held constant:

$$k_m \propto \rho^{0.2597} \mu^{-0.2597} D^{0.6667} \quad (\text{A.4})$$

The diffusivity, D , may be estimated for the each species in each carrier gas according to the Fuller correlation:

$$D = \frac{1 \times 10^{-7} T^{1.75} \left(\frac{1}{m_a} + \frac{1}{m_b} \right)^{1/2}}{P (v_a^{1/3} + v_b^{1/3})^{1/2}} \quad (\text{A.5})$$

Where: T = temperature in K
 P = pressure in atm.
 m_a = molecular weight of species a
 v = molecular diffusion volume

For either reactant species, CO or NO, the ratio of k_m in helium over k_m in argon may be calculated. For NO the ratio is:

$$\frac{k_{m \text{ He}}}{k_{m \text{ Ar}}} = \left(\frac{\mu_1}{\mu_2} \right)^{-0.2597} \left(\frac{\rho_1}{\rho_2} \right)^{0.2597} \left(\frac{D_1}{D_2} \right)^{0.6667} \quad (\text{A.6})$$

$$\frac{k_{m \text{ He}}}{k_{m \text{ Ar}}} = \left(\frac{3.6 \times 10^{-5}}{4.6 \times 10^{-5}} \right)^{-0.2597} \left(\frac{0.06}{0.6} \right)^{0.2597} \left(\frac{3.69 \times 10^{-4}}{1.03 \times 10^{-4}} \right)^{0.6667} \quad (\text{A.7})$$

$$= 1.4$$

(μ in kg/(ms), ρ in kg/m³, D in m/s)

The ratio is also about 1.4 for CO. Therefore, if the diffusion of one of the reactants to the pellet surface was the rate limiting step, then by switching the carrier gas to helium from argon the rate should have increased by 1.4 times.

If, instead of changing the diluent gas, G had been doubled, then k_m (and the rate) should have risen by a factor of 1.5 ($k \propto G^{0.593}$; $1.5 = 2^{0.593}$) under mass transfer control.

Appendix D Survey of Analytical Methods

The gases expected in the NO - CO - O₂ reaction system were NO, NO₂, N₂, O₂, CO, CO₂, and inerts (argon and/or helium diluent). N₂O was not likely to appear in significant amounts, but adaptability to its measurement was desired. Flexibility for the future measurement of NH₃ and light hydrocarbons was also deemed important. The use of helium as a diluent was an option, but it was recognized that the direct measurement of both helium and argon at the same time was unlikely.

A gas chromatograph (GC) fitted with a thermal conductivity detector (TCD), two columns, and an actuated bypass valve to allow for programmed bypass of the second column was available, but an initial study of the literature suggested that the measurement of NO by GC would be difficult, and that the measurement of NO₂ would be nearly impossible. The separation of O₂ and Ar by GC is also known to be difficult, necessitating the use of extreme conditions. With these problems in mind a survey of alternate methods of analysis was undertaken. This section is a summary of the findings.

Previously reported methods of analysis of the expected gasses include a wide range of techniques. The methods covered include wet chemical analysis, mass spectroscopy, infra-red spectroscopy (IR, FTIR), chemiluminescence spectroscopy, GC, and other miscellaneous means. The determination of nitrogen oxides is of the greatest difficulty and is discussed at greater length.

D.1 Wet Chemical Methods

Specifically considered for the measurement of NO and NO₂, most of these methods date back decades, yet none are satisfactory over a wide range of input conditions. Most were originally developed for use in measuring high concentrations of nitrogen oxides, as would be found in nitric acid plant tail gas. All have poor reproducibility and are slow and labour intensive. (Margeson *et al.*, 1980 ; Miyamoto *et al.*, 1979; Fisher and Becknell, 1972 ; Faucett *et al.*, 1966; Saltzman, 1954; Johnson, 1952)

D.2 Mass Spectroscopy

Sector and quadrupole mass spectrometers are commonly used for analyzing nitrogen oxides containing mixtures. The results are fast and the device can be used on line to measure all of the reaction components. Interpretation of the results involves solving mass balances which for complicated mixtures may be impossible, due to the cracking of the gasses being measured, particularly NO, NO₂, and N₂O. Because of the cracking, some researchers use chemiluminescence spectroscopy in addition to mass spectroscopy to measure NO_x. A fundamental drawback of the use of this tool is its expense; however it is probably the most accurate method available for the measurement of the other components in the reaction mixture. (Li and Hall, 1991 and 1990; Papolymerou and Schmidt, 1985; Izuka and Lunsford, 1980; Jansen and van der Kerkhof, 1979; Otto et al, 1973 and 1970)

D.3 Infrared Spectroscopy and UV Absorption

Fourier transform infra-red spectroscopy (FTIR) is convenient because several components in one sample can be easily analyzed by scanning at different wavelengths and the device can also be used on line. Noble gasses and homopolar diatomic gasses cannot be measured. NO and NO₂ can be measured, but complications arise due to changes in the oxidation state of NO and the phase (gas or liquid) of NO₂. Window degradation due to the corrosive natures of NO₂ and its liquid dimer can be a problem. The technique may be improved by its use in conjunction with an ultraviolet analyzer to determine NO₂. Most researchers have abandoned the use of IR and UV absorption for the measurement of NO_x, but IR is still a popular tool for the measurement of CO and CO₂. (Muraki *et al.*, 1986; Kim, 1982; Courty *et al.*, 1980; Bauerle *et al.*, 1978; Kudo *et al.*, 1978; Matsuda *et al.*, 1978; Bartholomew, 1975; Walker, 1974; Klimisch and Taylor, 1972)

D.4 Chemiluminescence Spectroscopy.

With the exception of M.S., these instruments cover the widest range of NO concentration. With an optional converter, the total NO_x (NO + NO₂) can also be determined, and, if present, NH₃ can also be measured by means of an additional converter. Nitrous oxide cannot be measured by chemiluminescence. (Blanco *et al.*, 1986; Kato *et al.*, 1981; Shikada *et al.*, 1981; Courty *et al.* 1980; Jansen and van der Kirkhof, 1979; Bauerle *et al.*, 1978; Klimisch and Taylor 1972)

D.5 Gas Chromatography

Chromatography has been used extensively to analyze mixtures containing nitrogen oxides as well mixtures of the "permanent" gasses Ar, O₂, and N₂. The isolation of the heavier components N₂O and CO₂ by GC is straightforward. In contrast, NO₂ cannot be measured using ordinary techniques and must be trapped out prior to the analysis. Because different target gasses within the sample require different approaches with GC, it has often been used in conjunction with other techniques, especially for the analysis of automobile exhausts and other complex mixtures.

Zeolite column packings, such as Molecular Sieve 5A are commonly used to separate mixtures containing O₂, N₂, H₂, and CO. Ar and O₂ can be separated at -80°C, although N₂ is permanently adsorbed at this low temperature. NO and O₂ cannot be measured simultaneously because they react on the column if present together. Poor reproducibility and serious tailing of the NO peak are known to occur, and CO₂ is permanently adsorbed under normal operating conditions. Water vapour in the sample will cause irreversible deterioration by gradually damaging the structure of these solids, so these columns cannot be exposed to water-containing samples or ambient air for long durations.

Porous polymers can be used for separations of NO mixtures, and are often chosen for their ability to resolve both CO₂ and N₂O. The separation of permanent gasses on porous polymers has been studied extensively; however for the separation of O₂ and Ar low temperatures and very long columns are needed.

To overcome the limitations and problems associated with individual packings, exhaust analysis is often done using dual column arrangements. (Hayes, 1992; Novkikov and Saskovets, 1991; Li and Hall, 1991 & 1990; Willey *et al.*, 1985; Hardee and Hightower, 1984; Yang, 1982; Hecker and Bell, 1981; Izuka and Lunsford, 1980; Bauerle *et al.*, 1978; McCandles and Hodgson, 1978; Arakawa *et al.*, 1977; Peters and Wu, 1977; Clay and Lynn, 1975; Walker, 1974; Amirmazmi *et al.*, 1973; Ayen and Amirmazmi, 1973; Jamieson, 1971)

D.6 Miscellaneous Techniques

Gas sensitive electrodes can be used in either the gas or liquid phase for both NO₂ and O₂ measurement. For NO measurement, ozonation of the sample stream is needed to oxidize the NO to NO₂. The results are accurate over only a limited range of concentrations, and the electrodes have a poor response times. The NO₂ gas sensing electrode (based on the nitrate specific-ion electrode) used to be on the market, but it is not now commercially available due to its limited use. The nitrate specific-ion electrode can be used to measure dissolved NO₂, but as would be expected, it suffers from interference from other volatile weak acids, in particular CO₂. In some cases, specific-ion electrodes can be used in combination with the wet chemical methods, speeding up the wet analysis somewhat. Oxygen electrodes also suffer from interference.

Paramagnetic susceptibility meters are often used for O₂ analysis of NO_x containing mixtures. Analysis of the measurement output would have to take into account the levels of nitrogen oxides present, as they are also paramagnetic, although less so than O₂ which has two unpaired electrons per molecule. Solid state sensors for NO and O₂ are less reliable and non-specific.

Flow colorimetry has been used to measure NO₂ in complex mixtures. The meters have a long residence time during which additional amounts of NO₂ tend to form from NO and O₂, skewing the results.

A volumetric analysis of NO₂ was reported wherein a cold trap downstream of the reactor captured the NO₂. It was subsequently transferred to a stainless steel

vacuum system and the pressure measured with a high accuracy Baratron pressure gauge after the temperature was set. (Li and Hall, 1991 & 1991; Mass *et al.*, 1986; Naruse *et al.*, 1980. Kiyomia and Kawai, 1979; Bauerle *et al.*, 1978; Di Martini, 1972; , Anderson *et al.*, 1961)

Appendix E GC Column and Program Selection

Several combinations of packing material and column length were tested with varied temperature programs for use in analyzing the gas mixtures. All of the columns tested were of standard 1/8 inch (3.18 mm) o.d. stainless steel with packings of 80/100 mesh size. The first combination, commonly in use for similar applications involving the analysis of stack gasses, had a 4 foot (1.2 m) column of Porapak QS (QS) followed by the bypass valve and then 3 feet (0.9 m) of Molecular Sieve 5A (MS5A). According to the sales literature and published results, the QS should have been able to separate the CO₂ and oxides of nitrogen, and the molecular sieve the CO, N₂ and O₂-with-Ar at room temperature. No separation of NO from the "permanent" gasses (N₂, Ar, O₂) and CO was observed with the QS. The molecular sieve was able to separate the NO from Ar at temperatures nearing ambient. For 100 µl of 4.98% NO in Ar, the peak-to-peak separation was 0.72 minutes at 30°C. Unfortunately, the molecular sieve also separated the N₂ from Ar/O₂ at a similar rate, thus giving no resolution of the NO and N₂ peaks.

An additional eight feet of porapak QS column was purchased in order to improve the separation of the NO from N₂. With twelve feet of this column only a very poor separation was achieved; the two peaks were almost completely merged. A further difficulty was encountered when repeated calibration of the NO using the MS5A revealed that reproducible area *versus* sample size results were not being achieved, particularly for small samples. This was partly due to severe tailing, as is consistent with reports from Amirnazmi et al. (1973), Walker (1974), and Yang (1982).

Various cooling configurations were tested to achieve better separation. 0°C (ice) and -18°C (saturated salt/ice) baths were employed with the three columns used alone or in combination. With 12 feet of QS at -18°C four peaks were found: In order, they were N₂, O₂/Ar/CO as one peak, NO, and much later CO₂ at retention times of about 2.19, 2.51, 2.98, and 25.41 minutes, respectively. This was promising as it then seemed possible to have the N₂ and the O₂/Ar/CO pass through to the Molecular Sieve, switch the bypass valve to have the NO and CO₂ pass

directly to the detector and, after the measurement, return the valve so the N₂, O₂, Ar, and CO could be resolved on the MS5A and be measured. However, the pressure swing and flow adjustment associated with each change of the valve position was picked up by the detector. The change in the TCD response lasted about 1 minute and it interfered with the measurement of the following peak. As there was little time separation between the O₂/Ar/CO and NO peaks, the NO peak could not be measured accurately with a valve switch in between them. The other option, of letting the NO through to the molecular sieve brought on the difficulty of the tailing which got worse at this lower temperature.

Further problems existed with the separation at -18°C. The CO₂ peak was very broad with a high area to height ratio, due to its long retention time of 26 min. This broadening resulted in poor reproducibility. In addition, the N₂ which entered the molecular sieve as the lead gas was the slowest gas to pass through this column, and as such it exited with and interfered with the measurement of the CO, often spoiling the analysis of both gasses. A better program was developed with the N₂ bypassing the second column, the O₂/Ar/CO being passed on to the sieve, and finally the NO and CO₂ bypassing the sieve.

The program involved four valve switches, three during the separation and only two of which could be performed automatically by the GC. The problem of the valve switches interfering with the peak analysis still existed and the timing had to be perfect (within two seconds) to avoid cropping of the gas peaks. The potential for operator error was high, and the maintenance of the temperature at -18°C took constant attention. In effect, this program was usable but poor.

In an attempt to eliminate the effect of the valve interference, the GC was configured so that the recorded signal was actually the difference between the signal generated by the TCD for the current run and that of a previously recorded run. For the recorded run no sample was introduced, but the GC program, with valve changes, was conducted as usual yielding a chromatogram showing only the interference peaks. Ideally, a chromatogram generated by comparison to this recorded one would show all of the expected gas peaks but not the interference

peaks caused by the valve changes. In practice, however, the TCD response to the valve changes was not a constant, instead, it showed significant variation from run to run, even after maintenance work on the valve assembly. Furthermore, since one of the valve switches has to be made by the operator an additional error due to imperfect timing often existed. Because of these problems this tool could not be used effectively, and it was conceded that there was no way to eliminate the valve disturbances from the chromatograms.

After testing the MS5A and QS columns at -79°C (with a dry ice slurry) it was concluded that the major difficulties associated with the analysis at -18°C would be overcome. By introducing a new primary column to separate out the CO_2 at room temperature or higher and having the 12 feet of QS at this much colder temperature, the separation of the other gasses could be achieved. At this stage in the research it was also desired to measure CH_4 in addition to the other gasses - using the same column combination - for related work. Accordingly, Porapak Q was selected for the new primary column. Columns of the Haysep series of packings, made for permanent and light gas separation at room temperature were considered as new column alternatives, and would have eliminated the problems related to cryogenic work if used in the place of the second column (leaving the QS for the primary column), but an unreasonable length would have been needed to resolve the O_2 and Ar.

Appendix F Measurement of NO in the Product Stream in the Absence of O₂, and Calculation of x_{NO}

Comparison of the measured amount of NO from a product sample to the measured amount of NO in feed samples which were of known concentration and which were measured immediately before and after the product analysis gave accurate relative results. By averaging the results from the two feed injections, the drift of the measured NO peak size m_{NO} was taken into account. That is, even though

$$m_{NO} \neq n_{NO} \quad \text{and} \quad \frac{m_{NO}}{m_{Ar}} \neq \frac{n_{NO}}{n_{Ar}} \quad (\text{A.8})$$

it was observed that, after averaging,

$$\frac{\frac{m_{NO}^p}{m_{Ar}^p}}{\left(\frac{m_{NO}^f}{m_{Ar}^f}\right)} = \frac{\frac{n_{NO}^p}{n_{Ar}^p}}{\frac{n_{NO}^f}{n_{Ar}^f}} \quad (\text{A.9})$$

Using this equation, the conversion of NO was calculated:

$$x_{NO} = \frac{F_{NO}^f - F_{NO}^p}{F_{NO}^f} \quad (\text{A.10})$$

$$x_{NO} = 1 - \frac{\frac{m_{NO}^p}{m_{Ar}^p}}{\left(\frac{m_{NO}^f}{m_{Ar}^f}\right)} \quad (\text{A.11})$$

Likewise, the molar flow rate of NO in the product stream can be calculated:

$$F_{NO}^P = \frac{n_{NO}^P}{n_{Ar}^P} * F_{Ar} \quad (A.12)$$

$$F_{NO}^P = \frac{\frac{m_{NO}^P}{m_{Ar}^P}}{\left(\frac{m_{NO}^f}{m_{Ar}^f}\right)} * \frac{n_{NO}^f}{n_{Ar}^f} * F_{Ar} \quad (A.13)$$

and therefore, by Equation 5.6,

$$F_{NO}^P = \frac{m_{NO}^P}{m_{Ar}^P} * \left(\frac{m_{NO}^f}{m_{Ar}^f}\right)^{-1} * 0.0524 * F_{Ar} \quad (A.14)$$

A similar analysis of NO by GC was performed by Walker (1974). In his work NO concentrations were calculated from the ratio of the peak area from one sample to the peak area given by a sample of known concentration, usually from his reactor feed stream. No calibration was used, and a linear area-to-mole response was assumed. The reported accuracy of the method is "to within several percent," while the method used in this research yielded an agreement of within 2% of the values determined by the N₂ production. For Walker's method, as well as the method shown here, such accuracies were only produced in the limited cases where the O₂ concentration was very low, or not present.

Appendix G Measurement of N_2 and Calculation of x_{N_2}

Nitrogen was found to be contaminating the reactor or analytical system. To ensure that the extra N_2 was not formed by reaction of NO in the handling system, the average background level of N_2 in a typical experiment was compared to the N_2 peak from samples of a CO, O_2 , and Ar mixture. No variation was noted, ruling this possibility out. Diffusion upstream from the exit was also ruled out since variation in N_2 response with sampling location would have existed. Had the contamination been due solely to diffusion upstream from the exit, higher concentrations downstream would have been present, but none were observed. Furthermore, a direct correspondence to the sample size at any sample port would have been observed, but only a partial correspondence was seen. Therefore, some of the N_2 was from either diffusion upstream from the exit or impurity in the feed and some, the portion independent of injection size, must have been from the sampling and measurement procedure. As a double check, a bubbler was installed at the exit of the system. No change was observed. Had the N_2 been diffusing upstream from the exit, the bubbler would have made a large, or complete reduction in the amount of N_2 measured. Therefore, the extra N_2 was due to both feed impurity and co-injection.

Figure A.2 reveals that the extra N_2 amount is largely independent of the injection size. The figure shows the N_2 measured in the feed injections during a typical experiment. These data were taken in a period of over 15 hours, with no change in the feed composition. Only a slight drop in the N_2 level was seen after dropping the sample size from 100 μL to 44 μL . It was concluded that co-injection of a relatively large amount of N_2 (air) with the sample was the main problem.

That portion of the N_2 that was dependent on injection size suggests the impurity in the feed stream. Reviewing the calibration results for the various pure feed gasses revealed that while small amounts of N_2 were measured in all samples, the CO and NO/Ar supplies had significantly larger quantities. Figure A.3 shows the N_2 measured in one set of calibration data for CO. A least squares fit was made yielding the formula relating the volume of N_2 measured to the total injection

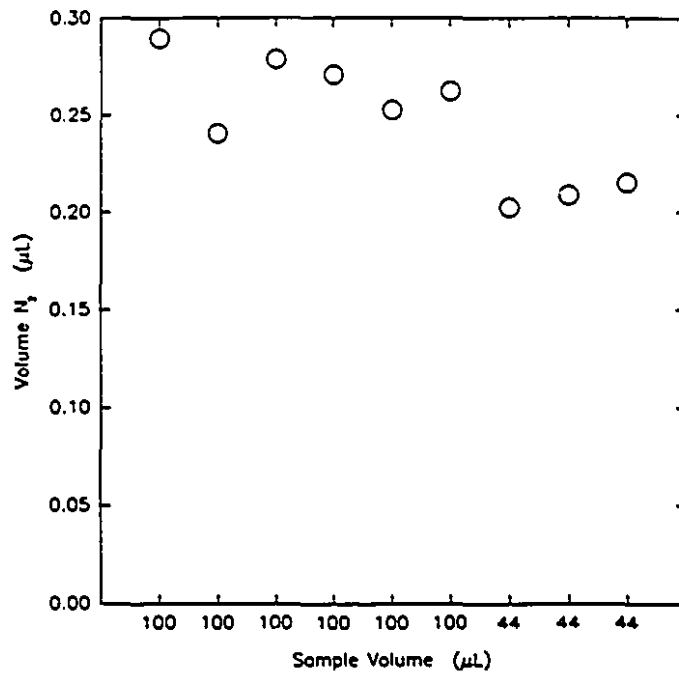


Figure A.2 N₂ measured in consecutive feed samples.
 (10% CO, 2% NO, 4% O₂, 38% Ar, 0% N₂)

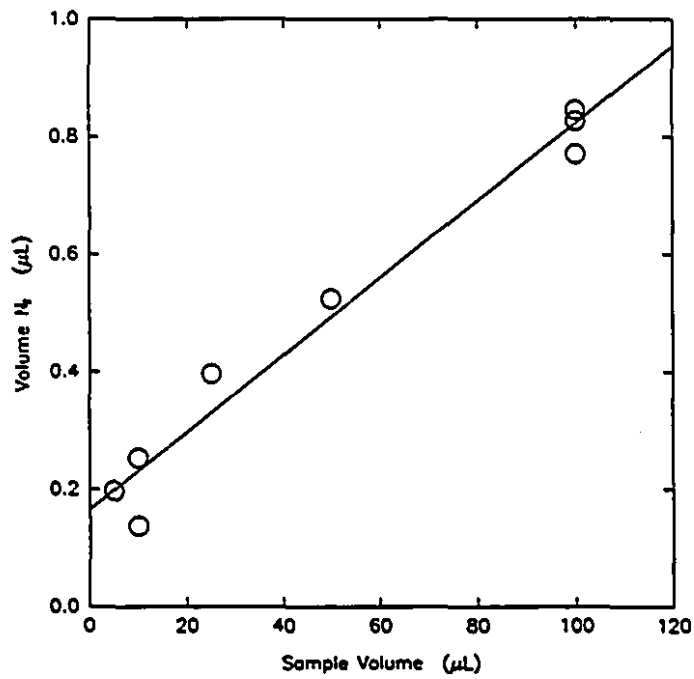


Figure A.3 The N₂ measured in the CO supply

volume:

$$v_{N_2} = 6.58 \times 10^{-3} * v_{inj} + 0.166 \mu L \quad (A.15)$$

The CO supply gas contains 0.658% N_2 while an average of 0.166 μL of N_2 has been co-injected with each sample. This exercise was repeated to determine the N_2 concentration in the NO/Ar mix.

If the data from Figure A.2 is replotted with volume N_2 measured against total injection size, Figure A.4 is obtained. The regression formula for the data is:

$$v_{N_2} = 0.00101 * v_{inj} + 0.163 \mu L \quad (A.16)$$

Note that the regression intercept, 0.163 μL , is almost the same as was found with the pure CO feed. This agreement affirms the conclusion that, in addition to the sample, with each injection a constant amount of N_2 ($\sim 0.165 \mu L$) enters the GC.

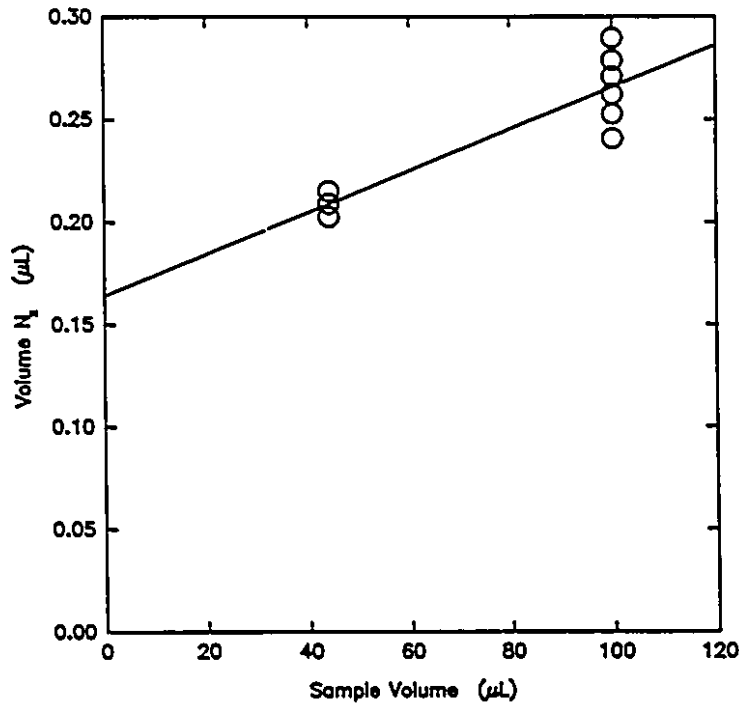


Figure A.4 Data from Figure A.2; the N_2 measured in feed gas mix with 0% N_2

The amount of N_2 measured by the GC (in moles) for a sample from any stream s is the sum of the co-injected amount of N_2 , k , and the sampled amount of N_2 , n :

$$m_{N_2}^s = k_{N_2}^s + n_{N_2}^s \quad (\text{A.17})$$

In the feed samples, the sampled N_2 is from feed impurities only, while the sampled N_2 in the product samples also contains N_2 as a reaction product. Since the N_2 impurity in the feed gas mixture is known to come from the CO and the NO/Ar mix supplies, it can be calculated from the measured amounts of CO and Ar in the feed sample

$$n_{N_2}^f = \left(r_{\frac{N_2}{CO}} * n_{CO} + r_{\frac{N_2}{NO/Ar}} * n_{Ar} \right) \quad (\text{A.18})$$

$$\therefore n_{N_2}^f = \left(r_{\frac{N_2}{CO}} * m_{CO} + r_{\frac{N_2}{NO/Ar}} * m_{Ar} \right) \quad (\text{A.19})$$

where r is the ratio giving the impurity N_2 content in each feed supply gas and n_i and m_i are the sampled and measured amounts of the feed component i (for CO, the ratio is calculated from the slope in Equation A.15). Therefore, from Equation A.17, the quantity of co-injected N_2 is given by

$$k_{N_2}^f = m_{N_2}^f - \left(n_{CO} * r_{\frac{N_2}{CO}} + n_{Ar} * r_{\frac{N_2}{Ar}} \right) \quad (\text{A.20})$$

Over the course of most experiments, the amount of co-injected N_2 drifted slightly, although a smooth trend was usually observed. To account for this drift, k_{N_2} was quantified on an ongoing basis. The level of background N_2 was found by continually taking samples of the feed gas throughout the experiment. A running average of the feed k_{N_2} values was made and used in the analysis of the product sample data.

Figure A.5 shows the variation in N_2 measured for feed injections in a typical experiment (as always, no N_2 was added to the feed mixture). While the level

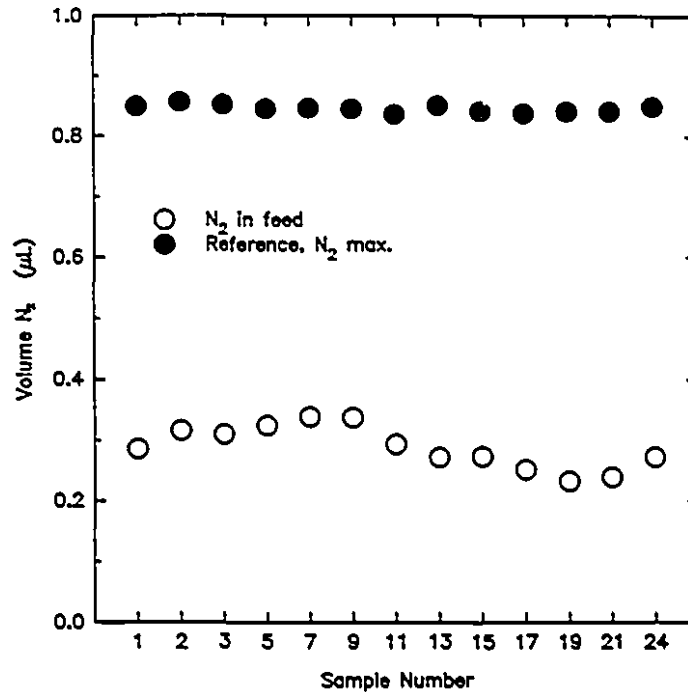


Figure A.5 N₂ measured in feed gas samples of constant volume, and, for reference, maximum amount producible by reaction of the feed mixture. For clarity, the product analyses have been removed from the figure.

varies, it generally follows a smooth path justifying the use of a running average. For reference, the maximum amount of N₂ that could be produced by reaction of the NO in the feed is also shown. Following the variation in the co-injected N₂ was necessary because this amount was often comparable to the amount of N₂ sampled. In the case of the lower temperature experiments, where very little or no reaction was taking place, the N₂ measured in the product samples was largely the co-injected N₂. Unfortunately, the sample size could not be enlarged to reduce the relative size of this N₂ without compromising the separation of other gasses being analyzed.

Typically, the feed (F) and product (P) samples in an experiment were ordered F, P, F, P, F, P... or F, P, P, F, P, P..., so that there was a close reference of feed k_{N_2} , measured near every product sample. For the product injections, the co-injected N₂ was assumed to be about the same as the running average of the amount of co-injected N₂ found in the feed samples:

For these measurements, the actual amount of N₂ sampled is then

$$k_{N_2}^p = \bar{k}_{N_2}^f \quad (\text{A.21})$$

$$n_{N_2}^p = m_{N_2}^p - \bar{k}_{N_2}^f \quad (\text{A.22})$$

The change in the molar flow rate of nitrogen can be calculated

$$\Delta F_{N_2} = F_{N_2}^p - F_{N_2}^f \quad (\text{A.23})$$

Combining Equations 5.1 and A.23 yields

$$\Delta F_{N_2} = \left(\frac{n_{N_2}^p}{n_{Ar}^p} - \frac{n_{N_2}^f}{n_{Ar}^f} \right) F_{Ar}$$

and substitution from 5.2, A.19 and A.21 gives

$$\Delta F_{N_2} = \left(\frac{m_{N_2}^p - \bar{k}_{N_2}^f}{m_{Ar}^p} - \frac{m_{CO}^f * r_{N_2} + m_{Ar}^f * r_{N_2}}{m_{Ar}^f} \right) F_{Ar} \quad (\text{A.25})$$

where k^f must be determined using Equations A.11 and A.12.

The change in the molar flow rate of N_2 , from Equation A.16, is used to calculate x_{N_2} , the conversion of NO to N_2 , by Equations 4.8 and 5.6:

$$x_{N_2} = \frac{2 \Delta F_{N_2}}{F_{NO}^f} \quad (\text{A.26})$$

$$x_{N_2} = \left(\frac{m_{N_2}^p - \bar{k}_{N_2}^f}{m_{Ar}^p} - \frac{m_{CO}^f * r_{N_2} + m_{Ar}^f * r_{N_2}}{m_{Ar}^f} \right) * 19.02 \quad (\text{A.27})$$

List of References

- Adams, K.M.; Gandhi, H.S., "Palladium Tungsten Catalysts for Automotive Exhaust treatment," *Ind. Eng. Chem. Prod. Res. Dev.*, **22**, 207 (1983)
- Anderson, H.C.; Green, W.J.; Steele, G.R., "Catalytic Treatment of Nitric Acid Plant Tail Gas," *Ind. Eng. Chem.*, **53**, 199 (1961)
- Amirnazmi, A.; Benson, J.E.; Boudart, M., "Oxygen Inhibition in the Decomposition of NO on Metal Oxides and Platinum," *J. Catal.*, **30**, 55 (1973)
- Ando, J., "Review of the Japanese NO_x Abatement Technology for Stationary Sources," in "NO_x Symposium," O. Renz, F. Iszle, and M. Weibel, Eds., Internationale Betriebsverfahren, Karlsruhe (1985)
- Arakawa, T.; Mizumoto M.; Takita, Y.; Yamazoe, N.; Seiyama, T., "Mechanism of Reduction of Nitric Oxide with Ammonia over Cu(II) Ion-Exchanged Zeolite," *Bull. Chem. Soc. Jpn.*, **50**, 1431 (1977)
- Ayen, R.J.; Amirnazmi, A., "Catalytic Reduction of Nitrogen Dioxide with Hydrogen," *Ind. Eng. Chem. Proc. Des. Dev.*, **9**, 247 (1970)
- Bartholemew, C.H., "Reduction of Nitric Oxide by Monolithic-Supported Palladium-Nickel and Palladium-Ruthenium Alloys," *Ind. Eng. Chem. Prod. Res. Dev.*, **14**, 29 (1975)
- Bauerle, G.L.; Wu, S.C.; Nobe, K., "Paramagnetic and Durability studies of NO reduction with NH₃ on V₂O₅ Catalysts," *Ind. Eng. Res. Prod. Dev.*, **17**, 117 (1978)
- Bhatia, S., "Zeolite Catalysis: Principles and Applications," CRC Press, Boca Raton, 1990
- Blanco, J.; Garcia de la Banda, J.F.; Aviva, P.; Melo, F., "Selective Reduction of Nitric Oxide on Nickel Oxide-Copper Oxide Supported Catalysts," *J. Phys. Chem.*, **90**, 4789 (1986)
- Bosh, H.; Jansen, F., "Catalytic Reduction of Nitrogen Oxides - A Review of the Fundamentals and Technology," *Catal. Today*, **2**, 4 (1987)
- Butcher, S.S.; Ruff, R.E., "Effect of Inlet Residence Time on Analysis of Atmospheric Nitrogen Oxides and Ozone," *Anal. Chem.*, **43**, 1890 (1971)
- Cadle, S.H.; Gorse, R.A.; Lawson, D.R., "Real World Vehicle Emissions: A Summary of the Third Annual CRC-APRAC On-Road Vehicle Emissions Workshop," *Air & Waste*, **42**, 1085 (1993)
- Church, M.L.; Cooper, B.J.; Willson, P.J., "Catalysis in Automobiles: A History," *A.E.*, **97**, 6 (1989)
- Church, M.L.; Cooper, B.J.; Willson, P.J., "Catalyst Formulations 1960 to Present," SAE 890815 (1989)
- Clarke, A.J., "Emissions Trends and Legislative Requirements in the United Kingdom," *VDI Berichte*, 495 (1984)
- Clay, D.T.; Lynn, S., "Iron Catalyzed Reduction of NO by CO and H₂ in Simulated Flue-Gas" in "The Catalytic Chemistry of Nitrogen Oxides," R.L. Klimisch, J.G. Larsen, and J.G. Plenum, Eds. Plenum Press, New York, 1975
- Cleemput, O.V., "Gas Chromatography of Gases Emanating from the Soil Atmosphere," *J. Chromat.*, **45**, 315 (1969)
- Courty, P.; Raynol, B.; Rebours, B.; Prigent, M.; Sugier, A., "Exhaust Gas Catalytic Reduction of Nitrogen Oxides over NiFe₂O₄-NiCr₂O₄ Solid Solutions" *Ind. Eng. Chem. Prod. Res. Dev.*, **19**, 227 (1980)
- Dijkstra, P.C.; Nicolaidis, C.P.; Weiss, K.I.G., "Evidence for non-site-isolation in ZSM-5 from Ion-Exchange and Catalytic Studies," *Catal. Lett.*, **10**, 383 (1991)
- Di Martini, R., "Determination of Nitrogen Dioxide and Nitric Oxide in the Parts Per Million Range in Flowing Gaseous Mixtures by Means of the Nitrate-Specific-Ion Electrode," *Anal. Chem.*, **42**, (1970)
- Douglas, D.C.; Greenaway, J.W. eds. "The English Historical Document," Eyre and Spottiswoode, London, 1961, p417
- Faucette, H.L.; McRight, T.C.; H.G. Graham Jr., "Analysis of Gases for Nitric Oxide, Nitrogen Dioxide, and Oxygen in a Pressure Nitric Acid Pant," *Anal. Chem.*, **38**, 1090 (1966)

- Fisher, G.E. and Becknell, D.E., "Saltzman Method for Determination of Low Concentration of Oxides of Nitrogen in Automobile Exhaust," *Anal. Chem.*, **44**, 863, (1972)
- Geankoplis, C.J., "Transport Processes and Unit Operations," 2nd ed., Allyn and Bacon, Boston, (1983)
- Hardee, J.R.; Hightower, J.W., "Nitric Oxide Reduction by Methane over Rh/Al₂O₃ Catalysts," *J. Catal.*, **86**, 137 (1984)
- Harrison, B.; Wyatt, M.; Gough, K. G., in "Catalysis," Royal Society of Chemistry, London, 1982, **5**, p 127
- Hayes, W., Personal Communication (1992)
- Hecker, W.C.; Bell A.T., "Gas Chromatographic Determination of Gasses Formed in Catalytic Reduction of Nitric Oxide," *Anal. Chem.*, **53**, 817 (1981)
- Held, W.; Konig, A.; Richter, T.; Puppe, L., "Catalytic NO_x Reduction in Net Oxidizing Exhaust Gas," SAE 900496 (1990)
- Herz, R.K.; Klela, J.B.; Sell, J.A., "Dynamic Behaviour of Automotive Catalysts. 2. Carbon Monoxide Conversion under Transient Air/Fuel Ratio Conditions," *Ind. Eng. Chem. Prod. Res. Dev.* **22**, 387 (1983)
- Hightower, J.W.; Van Leirsburge, in "The Catalytic Chemistry of Nitrogen Oxides," R.L. Klimisch, J.G. Larson, Eds., Plenum Press, New York, 1975
- Inui, T.; Okawa, T.; Takegami, Y., "Complete Conversion of NO over the Composite Catalyst Supported on Active Carbon," *Ind. Eng. Chem. Prod. Res. Dev.*, **21**, 56 (1984)
- Iwamoto, M.; Furukawa, H.; Kagawa, S., "Catalytic Decomposition of Nitrogen Monoxide over Copper Ion-Exchanged Zeolites," in "New Developments in Zeolite Science and Technology, Proceedings of the 7th International Zeolite Conference, Tokyo", Y. Murakami, A. Iijima, J.W. Ward, Eds., Elsevier, New York, 1986, p943
- Iwamoto, M.; Yahiro, H.; Mine, Y.; Kagawa, S., "Excessively Copper Ion-Exchanged ZSM-5 Zeolites as Highly Active Catalysts for Direct Decomposition of Nitrogen Monoxide," *Chem. Lett.*, 1989, 231
- Iwamoto, M.; Yahiro, H.; Torikai, T.; Yoshioka, T.; Mizuno, N., "Novel Preparation Method of Highly Copper Ion-Exchanged ZSM-5 Zeolites and Their Catalytic Activities for NO Decomposition," *Chem. Lett.*, 1990, 1967
- Iwamoto, M.; Yahiro, H.; Yu-U, H.; Shundo, s.; Mizuno, N., "Selective Reduction of NO by Lower Hydrocarbons in the Presence of O₂ and SO₂ over Copper Ion-Exchanged Zeolites," *Shokubai*, **32**, 6, 433 (1990). In Japanese.
- Izuka, T., Ikeda, H.; Terao, T.; Tanabe, K., "Support Effects on Iron III Oxide Catalysts in the Reduction of Nitrogen Oxide with Hydrogen," *Aust. J. Chem.*, **35**, 927 (1982)
- Izuka, T.; Lunsford, J.H. "The Reduction of Nitric Oxide by Carbon Monoxide Over Rhodium-Y-Zeolites," *J. Mol. Catal.* **8**, 391 (1980)
- Jamieson, A.M., "A Gas Chromatographic Method for the Determination of the Argon and Oxygen Contents of Air in Bottled Beverages," *J. Chrom. Sci.*, **9**, 750 (1971)
- Jansen, F.J.J.G.; van der Kerkhof, F.M.G., "Selective catalytic removal of NO from Stationary Sources," *Kema Scientific & Technical Reports*, **3**, 71 (1979)
- Johnson, C.L., "Analysis of Gas Mixtures Containing Oxides of Nitrogen," *Anal. Chem.*, **24**, 1572 (1952)
- Kato, A.; Matsuda, S.; Kamo, T.; Nakajima, F.; Kuroda, H.; Narita, T., "Reaction Between NO_x and NH₃ on Iron Oxide-Titanium Oxide Catalyst," *J. Phys. Chem.*, **85**, 4099 (1981)
- Kim, G., "Ceria-Promoted Three-Way Catalysts for Auto Exhaust Emission Control," *Ind. Eng. Chem. Prod. Res. Dev.* **21**, 267 (1982)
- Kiyomia M.; Kawai, M., "The Effectiveness of Laterite as a Catalyst for the Reduction of NO with NH₃," *Atmos. Env.*, **13**, 559 (1979)
- Klimish, R.L.; Taylor, K.C., "Dual Functionality and Synergism in the Catalytic Reduction of Nitrogen Oxide," General Motors Research Publication GMR-1195 (1972). Reference from: Klimish, R.L.; Komary, J.M., "Approaches to Catalytic Control of Automotive NO_x

- Emissions," in "The Catalytic Chemistry of Nitrogen Oxides," R.L. Klimisch, J.G. Larson, Eds., Plenum Press, New York, 1975
- Kokotailo, G.T.; Lawton, S.L.; Olson, D.H.; Meier, W.M., "Structure of Synthetic Zeolite ZSM-5," *Nature*, 272, 437 (1978)
- Kudo, T.; Gejo, T.; Yoshida, K., "New Oxide Catalysts with Perovskite-Related Structure for Reduction of Nitric Oxide with Ammonia," *Env. Sci. Tech.*, 12, 185 (1978)
- Lester, G.R.; Joy, G.C.; Brennan, J.F., "The Selective Catalytic Reduction of Nitric Oxide in the Presence of Oxygen," SAE 780202 (1978)
- Li Y.; Hall, W.K., "Stoichiometric Catalytic Decomposition of Nitric Oxide Over Cu-ZSM-5 Catalysts," *J. Phys. Chem*, 94, 6145 (1990)
- Li Y.; Hall, W.K., "Catalytic Decomposition of Nitric Oxide over Cu-Zeolites," *J. Catal.* 129, 202 (1991)
- Margeson, J.H.; Suggs, J.C.; Midgett, M.R., "Reduction of Nitrate to Nitrite with Cadmium" *Anal. Chem.*, 52, 1955, (1980)
- Markvart, M.; Pour, V., "The Influence of Oxygen on the Catalytic Reduction of Nitric Oxide by Ammonia," *J. Catal.*, 7, 279 (1967)
- Mass, C.; Knittel, G.; Liens, R.; Unk, J.; Von Ammon, R., "An Automated Introduction System of Hydrogen During the Catalytic Reduction Of O₂ and NO_x in the Flue-Gas Treatment," *Chem. Ing. Tech.*, 58, 43 (1986)
- Matsuda, S.; Takeuchi, M.; Hishinuma, T.; Nakajima, F.; Narita, T.; Watanabe, Y.; Imari, M., "Selective Reduction of Nitrogen Oxides in Combustion Flue Gasses," *J. Air Pollut. Cont. Assoc.*, 28, 350 (1978)
- McCandles, P.M.; Hodgson, K., "Reduction of Nitric Oxide with Metal Sulphides," Environmental Protection Agency Report EPA-600/7-78-213 Nov. 1978
- Meier H.; Gut, G., "Kinetics of the Selective Catalytic Reduction of Nitric Oxide with Ammonia on a Platinum Catalyst," *Chem. Eng. Sci.*, 33, 123 (1978)
- Minsono, M.; Kondo, K., "Catalytic Removal of Nitrogen Monoxide over Rare Earth Ion-Exchanged Zeolites in the Presence of Propene and Oxygen," *Chem. Lett.*, 1992, 1001
- Miyamoto, A.; Inove, B.; Murikami, Y., "Automotive Exhaust Emissions Control Using the Three-Way Catalyst System. 1. Computer Simulation of the NO-H₂-O₂ Reaction on Pt/Al₂O₃ Catalyst" *Ind. Eng. Chem. Prod. Res. Dev.*, 18, 104 (1979)
- Miyamoto, A.; Kobayashi, K.; Inomata M.; Murakami, Y., "Nitrogen-15 Tracer Investigation of the Mechanism of the Reaction of NO with NH₃ on Vanadium Oxide Catalysts," *J. Phys. Chem.* 86, 2945 (1982)
- Muraki, H.; Shinjoh, H.; Sobukawa, H.; Yokota, Y.; Fujitani, Y., "Palladium-Lanthanum Catalysts for Automotive Emission Control," *Ind. Eng. Chem. Prod. Res. Dev.* 25, 202 (1986)
- Muraki, H.; Yokota, Y.; Fujitani, Y., "Nitric Oxide Reduction Performance of Automotive Palladium Catalysts," *App. Catal.* 48, 93 (1989)
- Nakajima, F., "Air Pollution Control with Catalysis - Past, Present, and Future-," *Catal. Today*, 10, 1, (1991)
- Naruse, Y.; Ogasawara, T.; Hata, T.; Kishitaka, H., "Properties and Performances of Various Iron Oxide Catalysts for NO Reduction with NH₃," *Ind. Eng. Chem. Prod. Res. Dev.*, 19, 57, (1980)
- Novkikov, S.G.; Saskovets, U.V.; Brzouskii, I.I.; Dubnova, N.Y., "Gas Chromatographic Analysis of Mixtures of O₂ in Nitrogen Oxides," *Ser. Khim. Nauvk.* 2, 114 (1991)
- Ohtaki, H., *Bull. Chem. Soc. Jpn.*, 45, 1735 (1972); referenced from Iwamoto, 1990
- Otto, K.; Shelef, M.; Kummer, J.T., "Studies of Surface Reactions of Nitric Oxide by Nitrogen-15 Isotope Labelling; Part I. The Reaction Between Nitrogen Oxide and Ammonia over Supported Platinum at 200-225°C," *J. Phys. Chem.*, 74, 2690 (1970)
- Otto, K.; Shelef, M., "Studies of Surface Reactions of NO by Isotope Labelling; Part VI. The Reduction Nitric Oxide by Ammonia and Hydrogen over Supported Ruthenium," *Z. Phys. Chem. NF*, 85, 308 (1973)

- Papolymerou G.A.; Schmidt, L.D. "Unimolecular Reactions of NO, N₂O, NO₂, and NH₃ on Rh and Pt," *Langmuir*, **1**, 488 (1985)
- Peters, M.S.; Wu, J.L., "Catalytic Reduction of Nitric Oxide with Carbon Monoxide by Rare Earth Oxides," *Atmosph. Environ.*, **11**, 459 (1977)
- Powell, D.E.; Nobe, K., "Reduction of NO with NH₃ on Fe-Cr Oxides Catalyst," *Chem. Eng. Commun.* **10**, 103 (1981)
- Sarkanay, J.; d'Itri, J.L.; Sachtler, W.M.H., "Redox Chemistry in Excessively Ion-Exchanged Cu/Na-ZSM-5," *Catal. Lett.* **16**, 241 (1992)
- Shelef, M.; Otto, K.; Gandhi, H.S., "The Oxidation of CO by O₂ and NO on Supported Chromium Oxide and Other Metal Oxide Catalysts," *J. Catal.*, **12**, 361 (1968)
- Shikada T.; Fujimoto, K.; Kunugi, T.; Tominga, H.; Kaneko, S.; Kubo, Y., "Reduction of Nitric Oxide with Vanadium Oxide Catalysts Supported on Homogeneously Precipitated Silica-Titania," *Ind. Eng. Chem. Prod. Res. Dev.* **20**, 91 (1981)
- Shikada T.; Fujimoto, K.; Kunugi, T.; Tominga, H., "Reduction of Nitric Oxide with Ammonia on Vanadium Oxide Catalysts supported on Homogeneously Precipitated Silica-Titania," *J. Chem. Tech. Biotech.*, **33A**, 446 (1983)
- Sigsby J.E.Jr.; Black, F.M.; Bellar, T.A.; Klosterman, D.L., "Chemiluminescent Method for Analysis of Nitrogen Compounds in Mobile Source Emissions (NO, NO₂, and NH₃)," *Env. Sci. & Tech.*, **7**, 51 (1973)
- Smith, J.M., "Chemical Engineering Kinetics," 3rd Ed., McGraw Hill, New York, 1981
- Taylor, F.R. "The Elimination of Oxides of Nitrogen From Automobile Exhaust," Special Publication, Air Pollution Foundation, San Marino, California (1959)
- Tzou, M.S.; Asakura, K.; Yamazaki, Y.; Kuroda, H., "Zeolite Supported PtRh Catalysts for CO Oxidation and NO Reduction: Evidence for Bimetallic Particles Formation and Synergism Effect," *Catal. Lett.* **11**, 33, (1991)
- Walker, J.W., "The Catalytic Reduction of Nitric Oxide With Ammonia," Thesis, McGill University, Montreal, Canada (1974)
- Waren, W.L., "Henry II," *Eyre Methven*, London, 1973, p391
- Willey, R.J., Eldrige J.W.; Kittrel, J.R., "Mechanistic Model of the Selective Catalytic Reduction of Nitric Oxide with Ammonia," *Ind. Eng. Chem. Prod. Res. Dev.* **24**, 226 (1985)
- Yang, Li. "Catalytic Decomposition of Nitric Oxide on Sodium Ferrite," *Ind. Eng. Chem. Prod. Res. Dev.*, **21**, 405 (1982)